AD-A166 141 USE OF HOLOGRAPHIC FRINGE LINEARIZATION INTERFEROMETRY 1/1
(FLI) FOR DETECTIO.. (U) HONEYWELL ELECTRO-OPTICS DIV
LEXINGTON MA G O REYNOLDS ET AL NOV 85
UNCLASSIFIED AFOSR-TR-86-0108 F49620-82-C-0001 F/G 14/5 NL

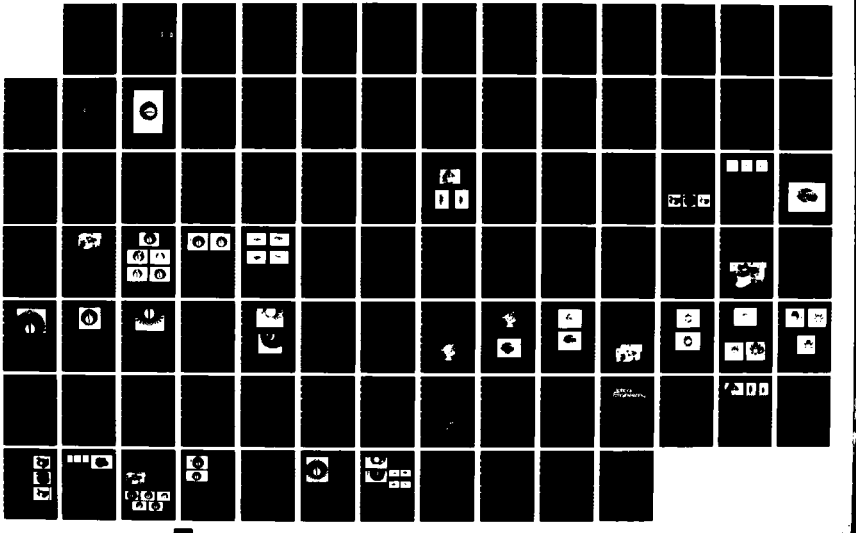

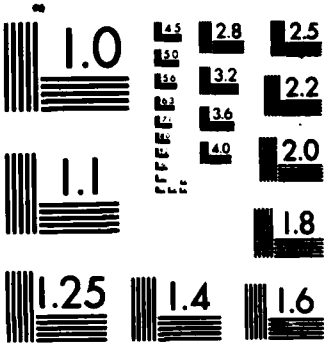

AFOSR-TR- 86-0108

(2)

Use of Holographic Fringe Linearization Interferometry (FLI) for Detection of Defects

Final Report

November 1985

Honeywell

UNCLASSIFIED

SECURITY CLASSIFICATION OF THIS PAGE (When Data Entered)

REPORT DOCUMENTATION PAGE	READ INSTRUCTIONS BEFORE COMPLETING FORM
1. AFOSR-TR- 86-0108 2. GOVT ACCESSION NO.	3. RECIPIENT'S CATALOG NUMBER
4. TITLE (and Subtitle) USE OF HOLOGRAPHIC FRINGE LINEARIZATION INTERFEROMETRY (FLI) FOR DETECTION OF DEFECTS	5. TYPE OF REPORT & PERIOD COVERED Final Jan. 15, 1984 Aug. 1985
	6. PERFORMING ORG. REPORT NUMBER
7. AUTHOR(s) George O. Reynolds, P.I., Donald A. Servaes, Luis Ramos, Honeywell EOD; Daniel Pierce, Ronald Mayville, Peter Hilton, Arthur D. Little, Inc., John B. DeVelis, Merrimack Col.	8. CONTRACT OR GRANT NUMBER(s) F49620-82-C-0001
9. PERFORMING ORGANIZATION Honeywell Electro-Optics Div. 2 Forbes Rd Lexington MA 02173 AFOSR/NE Bolling AFB DC 20332	10. PROGRAM ELEMENT, PROJECT, TASK AREA & WORK UNIT NUMBERS 61102F 2306 B2
	12. REPORT DATE November 1985
	13. NUMBER OF PAGES 90
14. MONITORING AGENCY NAME & ADDRESS (if different from Controlling Office) Same as #11	15. SECURITY CLASS. (of this report) UNCLASSIFIED
	15a. DECLASSIFICATION/DOWNGRADING SCHEDULE NA

16. DISTRIBUTION STATEMENT (of this Report)

NA Approved for public release; distribution unlimited.

17. DISTRIBUTION STATEMENT (of the abstract entered in Block 20, if different from Report)

NA

18. SUPPLEMENTARY NOTES

NONE

19. KEY WORDS (Continue on reverse side if necessary and identify by block number)

Holographic Interferometry, Non-Destructive Evaluation, Lasers, Moire Techniques, Finite Element Analyses,

20. ABSTRACT (Continue on reverse side if necessary and identify by block number)

In this final report on contract #F49620-82-C-0001, we show that the two-exposure FLI holographic method is feasible. We describe how the two-exposure FLI technique can be utilized by increasing the linear fringe frequency. Reprints of the published papers from this contract describing the modeling/experiment program are appended. The feasibility of an automatic readout for the linear fringe method is demonstrated by showing that observable and measurable effects at the defect site can be monitored.

DD FORM 1 JAN 73 1473 EDITION OF 1 NOV 65 IS OBSOLETE

UNCLASSIFIED

SECURITY CLASSIFICATION OF THIS PAGE (When Data Entered)

20. ABSTRACT (Continued)

The sensitivity analysis and results from a simple dynamic loading model are presented. A preliminary FLI experiment on composite samples with both static and thermal loading failed to find defects. Finally, recommendations of work necessary to develop the FLI technique are given.

FINAL REPORT

on

Contract F49620-82-C-0001

USE OF HOLOGRAPHIC FRINGE LINEARIZATION INTERFEROMETRY (FLI) FOR DETECTION OF DEFECTS

November 1985

Principal Investigator

GEORGE O. REYNOLDS

Honeywell

ELECTRO-OPTICS DIVISION
2 Forbes Road
Lexington, MA 02173

TABLE OF CONTENTS

SECTION	TITLE	PAGE
1	OVERVIEW AND EXECUTIVE SUMMARY	1-1
1.1	OVERVIEW	1-1
1.2	SUMMARY OF SIGNIFICANT RESULTS	1-1
1.3	RECOMMENDATIONS	1-2
2	RESEARCH OBJECTIVE AND LOGISTICS	2-1
2.1	OBJECTIVE	2-1
2.2	LOGISTICS	2-1
2.3	CONTRIBUTORS TO THE REPORT	2-1
3	PROBLEMS ENCOUNTERED DURING THE PROGRAM	3-1
4	PUBLISHED RESULTS OF THIS RESEARCH PROGRAM	4-1
5	TECHNICAL RESULTS OF RESEARCH EFFORT ADDITIONAL TO THOSE IN APPENDIXES A THROUGH E	5-1
5.1	FINITE ELEMENT ANALYSIS OF FLI EXPERIMENTS	5-1
	5.1.1 Review of Static Loading	5-1
	5.1.2 Sensitivity Considerations with Static Loading	5-1
5.2	DYNAMIC LOADING CONSIDERATIONS	5-6
	5.2.1 Analysis	5-6
	5.2.2 Experimental Work	5-12
5.3	LOAD DESENSITIZATION WITH MOIRE TECHNIQUES	5-12
5.4	FLI EXPERIMENTS TO FIND DEFECTS IN COMPOSITE MATERIALS	5-13
5.5	COMMENTS ON DEFECTS AND MODELING	5-13
	5.5.1 Experimental Cracks Used in Study	5-13
	5.5.2 Real Cracks in Metals	5-13
	5.5.3 Composites	5-14
	5.5.4 Adhesive Joints	5-15
	5.5.5 Three-Dimensional Modeling Effort	5-15
6	CONCLUSIONS	6-1
7	RECOMMENDATIONS	7-1
8	REFERENCES	8-1

SECTION 1
OVERVIEW AND EXECUTIVE SUMMARY

1.1 OVERVIEW

Two exposure Holographic Interferometry has been successfully utilized in a number of applications. Its use in non-destructive evaluation has been limited in its full potential due to the inability to interpret the complicated interference fringe patterns which result from the test specimen being in different mechanical and/or thermal states at the time of the two exposures. For this reason many non-destructive production testing situations have abandoned holography in favor of other less desirable but more reliable technologies such as eddy currents, radiography, dye penetrants, magnetic particles, and acoustic sounding. However, these techniques are only effective over small areas.

The objective of this program was to demonstrate that the holographic Fringe Linearization Interferometry (FLI) process could remove fringe clutter and make fringe shifts due to defects more visible.

The work performed under this contract experimentally demonstrated that the location of through and rear-surface cuts (which are difficult to detect with conventional double exposure holographic interferometry) were rendered visible with the holographic FLI technique. Further work demonstrated that these defects had measurable Fourier signatures which were characteristically different from the signature of the carrier. The FLI process is thereby amenable to automatic readout technology. We also developed a computer model for static loading and the resulting analytical FLI fringe patterns were in excellent agreement with those obtained experimentally.

In any practical NDE application it will be necessary to utilize FLI with dynamic loading conditions and pulsed lasers to avoid overall mechanical motions between the hologram and structure under evaluation.

1.2 SUMMARY OF SIGNIFICANT RESULTS

Results obtained with static loading techniques were significant;

- The experimental feasibility of the FLI concept has been demonstrated;
- FLI removes fringe clutter and simplifies defect location;
- Experimental results showed linearization of fringes and location of both a through cut and a rear surface cut;
  - no spatial filtering required;
- Experiments with a Fourier diffractometer showed that both the through cut and the rear surface cut had Fourier signatures significantly different from those of the defect free fringe area;
  - Automatic readout techniques utilizing computer software algorithms are possible with such characteristic signatures;
- Finite element analysis showed that the FLI process can be modeled accurately; agreement with the experimental results was excellent;

- Further desensitization, if necessary, can be achieved by using the two-color, four-exposure holographic moire technique;
  - Spatial filtering will be required;
- The sensitivity analysis showed that best detectivity of sub-surface cracks is obtained when the fringes cross the crack at an angle of 45°.
- Cracks not emanating from the hole were not rendered visible with static or analytical dynamic loading but were found with pressure loading experimentally.
  - These types of defects are not as common as the types emanating from the holes which closely simulate cracks growing from a fastener hole.
- We also modeled dynamic loading with various harmonics showing that sub-surface cracks emanating from holes (similar to real cracks emanating from fastener holes in aircraft) are detectable with FLI.
  - Impulse loading would result in a superposition of such modes.
- Two composite samples with defects (delaminations) were experimentally investigated with both static and thermal loading techniques. The defects were not found with these loading methods. Pressure loading is usually used to holographically find debonds in laminated materials but this may not be practical for aircraft measurements in the field.
- The utility of dynamic loading on composite materials in finding delaminations remains to be determined.
- We were not able to do dynamic measurements on this program because of problems encountered with the high power lasers available to us.

1.3 RECOMMENDATIONS

THE SUCCESSFUL RESEARCH RESULTS OBTAINED ON THIS PROGRAM WITH STATIC LOADING SUGGEST TRANSITIONING THE TECHNOLOGY TO INCORPORATE THE DYNAMIC LOADING CAPABILITY IN A FUTURE STUDY.

The implications of this situation are that holographic FLI could revitalize large area inspection of military aircraft (both metal and composite structures) and thereby increase the aircraft's useful lifetime.

We therefore recommend generating a three-dimensional model to describe realistic flaws. These defects should be fabricated in experimental specimens and located with FLI technology. Defects in metals and composite materials should be experimentally located and evaluated with this dynamic loading technology. In addition, the integrity of adhesive joints in composite materials should be determined.

Specifically, this future study should consist of:

1. Model development for FLI with (a) dynamic loading, (b) realistic defects in three-dimensional metallic structures, and (c) debonds in composite materials and adhesive joints.
2. An experimental demonstration of the feasibility of dynamically loaded FLI for detecting flaws in metal and in composite samples.
   - Define range of loading forces as a function of sample and defect type.

3. A comparison of the model results with experimental results and a determination of the sensitivity limitations of dynamic FLI in various types of materials.

4. A measurement of defects in structures of interest to the Air Force with the FLI technique.

The different combinations of materials, defects, model geometry and loading types that should be investigated theoritically and experimentally in such a study are shown in Figure 1-1. The results of such a study would show the viability for developing a holographic FLI hardware/software system for use in the important NDE applications of testing military aircraft. Implementation of a practical surface testing program could extend the lifetime of military aircraft and thereby result in savings to the U.S. government.

DEFECT TYPE/TASK	GEOMETRY	MODEL AND LOADING TYPE		FEASIBILITY EXPERIMENTS		SENSITIVITY STUDY	
		Static	Dynamic	Static	Dynamic	Static	Dynamic
Real Cracks In Metals	2-Dim	*	*	*	✔	*	✔
	3-Dim	✔	✔	✔	✔	—	✔
Debonds In Composites	2-Dim	✔	✔	✔	✔	—	✔
	3-Dim	✔	✔	✔	✔	—	✔
Adhesive Joints In Composites	3-Dim	✔	✔	✔	✔	—	✔

— N.A.
✔ To be investigated in the recommended program
* Investigated under this contract

Figure 1-1. Subjects to be Addressed in the Recommended Program

SECTION 2
RESEARCH OBJECTIVE AND LOGISTICS

2.1 OBJECTIVE

The objective of this research program was to prove the concept of Holographic Fringe Linearization Interferometry (FLI) and determine its degree of utility. The former objective was met but the utility of the concept to practical situations still awaits further study.

In the FLI technique, linear fringes are introduced in the formation step of double exposure holographic interferometry by using a beam deflector in the object beam between two holographic exposures. The addition of the linear fringe of the appropriate spatial frequency to the interferogram dominates the random fringes that commonly appear in double exposure holography. The superposition of the linear fringes with the random fringes yields a resultant pattern, that is comprised of straight line fringes everywhere except at the defect region.

The goal of this research program was the experimental demonstration of the FLI technique for detecting and locating (not necessarily identifying or classifying) subsurface cracks and defects in various structures. Since FLI is a potentially large area inspection technique that is compatible with image processing, its success can simplify the Non-Destructive Evaluation (NDE) process for large military structures such as aircraft.

2.2 LOGISTICS

The experimental work was performed by Honeywell at its Electro-Optics Division, Advanced Concepts Group in Wilmington, MA. Initial experimentation at NADC was performed but dropped because of reliability problems with their pulsed ruby laser.

2.3 CONTRIBUTORS TO THE REPORT

This study's principal investigator was George O. Reynolds from the Honeywell Electro-Optics Division. Donald A. Servaes, the Project Experimentalist, Luis Ramos and Adrian Ho the Experimental Assistants, were also Honeywell employees on this program. Dr. John B. DeVelis, a consultant to Honeywell from Merrimack College, has contributed to the study. Ronald A. Mayville, Peter D. Hilton and Daniel C. Peirce from Arthur D. Little, Inc. performed mechanical designs, modeling work and deformation analysis under a subcontract to Honeywell.

SECTION 3
PROBLEMS ENCOUNTERED DURING THE PROGRAM

In addition to the two moves of the Advanced Concepts group within Honeywell EOD during the program, the GFE laser at NADC was not extensively used because of reliability problems encountered during our visits. The Honeywell argon ion laser tube was broken during the second move, and a new tube was installed at Honeywell's expense during 1984. The water supply to the lab in Wilmington was increased to accommodate the flow rate required by the laser cooling system. This fix was inadequate due to the low water pressure at the Honeywell facility in Wilmington, Mass. A holding tank and pump was installed and the laser worked for two days until the hose on the pump let go and flooded the Wilmington facility. A new holding tank was ordered, the lab remodeled to hide it in the wall and the tank finally installed. By this time the laser tube had gone dead and we could not get the unit to lase. The vendor suggested a new tube which is currently on order. Our argon laser was at the vendors shop at the conclusion of the program. Needless to say, the dynamic loading and two color moire experiments were not conducted during this program because of these laser problems.

SECTION 4
PUBLISHED RESULTS OF THIS RESEARCH PROGRAM

The theoretical and experimental work conducted on this program resulted in five publications which are listed below and reprints included in Appendixes A through E.

Appendix A G.O. Reynolds, D.A. Servaes, L. Ramos-Izquierdo, and J.B. DeVelis, "Holographic Fringe Linearization Interferometry (FLI) for Defect Detection; Part I - The Basic Concept" in Applications of Holography L. Huff, editor, Proceedings SPIE Vol. 523, pg. 160, 1985.

Appendix B G.O. Reynolds, D.A. Servaes, L. Ramos-Izquierdo, J.B. DeVelis, D.C. Peirce, P.D. Hilton and R.A. Mayville, "Holographic Fringe Linearization Interferometry (FLI) for Defect Detection; Part II - Comparison of Observation with Predictions" in Applications of Holography L. Huff, editor, Proceedings SPIE Vol. 523, p. 176, 1985.

Appendix C G.O. Reynolds, D.A. Servaes, L. Ramos-Izquierdo and J.B. DeVelis "Holographic Fringe Linearization Interferometry (FLI) for Defect Detection; Part III - Load Desensitization with Moire Techniques" in Application of Holography L. Huff, editor, Proceedings SPIE Vol. 523, p. 186, 1985.

Appendix D G.O. Reynolds, "Holographic Fringe Linearization Interferometry (FLI) for Defect Detection" ACTA POLYTECHNICAL SCANDINAVICA Applied Physics, Series No. 150, Image Science '85 ed. by A.T. Friberg and P. Oittinen Vol. 2 Ph150, p. 53, 1985. Helsinki, Finland VDC 778.3:681.3:535.3/.6.

Appendix E G.O. Reynolds, D.A. Servaes, L. Ramos-Izquierdo, J.B. DeVelis, D.C. Peirce, P.D. Hilton and R.A. Mayville "Holographic Fringe Linearization Interferometry for Defect Detection" Opt. Eng. 24(5) 757 Sept/Oct 1985.

Papers Presented

- The material in Appendixes I through III was presented in three papers at the SPIE Symposium, January 21-23, 1985, Los Angeles, California, by G.O. Reynolds, D.C. Peirce and D.A. Servaes respectively.
- The material in Appendix D was presented at the ICO Conference, Image Science '85 held on the campus of the Helsinki University of Technology in Otaniemi Finland, June 11 through 14, 1985, by G.O. Reynolds.
- The material in Appendixes A through E was presented in a colloquium at the University of Erlangen:Nurnberg, Erlangen Germany on June 5, 1985 by G.O. Reynolds.
- Some of the material in Appendix E was presented at the New England Experimental Stress Society meeting in Newton, Mass., on October 4, 1984, by G.O. Reynolds.

SECTION 5
TECHNICAL RESULTS OF RESEARCH EFFORT ADDITIONAL TO THOSE IN APPENDIXES A THROUGH E

5.1 FINITE ELEMENT ANALYSIS OF FLI EXPERIMENTS

Throughout this research program, finite element calculations have been performed in support of laboratory tests which demonstrate fringe linearization interferometry. These computations, carried out primarily with the commercial software package ANSYS, serve not only as a guide to specification of those loads which best reveal the presence of a flaw, but also as a flexible means of checking which fringe frequencies and orientations are most effective in detecting a particular defect. In the following section, we summarize our previously reported success in detecting a part-through crack emanating from a hole in a plate subjected to a static bending load. From further computations based on the same configuration, we also offer some likely rules of thumb that should apply in general to detection of flaws using the FLI technique. Finally, we show results from a modal analysis of the experimental test plate, and we comment on the potential for using dynamic loading to elucidate the locations of defects.

5.1.1 Review of Static Loading

The finite element mesh (Figure 5-1) which was generated by ANSYS has relatively fine line separation near the two cracks in the plate, which is four inches square. One crack emanates from the upper left of the hole, while the second is horizontal and is located one inch below the hole. In ANSYS, the cracks are modeled by narrow elements (too small to be visible on the plot) which are assigned a thickness of 0.0005 inches, while the plate itself is 0.1 inches thick. A Young's modulus of 10×10^6 psi and a Poisson ratio of 0.34, both characteristic of aluminum, are used throughout. Equal and opposite loads of 4 pounds at the top and the bottom of the hole provide the static loading. To model the test configuration, the plate is clamped on three sides and is free on the top edge. The analytical results, with linear fringes, are shown in Figure 5-2. (In the model, the linear fringes are created by superposing contours corresponding to a rigid body rotation. The amount of this rotation corresponds exactly to the rotation of the object beam in the experiments.) The subsurface crack emanating from the hole is readily detectable, as in the corresponding experimental result shown in Figure 5-3. The horizontal crack below the hole, however, is not visible in either the model or the experiment. Thus, the model and the experiment are in excellent agreement; the fact that the crack below the hole remains obscured is most likely due to the load and plate configuration. The deformations in the area of the horizontal crack are quite small and, IN FACT, ONE WOULD TYPICALLY NOT EXPECT A CRACK TO DEVELOP IN THIS LOCATION. Experiments with plug (pressure) loading showed that this defect was easily detectable (see Figure 20 in Appendix E).

5.1.2 Sensitivity Considerations with Static Loading

The results shown in Figures 5-2 and 5-3 correspond to an object beam rotation of 600 μr, and the rotation is about a vertical axis. This raises the question of which linear fringe frequency and orientation is best suited to detecting a particular flaw. It is especially easy to change the fringe orientation using the computer model; an example showing an orientation 45° from the vertical is presented in Figure 5-4. This figure does not reveal the crack as well as Figure 5-2 and, in fact, the orientation of the fringes shown in Figure 5-2 proved to reveal the crack emanating from the hole better than any of the several orientations for which calculations were performed. From these results, one might postulate the following general rule: to be able to detect defects most

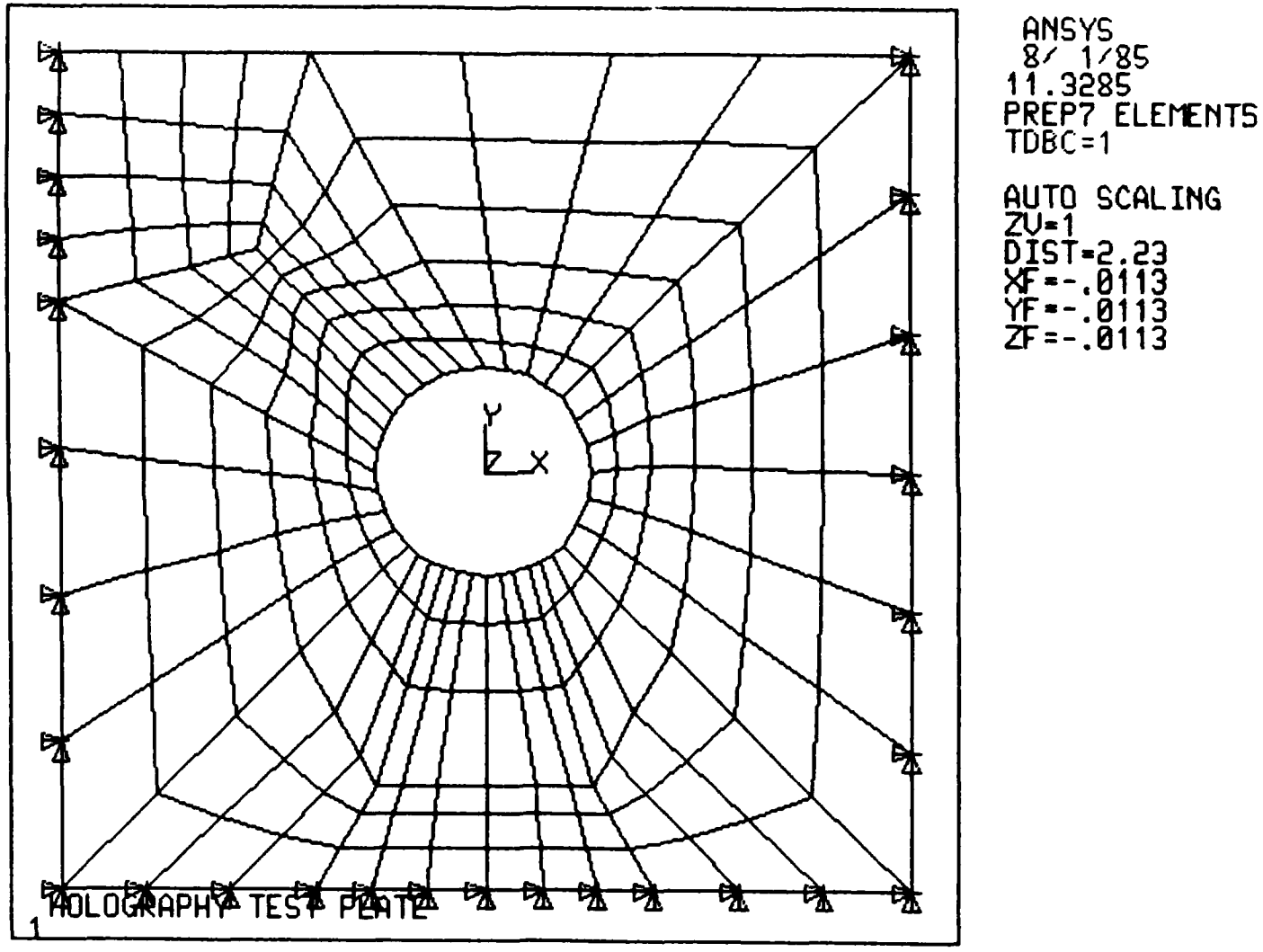

Figure 5-1. Finite Element Mesh for Test Plate Analysis

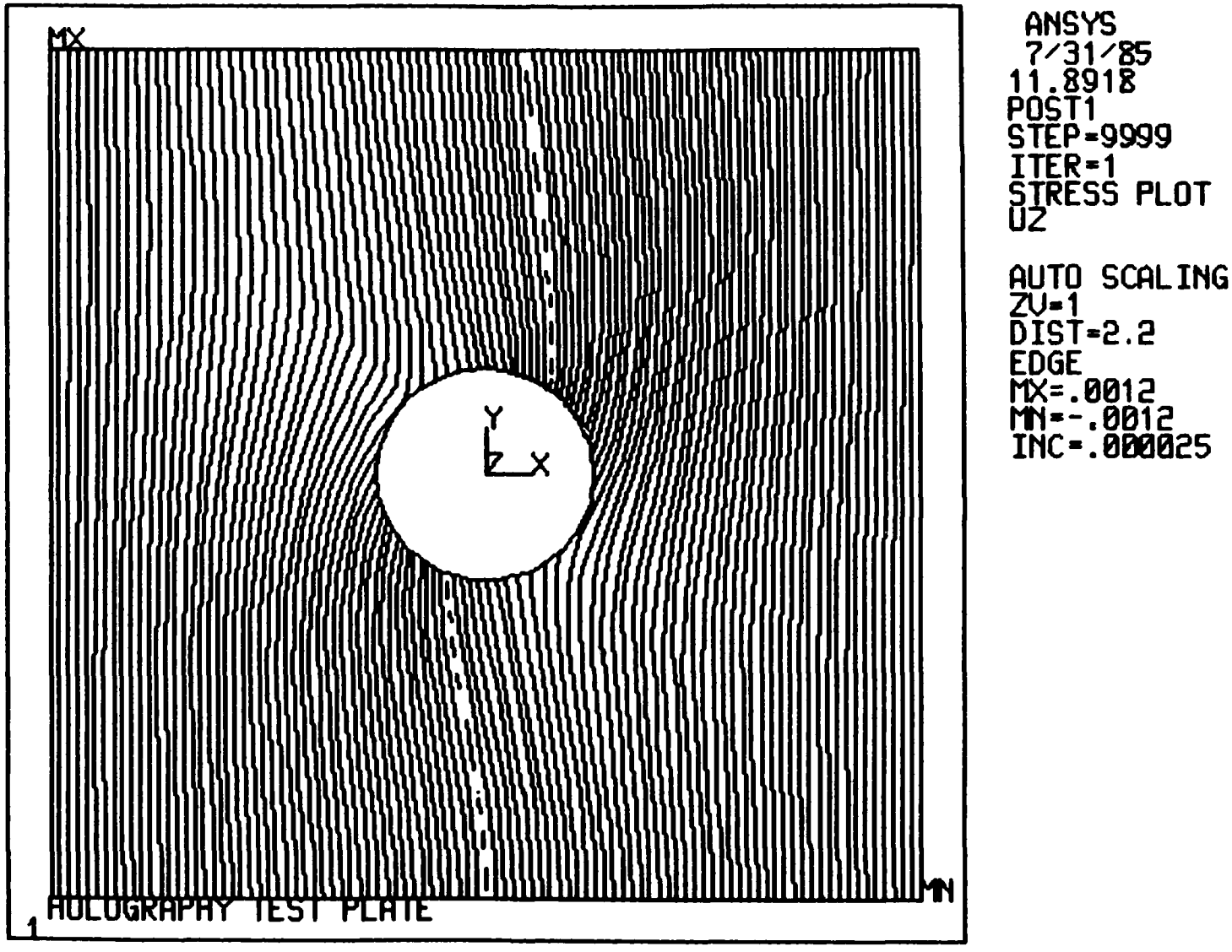

Figure 5-2. Model Results for Static Loading at the Top and Bottom of the Hole. Linear fringes corresponding to a 600 microradian object beam rotation have been added. The flaw extends from the upper left of the hole.

Figure 5-3. Experimental Results Corresponding to Figure 5-2, with the Same Object Beam Rotation

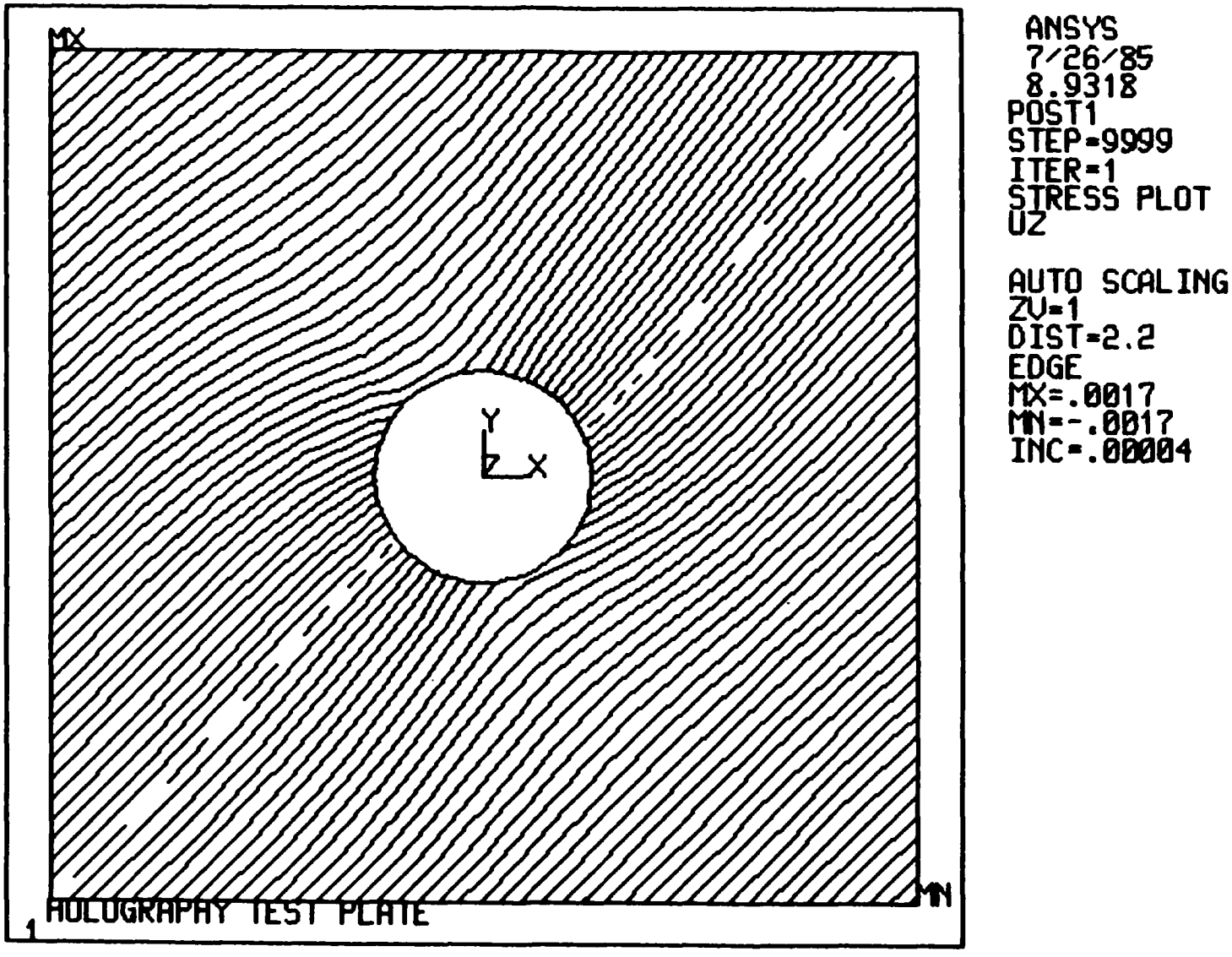

Figure 5-4. The Results of Figure 5-2 Plotted with Linear Fringes Arising from Rotation About a 45° Axis

readily, the object beam should be rotated about an axis which is oriented 45° from the line of the defect. In a structure containing defects of unknown orientation and location, a range of fringe orientations should be used.

Unfortunately, there seem to be some situations when a defect cannot be detected with any linear fringe configuration. The horizontal crack in Figure 5-1, statically loaded as discussed, seems to provide such a situation. The fringes in Figure 5-4, even though they are oriented 45° from the crack, do not reveal its location. Again, the tapered plug (pressure) loading shown in Appendix E, does visualize this crack. As suggested earlier, this implies that appropriate loading must be chosen for defects to show up. In practice, this should not prove difficult, since flaws usually will not develop in areas where the effect of the loads is small.

It is more difficult to specify which linear fringe frequency (i.e., object beam rotation) will best reveal a particular defect. The proper frequency, however, depends on the excitation of the flawed structure rather than on the nature of the flaws. A fringe frequency should be selected so that disturbances away from the defects are dominated by linear fringes, but the frequency should not be so great that the fringes at the flaws become completely linear themselves. As a practical matter, the object beam rotation should be increased gradually until the fringe frequency fits within this window.

Defect size is also critical to detection using the FLI technique. The crack that is revealed in Figure 5-2 is one inch long, and virtually the entire length can be located by the abrupt bends in the fringes. One end of the crack, however, intersects the hole and is, therefore, not constrained as greatly as the other end. The bends in the fringes, therefore, grow less distinct as one moves away from the hole. For a crack not intersecting a hole or a free boundary, therefore, detection may prove difficult if it is less than about 1/2 in. in length. This conjecture assumes, of course, that the crack is as deep or deeper than those investigated here. Since the numerical model used here was two-dimensional, an accurate study of sensitivity to depth was not possible, but three-dimensional finite elements analyses could be performed to determine just how deep a crack is detectable with FLI.

5.2 DYNAMIC LOADING CONSIDERATIONS

5.2.1 Analysis

Because different load configurations may be required to reveal all the defects in a structure, dynamic loading may provide an opportunity to excite observable disturbances in a variety of different flaws simultaneously. With this in mind, the configuration in Figure 5-1 was subjected to a modal analysis in ANSYS. Ten modes were examined, and fringe patterns for the first five modes are shown here in Figures 5-5 through 5-9. Linear fringes have been added in these figures, but because the amplitude of the modes is arbitrary, the beam rotation to which these fringes correspond cannot be specified. Modes two, three, and four (Figures 5-6 through 5-8) reveal clearly the crack emanating from the hole, but this defect is not readily detected in modes one and five (Figures 5-5 and 5-9). Again, this shows that different deformation modes can dramatically affect the amount of disturbance around a flaw. Indeed, in all the dynamic modes we investigated, we were unable to find a fringe pattern that successfully revealed the horizontal crack below the hole.

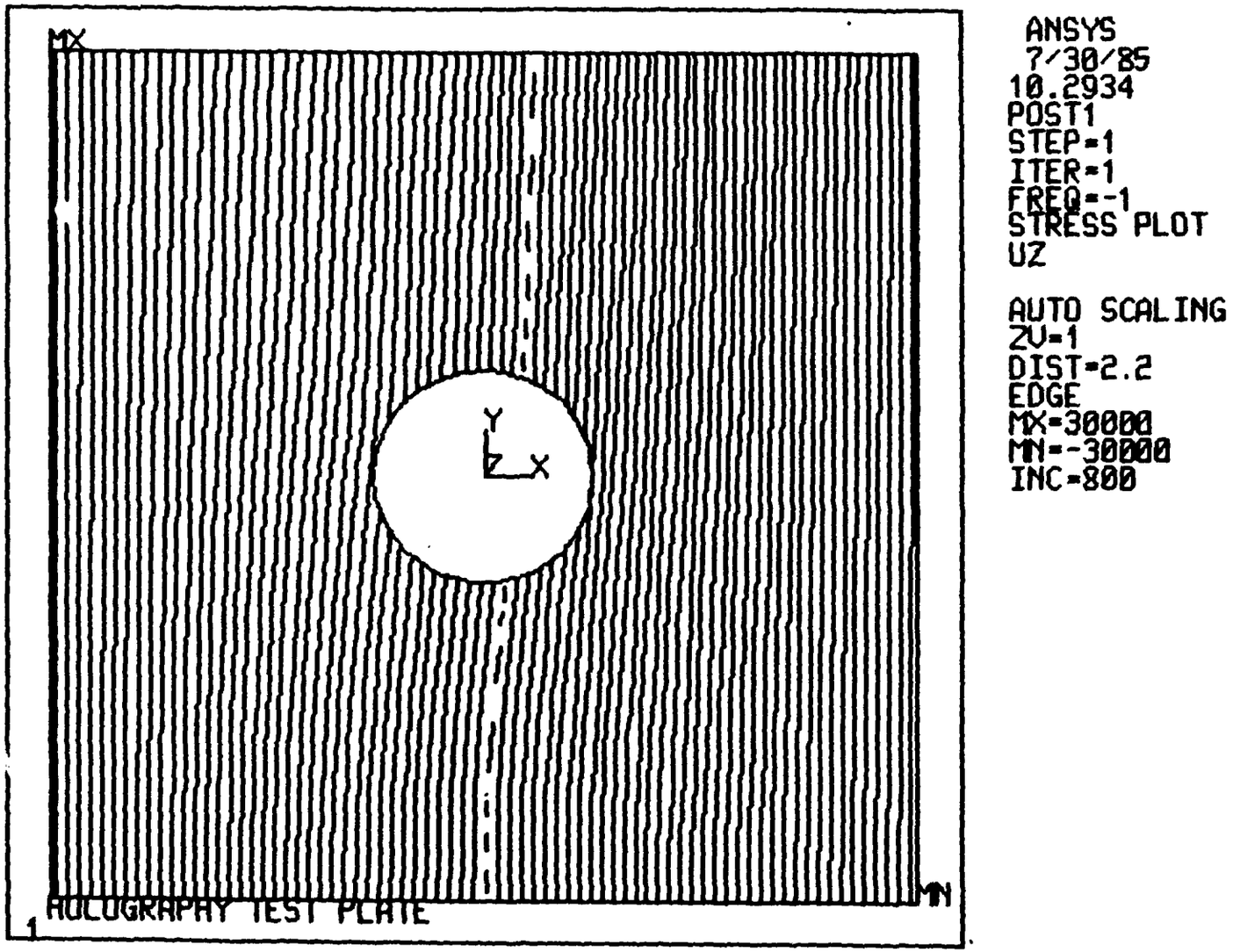

Figure 5-5. Mode One from a Dynamic Analysis of the Clamped Plate in Figure 5-1. Linear fringes have been added.

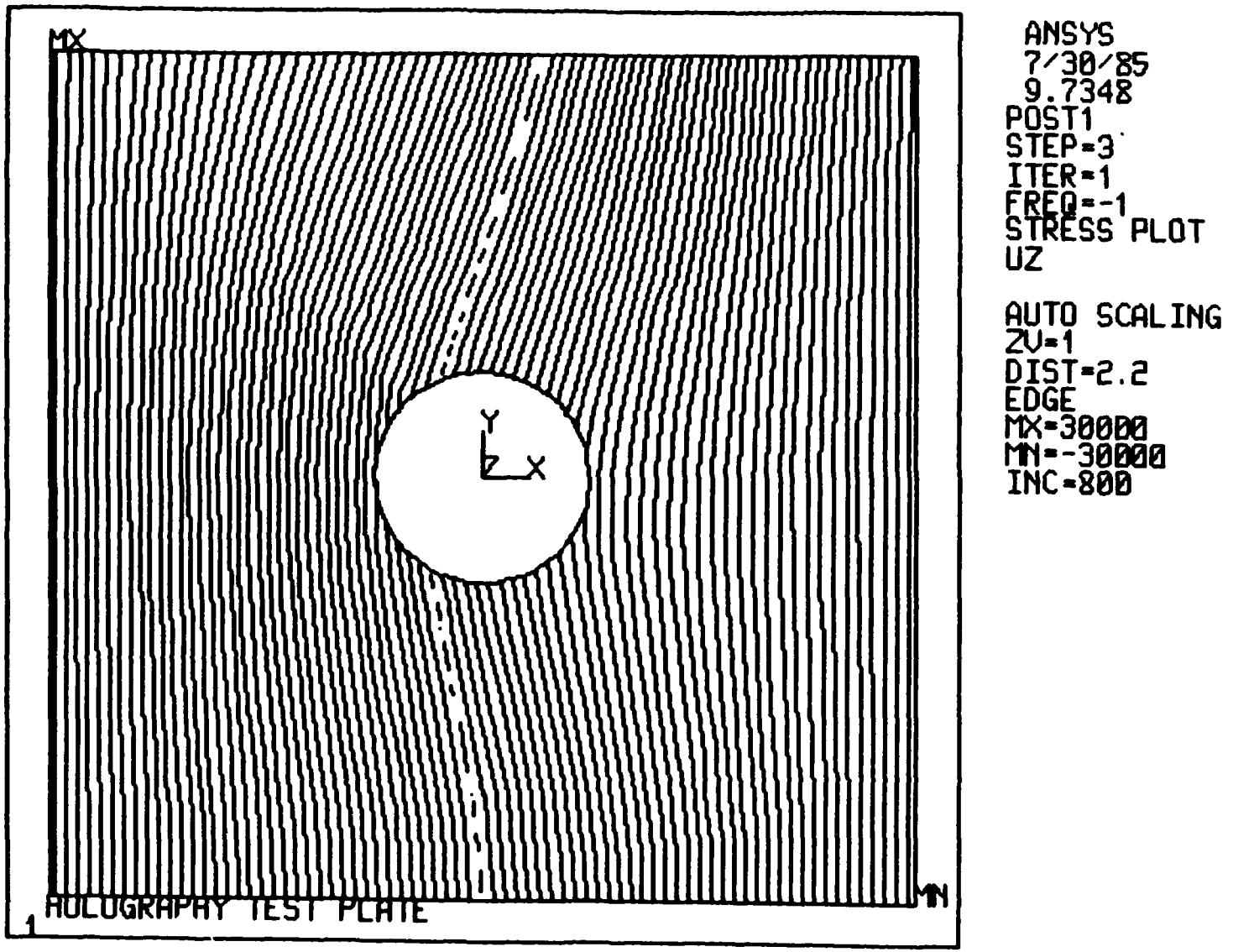

Figure 5-6. Mode Two from a Dynamic Analysis of the Clamped Plate in Figure 5-1. Linear fringes have been added.

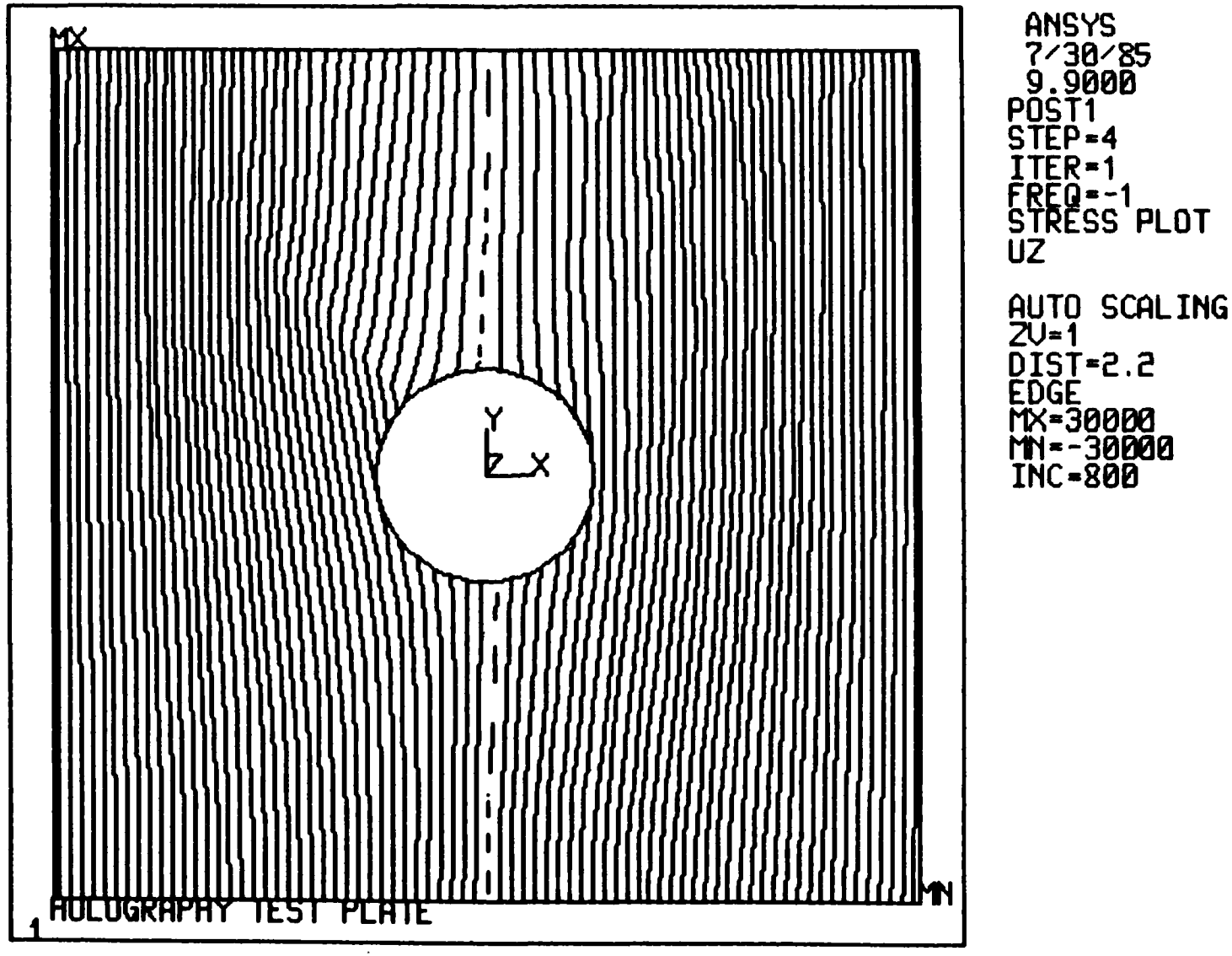

Figure 5-7. Mode Three from a Dynamic Analysis of the Clamped Plate in Figure 5-1. Linear fringes have been added.

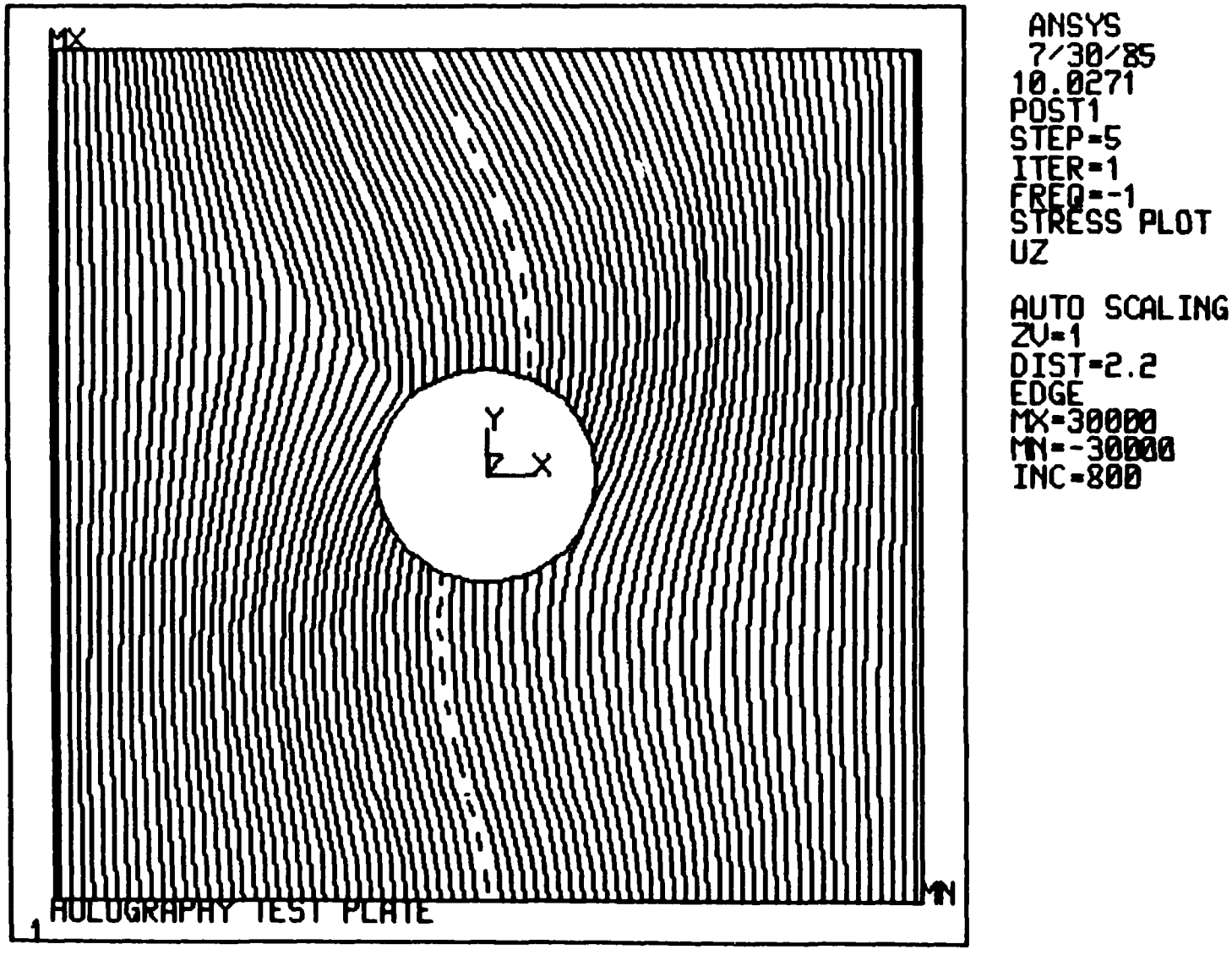

Figure 5-8. Mode Four from a Dynamic Analysis of the Clamped Plate in Figure 5-1. Linear fringes have been added.

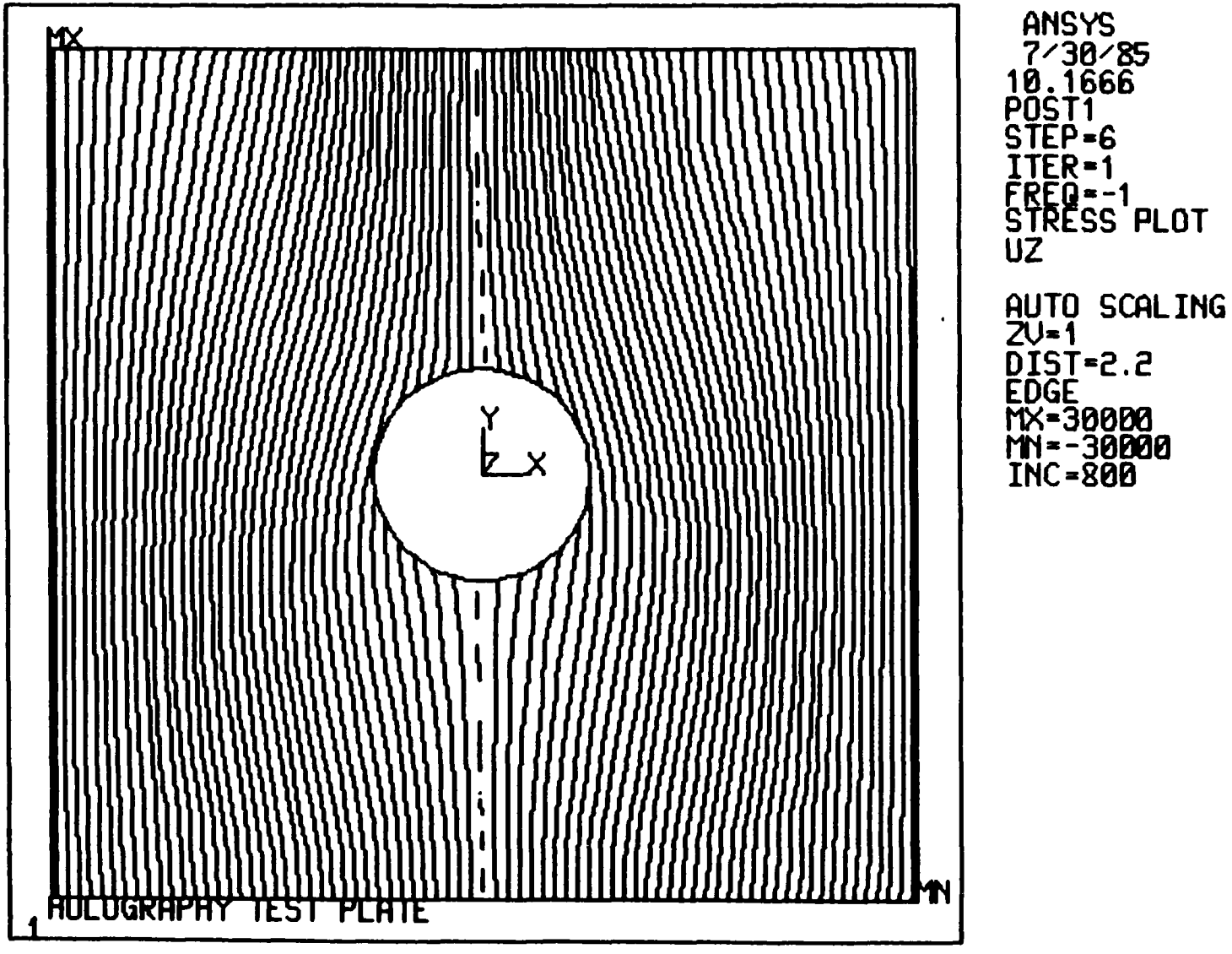

Figure 5-9. Mode Five from a Dynamic Analysis of the Clamped Plate in Figure 5-1. Linear fringes have been added.

Because the mode shapes seem to cover such a broad range of deformation behavior, we can only conclude that the horizontal crack is not the type of crack that would typically exist in this configuration.

The modal analyses also provided information on the natural frequencies of the cracked test plate. These are listed below.

Mode	Frequency (Hz)
1	1830
2	3000
3	4680
4	5470
5	5880

From this information, and on the basis of Figures 5-7 and 5-8, one might choose to excite the plate at 4680 or 5470 Hz to reveal most clearly defects like that emanating from the hole in Figure 5-1. Of course, impulse loading would create a superposition of many such modes.

Like the static analysis, therefore, the dynamic analysis provides a flexible and practical tool for assessing a corresponding flaw detection procedure based on the FLI technique. It is hoped that continued experimental work using dynamic loads will show good agreement with the results in Figures 5-5 through 5-9, corresponding to the favorable comparison between Figures 5-2 and 5-3.

5.2.2 Experimental Work

Experimentation with the pulsed laser system and dynamic loading at NADC was attempted early in the program but was discontinued during the second year due to unreliability of the data obtained because of the intermittent behavior of the ruby laser as described in the second annual report on this contrast issued in April 1984. Dynamic loading experiments on a small format were planned using the 200 mw Ag ion laser at Honeywell. However, this laser was still not operating at the conclusion of the program so this plan was also aborted.

5.3 LOAD DESENSITIZATION WITH MOIRE TECHNIQUES

During this contract we demonstrated that the FLI process can be made to work by moiring two double exposure holograms (Appendix C). This process desensitizes the system to the load when two colors are used because the moire difference frequency effectively appears as a laser of a longer wavelength. Since the moire FLI effect appears superimposed on the clutter produced in the moire process (the moire is one of sixteen terms contributing to the final image) a spatial filtering step would be needed to obtain a FLI result equivalent to those obtained by swinging the reference beam between exposures.

The two-color experiments were not done during this program because of the unavailability of the Ag ion laser at Honeywell.

5.4 FLI EXPERIMENTS TO FIND DEFECTS IN COMPOSITE MATERIALS

Static and thermal loading techniques were used in attempting to locate defects in specially prepared composite samples. One sample was supplied by the Air Force and the other was prepared by Arthur D. Little, Inc. The defects in the Arthur D. Little sample were induced by placing pieces of cellophane between the layers during the manufacturing of the material.

No fringe shifts were seen in any of the experiments, so the defects could not be located with these loading mechanisms. The literature search showed that pressure loading techniques were usually used to locate defects in laminated materials. Since pressure loading did not seem practical as a loading method for use on aircraft, it was not pursued further experimentally.

5.5 COMMENTS ON DEFECTS AND MODELING

5.5.1 Experimental Cracks Used in Study

The defects used in these experiments were through cuts and part-through cuts (from the back side of the specimen) emanating from holes in the center of metal plates. Fatigue cracks have characteristics that are different from these cuts and should be further investigated. The applicability of FLI for finding defects in composite materials and for testing the integrity of adhesive joints should also be investigated.

5.5.2 Real Cracks in Metals

Cracks often nucleate and grow in structural members during service as a result of cyclic loading and/or stress corrosion cracking. These cracks are generally closed when the structure is not loaded and have irregular and interpenetrating crack faces. Loading causes motion of the crack faces with respect to each other. In fracture mechanics, this motion is often divided into three mutually orthogonal directions denoted as Modes I, II, and III. Mode I refers to crack opening (separation of the faces) while Modes II and III refer to in-plane and transverse sliding of one crack face with respect to the other. Real cracks are likely to behave differently than the cuts used in the initial phase of the AFOSR study in that the localized deformation associated with Modes II and III will be resisted by friction on the crack faces unless it is accommodated by Mode I deformation separating the crack faces. Compressive stresses in the structure may keep the crack faces closed until some threshold tensile stress is applied to the crack region.

The applicability of FLI to fatigue cracks in metal components should be studied. For this purpose fatigue loading could be used to create cracks in specimens for experimental testing. These cracks could be made on computer controlled Instron Testing machine. Both through cracks and subsurface cracks emanating from a hole could be created using starter notches and fatigue loading. Similar specimens have been made by this technique in performing fatigue crack growth studies at Arthur D. Little, Inc.

The sensitivity of FLI to detection of through thickness fatigue cracks in terms of crack length and orientation and to rear surface fatigue cracks in terms of location size, depth and orientation should be determined. In particular we would test plates with corner cracks emanating from cylindrical holes, simulating the crack growth from fastener holes as illustrated in Figure 5-10.

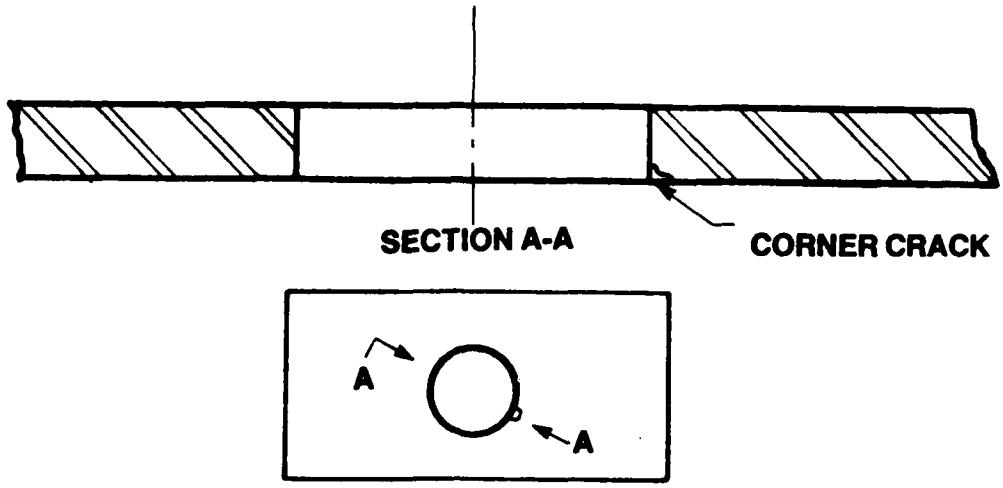

Figure 5-10. Schematic of Crack Growth from a Fastener Hole

In both cases of static loading and dynamic loading, it is of interest to predict the deformation increment between holographic exposures as a check on the FLI process, i.e., a comparison of predicted and observed deformation fields. Finite element calculations can be used for this purpose.

Arthur D. Little Inc. has performed two-dimensional analyses for through crack problems and developed adjusted two-dimensional models to approximate the behavior of specimens containing sub-surface cracks. The two-dimensional model is adjusted by the introduction of narrow elements filling in the crack and of smaller transverse thickness to represent the part-through crack geometry. As the test specimens become more complex, including representative structural components, and as the defects to be found become a geometrically smaller portion of the specimen, they would begin to perform separate analyses of the structure and of the defect region. For example, an analysis using plate elements for the specimen would be used to develop boundary conditions for a three-dimensional finite element analysis of the region containing the defect.

Arthur D. Little Inc. has been successful in using ANSYS to perform static and dynamic (steady state, forced oscillations) plate analyses in this program. Local three-dimensional analyses of regions containing surface cracks can be performed with the program APES-3D[1,2,3] which was developed specifically for three-dimensional crack problems.

5.5.3 Composites

High strength laminated fiber composites fail by different mechanisms than metals and are sensitive to different types of defects. The type of defect of concern for laminated fiber composites for which FLI may be applicable is delamination, a lack of adhesion over the interface

region between adjacent plies. Delamination may be the result of fabrication (ply build up) imperfections, or it may be caused by (compressive) overloads during service or in the form of impact damage. Delamination can significantly reduce compression strength of laminate composites. Various experimental conditions must be defined and evaluated to determine the applicability of FLI for NDE of composites.

Modeling of deformation and stress in lamina fibrous composites which will be required to predict FLI applicability is different from that in homogeneous materials. Models can be built at various levels of detail and the appropriate level depends on the output desired. Each layer should be treated as a homogeneous orthotropic material since we are not looking for fiber matrix interactions but rather for lamina scale effects. Lamina models treat the composite as made up of the loads applied to the composite and the layer properties. Finite element models for layered composites are available. Layered shell elements, based on the laminate theories, enable analysis of composite plates/shells of arbitrary geometry and with specified boundary conditions.

Arthur D. Little Inc. would use laminate theory and related finite element analysis techniques (available on the ANSYS code) to analyze composite test specimens including the load transfer to the specimen, the support condition for the specimen and the specimen geometry which may, for example, include a through hole.

Separate local modeling and analyses would be used to determine the deformation in the vicinity of a delamination defect. Approximate analysis procedures are available to obtain an estimate of out-of-plane deflection, ref. 4. These would be applied in the design of specimens and loading fixtures. A layered finite element model would be developed to accurately predict the out-of-plane deformation of the region in the specimen which contains the delamination and thereby simulate FLI results. The layered model would involve three-dimensional or thick plate orthotropic elements configured so as to model the debond region and the adjacent composite structures. Experiments on composites with dynamic loading techniques would be conducted.

5.5.4 Adhesive Joints

Adhesive joints, similar to laminar composites, are subject to debonding as a result of fabrication difficulties or service loading, (ref. 1, 5). Debonding in superscript adhesive joints under bending or axial loading result in transverse deformation (local separation of the members being joined). These defects should be observable with FLI. It would be of interest to determine if there is a region of debonding in an adhesive joint and, if so, to determine its size and location. This information is the basis for assessing the integrity of the joint.

Holographic FLI experiments would be defined to investigate the application of FLI to joined regions of laminated composites to assess adhesive joint integrity.

5.5.5 Three-dimensional Modeling Effort

The purpose of conducting a three-dimensional, finite-element analysis in the future is two-fold. The immediate purpose is to determine if sub-surface flaws of known shape, size, and location will produce surface displacements that are detectable using this holographic technique. The initial fringe spacing would establish the number of interference fringes associated with the calculated in-plane displacements. The initial fringe spacing can be varied in order to optimize the number of interference fringes associated with these flaws.

A secondary purpose of the three-dimensional finite element analysis is to reverse the process and determine the size, shape and location of flaws from the interference pattern. It is possible that size, shape and location cannot be uniquely determined from in-plane displacements. It may be necessary to assume the shape and calculate the size and location of the flaws. Moire techniques could be used in an experimental program to supplement this effort if more sensitivity is necessary.

SECTION 6
CONCLUSIONS

The FLI concept was experimentally demonstrated during this program and an analytical model was developed which gave excellent agreement with the experimental results. The model was two-dimensional so it is not capable of predicting crack depth. The fringe clutter noise was removed by choosing the frequency of the linear fringes to be high enough to dominate the clutter noise yet being low enough so that surfaces excursions due to the presence of a defect would still cause a fringe shift. The shifts on the fringes due to the defect were shown to have signature very different from those of the carrier alone, so that, potentially, automatic reading of the data is greatly simplified. It was also shown that Moire techniques could be used to desensitize the loading.

The sensitivity analysis showed that the defect is most observable when the FLI fringes cross the defect at an angle rather than being parallel or perpendicular to the defect. The experiments were limited to those utilizing static loading techniques due to various difficulties encountered with the higher power lasers at NADC and Honeywell. Therefore, the dynamic and two color moire experiments were not performed under this contract.

The static and plug (pressure) loading models were very accurate in locating cuts (cracks) emanating from a hole. These defects are quite realistic and approximate those anticipated in real structures. A modal analysis of a dynamic loading technique (impulse loading would be a superposition of such modes) also predicted that these cracks would be detectable.

Neither static or dynamic loading techniques were successful in locating a subsurface cut in the middle of the plate. Plug (pressure) loading made this defect visible but this would probably not be a practical loading method on a structure such as an airplane. SUCH DEFECTS IN REAL STRUCTURES WOULD BE HIGHLY UNLIKELY SO THIS NEGATIVE RESULT MAY ONLY BE OF ACADEMIC INTEREST.

Finally, two composite samples prepared with sub-surface defects were examined with both static and thermal loading being applied between the exposures. None of the defects were found with these loading techniques. The literature search showed that the few successes in holographic interferometry finding defects in laminate structures (debonds) were achieved with pressure loading methods. Dynamic and/or pressure loading methods were not attempted in our experiments due to the equipment limitations described in Section 4.

SECTION 7
RECOMMENDATIONS

The success of this program in demonstrating that sub-surface defects in metals can be modulated onto a spatial carrier such that the defect phase modulates the carrier under static loading conditions should be further pursued for applications of interest to the Air Force such as fatigue testing of aircraft.

FLI is potentially a large area inspection technique for defect location which is amenable to automatic readout. In any practical NDE application it will be necessary to utilize FLI with dynamic loading conditions and pulsed lasers to avoid overall mechanical motions between the hologram and the structure under evaluation. Therefore, we suggest that a basic study be performed to demonstrate that the FLI process is compatible with dynamic loading techniques for defect location over large areas.

> THE OBJECTIVE OF THIS STUDY WOULD BE TO DEMONSTRATE THAT HOLOGRAPHIC FLI WORKS WITH DYNAMIC LOADING FOR LARGE AREA DETECTION OF REALISTIC FLAWS IN METALS, DEBONDS IN COMPOSITES, AND ADHESIVE JOINTS.

The following classes of defects should be investigated:

- Realistic surface and sub-surface cracks
- Debonds in composite materials and adhesive joints
- Aircraft fastener defects

Based on the successful methodology demonstrated in this current contract a dual modeling/experimental parametric investigation should be followed to maximize the understanding of the dynamic loading problem.

Specifically, this effort should consist of:

1. Model development for FLI with (a) dynamic loading, (b) realistic defects in three-dimensional metallic structures, and (c) debonds in composite materials and adhesive joints.
2. An experimental demonstration of the feasibility of dynamically loaded FLI for detecting flaws in metal and in composite samples.
3. A comparison of the model results with experimental results and a determination of the sensitivity limitations of dynamic FLI in various types of three-dimensional materials.
4. A measurement of defects in structures of interest to the Air Force with the FLI technique.

The program should entail basic investigations concerning defects in both metal and composite materials including model development for various loading configurations and use of FLI to experimentally demonstrate the feasibility of locating/identifying the defects. The different

combinations of materials, defects, model geometry and loading types which should be investigated are shown in Figure 1-1. The results of this research should show the viability for developing a holographic FLI hardware/software system for use in the important NDE applications of testing military aircraft. Implementation of a practical testing program could extend the lifetime of military aircraft and thereby result in significant cost savings to the U.S. government.

SECTION 8
REFERENCES

1. Hilton, P.D., Kiefer, B.V., "The Enriched Element for Finite Element Analysis of Three-Dimensional Elastic Crack Problems," Journal of Pressure Vessel Technology, Vol. 102, November 1980, pp. 347-352.

2. Hilton, P.D., Peirce, D.C., "APES3D-Revision 1.0 Documentation and Theoretical Manual, report to David Taylor Naval Ship R&D Center, Bethesda, Maryland, contract N00167-81-C0260, January 1983.

3. Hilton, P.D., Peirce, D.C., "The Enriched Element Formulation for 3-D Combined Mode Elastic Crack Problems," presented at the 1984 Pressure Vessel and Piping Conference and Exhibition, San Antonio, Texas, June 17-21, 1984, The American Society of Mechanical Engineers, PVP, Vol, 85, 1984, pp. 65-76.

4. Whitcomb, J.D., "Approximate Analysis of Postbuckled Through Thickness Delaminations," Composite Technology Review, Vol. 4 No. 3, Fall 1982, pp. 71-77.

5. Hilton, P.D., Gupta, G.D., "Stress and Fracture Analysis of Adhesive Joints," presented at the Design Engineering Conference & Show, Philadelphia, PA, april 9-12, 1973, The American Society of Mechanical Engineers, 1983.

APPENDIX A

Holographic Fringe Linearization Interferometry (FLI) for Defect Detection
Part I
The Basic Concept

by

G.O. Reynolds, D.A. Servaes, L. Ramos-Izquierdo
Honeywell Electro-Optics Division
110 Fordham Road, Wilmington, Massachusetts 01887

and

J.B. DeVelis
Merrimack College, North Andover, Massachusetts 01860
Currently on sabbatical at Tufts University, Medford, Massachusetts 02153

Reprinted from: SPIE Vol. 523, p. 160, Applications of Holography (1985)

Reprinted from SPIE Vol 523 Applications of Holography

Holographic Fringe Linearization Interferometry (FLI) for defect detection

Part I
The basic concept

G.O. Reynolds, D.A. Servaes, L. Ramos-Izquierdo
Honeywell Electro-Optics Division
110 Fordham Road, Wilmington, Massachusetts 01887

and

J.B. DeVelis
Merrimack College, North Andover, MA
Current on sabbatical at Tufts University, Medford, MA

Abstract

In normal double exposure holography with impulse loading it is very difficult to locate defects because the fringe clutter, due to random motion between exposures, often swamps the fringe shifts caused by the presence of sub-surface defects (cracks, debonds, etc.).

We attempted to simplify the defect location problem by developing a concept more amenable to automatic readout techniques. Our approach to incorporate this change is quite simple. We swing the object beam between the two exposures which adds a linear fringe to the reconstructed image. Proper selection of the fringe frequency (angle of object beam swing) and the loading force creates a reconstructed image laced with linear fringes with fringe shifts at the defect locations which are highly visible.

We will describe the theory of the process. Experiments performed with a static load illustrate that the defect is seen as fringe shifts on a linear carrier. Both through cuts and rear surface cuts in a metal test plate were used to simulate defects. We further show that the defects have characteristic Fourier signatures different from those of the carrier.

1. Introduction

"Double Exposure Holographic Interferometry" has been successfully demonstrated in a number of applications including nondestructive testing and metrology.[1,2,3,4] This technique holds promise for many Non-Destructive Evaluation (NDE) applications. However, it has been limited in reaching its full potential due to the inability to interpret the complicated interference patterns which result from the test specimen being in different mechanical and/or thermal states at the time of the two exposures.

In this paper, we show that the complicated interference pattern resulting from double-exposure holography can be reduced to a simple linear fringe pattern using Fringe Linearization Interferometry (FLI), a modification of conventional double-exposure holographic interferometry. Furthermore, fringe shifts on the resulting linear fringe pattern clearly indicates the location of through cuts and sub-surface cuts in test plates under static loading conditions.

The fringe shifts at the site of the defects (cracks and sub-surface cracks) in the Holographic FLI method have characteristic Fourier signatures that are amenable to automatic readout techniques for defect location. This is experimentally demonstrated in a Fourier diffractometer where the interference effects at the site of defects using Holographic FLI have demonstrably different diffraction patterns (Fourier signatures) from those in the linear fringe region where no defects are present.

2. Objective of Holographic FLI

The objective of Holographic FLI is to replace the complicated interference pattern resulting from conventional double exposure holographic interferometry by a simple linear fringe pattern. Holographic FLI is potentially capable of detecting and locating defects in inspection applications involving large areas.

In the FLI technique, linear fringes are introduced in the formation step of double exposure holographic interferometry by utilizing a beam deflector in the object beam between the two holographic exposures. The addition of the linear fringes to the interferogram makes the pattern much easier to interpret. A distinctive signature (fringe shift) at the site of a defect is maintained while the clutter pattern is reduced to a field of linear fringes.

In Figure 1a we have a typical cluttered fringe pattern resulting from double exposure holographic interferometric testing of a panel. The stress corrosion cracking is indicated and highlighted by the fringe shifts in the boxed-in areas. It is apparent that locating the desired fringe shift information within the complicated fringe pattern is quite difficult.

In Figure 1b we show another, less complicated, fringe pattern. This pattern resulted from a double exposure hologram of an aluminum can stressed with an elastic band. Between exposures the elastic band was cut causing a large local deformation at the position of the elastic.

In Figure 1c, we see the effect of adding the linear fringe pattern by tilting the object beam between exposures of the two holograms. We see that the complicated fringe pattern in Figure 1b has been simplified to the linear fringe pattern of Figure 1c with a phase shift at the region of the elastic band where the differential force was applied. The fringes are not quite linear but rather more quad ratio in nature because of the curvature of the object. A higher frequency linear fringe is needed to linearize three quadratic fringes.

It is the simplification of this interference pattern which forms the basis for the holographic FLI concept.

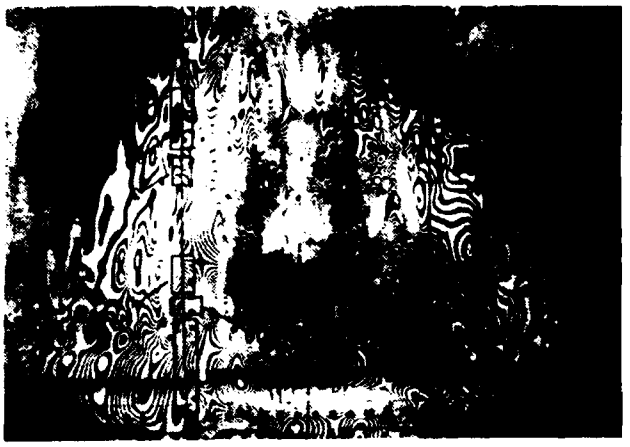

Figure 1a. Complicated fringe pattern on a 48 by 25 inch panel using the double pulsed holographic NDT technique. An impulse loading technique was utilized. The areas of stress corrosion cracking are indicated by fringe shifts in the boxed-in areas (from Ref. 4).

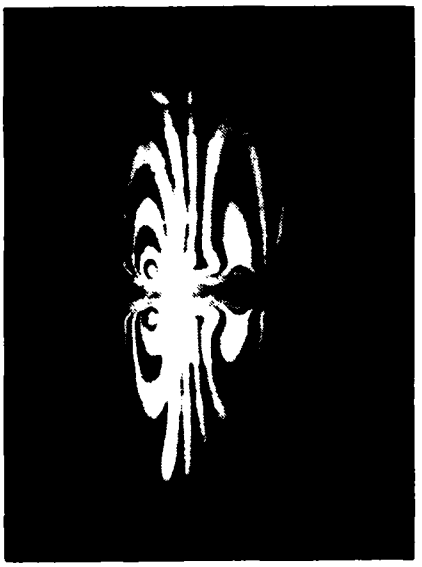

Figure 1b. HI of Coke Can Stressed with Elastic Band

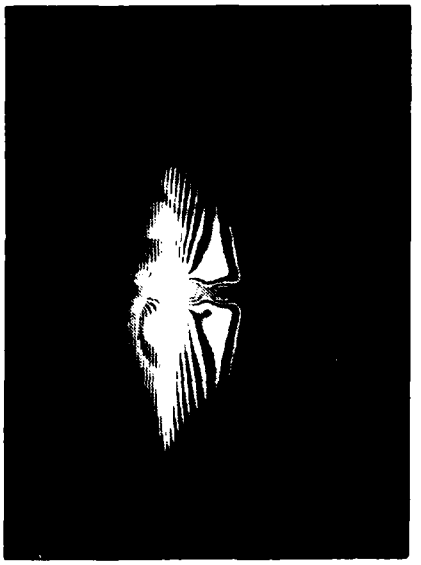

Figure 1c. FLI version of Figure 1b

Figure 1. Double Exposure Holographic Interferograms

3. Basic theory of Holographic FLI

3.1 Objective beam shifting to create linear fringes

The principle of shifting the object wave between exposures in double exposure holographic interferometry to create linear cosine fringes in the reconstructed interferogram has been illustrated in the literature.[6] The fringes have a period, $\lambda/\delta\theta$, where $\delta\theta$ is the amount of angular shift between the object beams and λ is the wavelength of the laser light. An analysis utilizing Fourier transform holography and a finite-sized object is given here to illustrate the principle of FLI.

3.2 Fourier transform Holographic FLI analysis

The Fourier transform configuration (Figure 2) will be analyzed for simplicity. An analysis for sideband Fresnel Holographic FLI appears in the Appendix. Fourier transform holograms reconstruct by performing Fourier transforms, rather than the more complicated procedure of focusing Fresnel transforms, which is necessary for sideband Fresnel holograms.

In the FLI process the first hologram is made when the object is in state #1. Between exposures the object beam is moved through an angle, $\delta\theta$, and the load on the object is changed to create state #2 of the object. A second exposure on the same film is made of the object in state #2. The reference beam is identical for both holograms. Upon reconstruction, the holographic images from the two exposures combine coherently and the phase difference describing the two different states of the object forms an interference pattern (laced with linear fringes) superimposed upon the image of the object. By controlling the frequency of the linear fringes, it is possible to remove the fringe shifts associated with small displacements (clutter) and keep the information concerning the larger displacements (defects) as a phase shift on the linear fringes (Figure 1c). We will now describe this process mathematically using the Fourier transform hologram recording process illustrated schematically in Figure 2.

The irradiance in the hologram plane of Figure 2 for the first exposure is

$$H(x) = | e^{ikx \sin(\xi_0/f)} + \tilde{f}(x,t) |^2, \tag{1}$$

where ~ denotes a Fourier transform and f(x,t) represents the surface deformations on the complex test object at time t.

If a prism of angle $\delta\theta$ is used to shift the direction of the object wave and another hologram is recorded on the same recording medium (note: in double exposure holographic interferometry, a different state of the dynamic object, $f(x,t_1)$, is usually captured on the hologram), the irradiance of the second hologram is:

$$H(x) = | e^{ikx \sin(\xi_0/f)} + \tilde{f}(x-x_{\xi_0},t_1)|^2. \tag{2}$$

where from the shift theorem of Fourier analysis

$$X_{\xi_0} = f \tan(\delta\theta) \tag{2a}$$

Reconstruction of the two holograms described in Equations 1 and 2 with a lens of focal length f results in a reconstructed image centered at the position $x' = \xi_0$ of the reconstructed image plane given by

$$I(x) = \text{image} = | f(x',t) + f(x',t_1)\, e^{ikx_0x'/f}|^2 \tag{3}$$

We will now investigate the implications of Equation (3) for various conditions of interest.

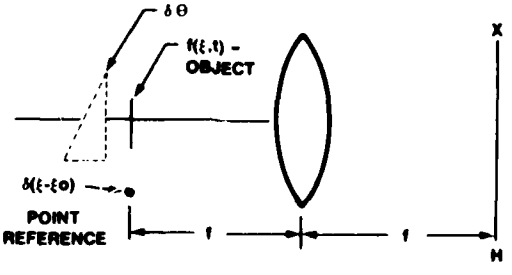

Figure 2. Schematic of Fourier transform hologram system for double exposure interferometry using a lens of focal length, f.

Case 1: linear fringes

$$\text{If } f(x',t) = f(x',t_1), \text{ then}$$

$$I(x') = [f(x',t)]^2 \, |1 + e^{ikx_0x'/f}|^2$$

$$= [f(x',t)]^2 [2 + 2\cos(kx_0x'/f)], \tag{4}$$

i.e., the image of the object is laced with "linear" cosine fringes of frequency

$$\upsilon = \tan \frac{\delta\theta}{\lambda}$$

Case 2: Response of the Defect

To extend this analysis to include the response of a defect, assume that the defect of interest causes a differential surface displacement, $\Delta\phi(x'')$ at the position of the defect when loaded between the two exposures. This displacement behaves as an optical phase function in the hologram. A simplified analysis would assume

$$f(x',t) = 1,$$

and

$$f(x',t_1) = e^{ik\Delta\phi(x'')} \text{ in Equation 3.}$$

The revised image of Equation 4 would be

$$I(x') = \text{ideal image} = (2 + 2\cos[k\,x_0x'/f + k\Delta\phi(x'')]). \tag{5}$$

where x'' denotes the position of the defect in the x' coordinate system.

The surface displacement differential appears as a phase modulation of the linear fringes and has a shape, size and location, $\Delta\phi(x'')$, characteristic of the defect. We call this the ideal image because of the simplifying assumptions used in deriving Equation 5.

Case 3: Response of the defect and random surface displacements (clutter noise).

In any situation where the object surface undergoes a differential loading between the two exposures $f(x',t_1)$ in Equation 3 would be

$$f(x',t_1) = f(x',t)\, e^{ik[\Delta\phi(x'') + \Delta\psi(x')]}, \tag{6}$$

where $\Delta\phi(x'')$ is the differential surface displacement due to the defect at the position of the defect, x'',

and $\Delta\psi(x')$ is the differential surface displacement of the remainder of the test object.

Use of Equation 6 in Equation 4 yields

$$I(x) = |f(x',t)|^2 \left[2 + 2\cos\left(\frac{kx_0x'}{f} + k[\Delta\phi(x'') + \Delta\psi(x')]\right)\right], \tag{7}$$

where $|f(x',t)|^2$ is the normal holographic image of the object at time t.

Equation 7 shows that in general a complex fringe pattern is superimposed upon the object.

If we assume that

$$\frac{x_o x'}{f} \quad > \Delta\psi(x'), \tag{8a}$$

and

$$\frac{x_o x'}{f} \quad < \Delta\phi(x'') \quad > > \Delta\psi(x'), \tag{8b}$$

then, Equation 7 becomes

$$I(x') = |f(x',t)|^2 \left[2 + 2\cos\left\{\frac{k x_o x'}{f} + k\,\Delta\phi(x'')\right\}\right] \quad . \tag{9}$$

Equation 9 shows that under the assumptions given in Equations 8a and 8b, the interferometric image is laced with linear fringes with fringe shifts at the locations of the defects.

The result in Equation 7 illustrates that the normal fringe pattern of holographic interferometry is phase-modulated onto the cosine carrier, which is created by shifting the object wave between the exposures. Therefore, we see that the basis of Holographic FLI is to create linear fringes in two-exposure holographic interferometry by shifting the object beam between exposures of the two holograms and to control either the loading and/or the fringe frequency to ensure that the assumptions given in Equation 8 are experimentally realizable. This approximation is nearly realized in Figure 1c where the loading was extremely localized and very large.

3.3 Fringe localization with Holographic FLI

The issue of fringe localization in holographic interferometry has been thoroughly investigated.[1] The linear fringes resulting from tilting the object beam between exposures in Holographic FLI appear to be localized in the space on and about the object. These fringes can be made to appear in front of or behind the reconstructed object or actually on the object surface. In the research presented in this paper the latter situation is most desirable. A thorough mathematic analysis[1] shows that fringe localization depends upon the geometry of the holographic recording and viewing systems.

In holographic interferometry, the fringe localization depends upon the curvature of the object illumination wavefront at the object surface. The curvature of the reference beam is unimportant as long as it is equivalent to the curvature of the reconstruction wave. To guarantee that the linear fringes in Holographic FLI will be localized on the surface of the reconstructed object, we utilize collimated object illumination in forming the holograms. The actual experimental holographic recording arrangement used in the experiments is shown in Figure 3.

4. Understanding FLI/vector addition of phases

4.1 Experiment demonstrating the vector addition of phases

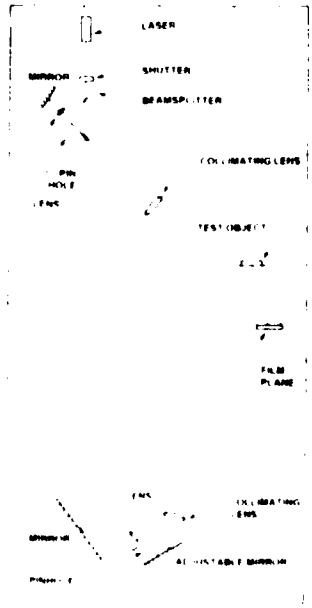

Figure 3. Experimental arrangement for Holographic FLI experiments showing collimated object illumination for obtaining fringe localization on the surface of the reconstructed image

The fundamental concept for the proper understanding of why the Holographic FLI process works is that of the Vector Addition of Phases in the holographic process, as shown in Equation 7. The phase of the linear fringes resulting from tilting the object beam between exposures of a double exposure hologram adds vectorially to the phase due to the surface deformation contours caused by differentially loading the object. The system, shown schematically in Figure 3, was used to demonstrate the vector addition principle for two-exposure holography. In Figure 4 we show the results for the case of an object tilt about one axis and a beam rotation about the other axis.

Figure 4a shows the linear fringes present in the reconstructed image of a double exposure hologram arising from tipping the test plate about the x-axis between exposures. Figure 4b shows linear fringes resulting from rotating the object beam about the y-axis between exposures. Figure 4c shows the linear fringes arising from the vector addition of the phases resulting from tilting the test plate as in Figure 4a and rotating the object beam as in Figure 4b between exposures. The resulting fringes in Figure 4c are rotated through an angle. The horizontal and vertical phases have been added vectorially to produce the rotated linear fringe pattern. Figure 4c also shows that the higher frequency x-axis phase due to tilting the test plate dominated the y-axis phase from a small rotation of the object beam rotation when the two are vectorially added in the two-exposure hologram.

To demonstrate that is the vector addition of phases which has occurred in the experiments shown in Figure 4, we examine the Fourier spectrum of each of the reconstructed images of Figure 4. In Figure 5 we show the spectra. Figure 5a is the Fourier Transform of Figure 4a; Figure 5b is the Fourier Transform of Figure 4b; Figure 5c is the Fourier Transform of Figure 4c. The higher diffraction orders are due to film nonlinearities.

If we now record and superimpose the position of the first harmonic along the y-axis of Figure 5a (see arrow in Figure 5a) with the first harmonic along the x-axis of Figure 5b (see arrow in Figure 5b) with the first harmonic in the x-y plane of Figure 5c (see arrow in Figure 5c), we obtain the result shown in Figure 6. Clearly, the first harmonic of Figure 5a has added vectorially to the first harmonic of Figure 5b to give the resultant first harmonic of Figure 5c. This series of experiments clearly demonstrates that the Holographic FLI process does indeed produce a vector addition of the phases which leads to the desired linear fringe pattern in the reconstructed image.

4.2 The basic Holographic FLI process

The experimental procedure for the Holographic FLI process is described as follows:

- Form a conventional hologram with the test specimen in a given stress state.
- Add an additional loading to the test fixture to change the stress state of the specimen.
- Tilt the object beam and keep the reference beam fixed.
- Form the second hologram on the same recording medium with a second exposure.
- Process and reconstruct the double exposure hologram.

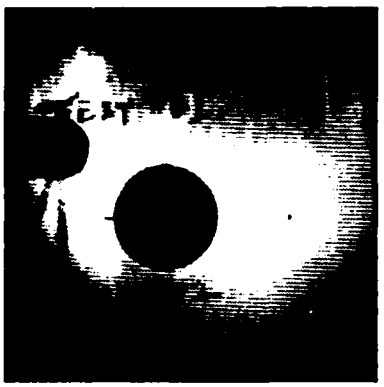

Figure 4a. Reconstructed image of double exposure hologram resulting from tipping the test plate about the x-axis between exposures

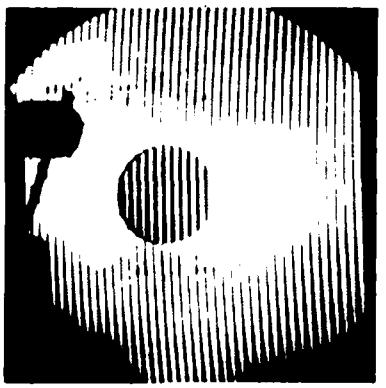

Figure 4b. Reconstructed image of double exposure hologram resulting from rotating the object beam about the y-axis between exposures

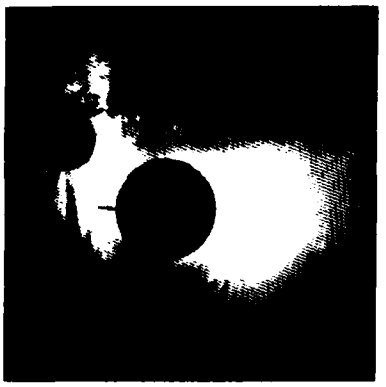

Figure 4c. Reconstructed image of double exposure hologram resulting from rotating the object beam about the y-axis and tipping the test plate about the x-axis between exposures

Figure 4. Experimental demonstration of the vector addition of linear fringes in double exposure holography

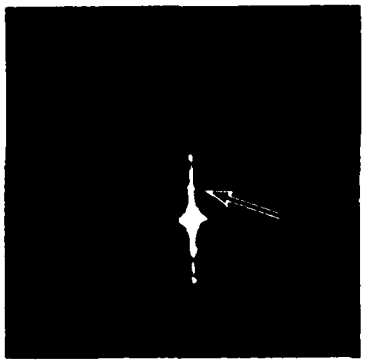

Figure 5a. Fourier spectrum of the reconstructed image of Figure 4a showing the delta functions along the y-axis

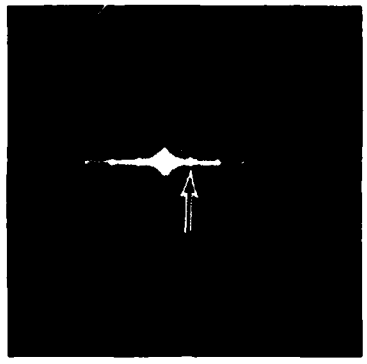

Figure 5b. Fourier spectrum of the reconstructed image of Figure 4b showing the delta functions along the x-axis

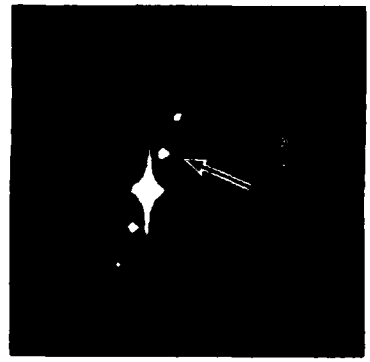

Figure 5c. Fourier spectrum of the reconstructed image of Figure 4c showing the delta functions in the (x-y) plane

Figure 5. Fourier spectra of the reconstructed images of Figures 4a, 4b and 4c

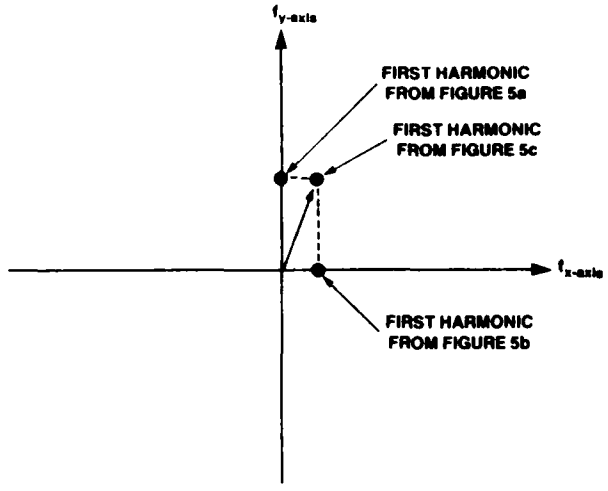

Figure 6. Fourier plane indicating the superposition of the first harmonics of Figure 5a, 5b and 5c demonstrating the vector addition of phases

As shown in Equation 7, the resulting reconstructed holographic interferogram has cosine fringes of the form:

$$\text{Fringes} \sim \cos\,[wx' + \Delta(x', y')] \tag{10}$$

where $(\omega x') = kx_s x'$ represents the phase of the linear fringe obtained from tilting the object beam between exposures of the two holograms and $\Delta(x',y') = k\,\Delta\phi(x'',y'') + \Delta x(x',y')$ represents the phase term describing the difference in the out-of-phase surface deformations resulting from the loading force added prior to forming the second hologram. Equation 10 is referred to as the FLI equation.

4.3 Interpretation of vector fringe addition leading to the loading limitation

Interpreting the experimental results demonstrated in Figure 5 in terms of the basic interference equation of two-exposure FLI holography, Equation 10, led to the following conclusion:

If the out-of-plane deformation of the test plate due to differential loading between exposures that yields the $\Delta(x',y')$ phase term in Equation 10 is greater than one-quarter wavelength per linear fringe period given by the $\omega x'$ term in Equation 10, then the vector addition of fringes would lead to the $\Delta(x',y')$ term dominating the linear fringe term in Equation 10. This would result in the linear fringe term being swamped by the fringes due to any differential loading, rendering the FLI concept ineffective.

This constraint can be overcome in two ways: (1) fixing the fringe frequency and desensitizing the effect of the deformation by using Holographic moire techniques as described in part 3 of the series of papers[6], or (2) increasing the fringe frequency ω so that the spatial period is smaller than the distance over which the deformation changes by $\lambda/4$.

Thus, the two-phase terms in Equation 10 can be controlled such that either term can predominate the other. In fact, in Figures 1b and 1c we have shown a case where the linear fringe term has been controlled so that it is larger than the phase term due to the deformation $\Delta(x',y')$ but not the phase of the defect $\Delta(x''y'')$. This effect was achieved by increasing the linear fringe frequency until it dominated the vector addition.

This same effect of linear fringe demonstration could have been accomplished by controlling the differential loading force (giving rise to the $\Delta(x',y')$ phase term in Equation 10) to ensure that the resulting deformations are less than one-quarter wavelength per linear fringe period. This is a very severe experimental restriction on the differential loading configuration and is very difficult to implement. We demonstrate that the differential loading phase term, $\Delta(x',y')$, can be made to dominate the linear fringe phase term, $\omega x'$, by examining the experimental results shown in Figure 7. In Figure 7 we show the linear fringes which have been introduced by shifting the object beam. They have been completely dominated by the random fringe pattern resulting from the differential loading. In this case the load was applied by two thumb screws mounted on the back side of the test plate. The linear fringes can be seen by using moire holography as described in part III of this paper.[6]

It is apparent from these results that if Holographic FLI is to be feasible and viable, we must control the linear fringe phase term, $\omega x'$, so that it dominates the phase term, $\Delta(x',y')$ resulting from the differential loading. Experimentally, this task was accomplished by increasing the fringe frequency until the $\omega x'$ phase term dominates the $\Delta(x',y')$ phase term resulting from the differential loading. Obviously, if the defect is to be found as a shift of the linear fringes at the defect site then its out of plane displacement must be greater than $\lambda/4$ per linear fringe period as described in Equation 8b.

Figure 7. The addition of a large differential load, $\Delta(x,y)$ leads to random fringes which dominate the linear fringes.

5. Experimental demonstration of Holographic FLI

5.1 Test specimen

The test specimen (Figure 8a) designed for the FLI experiments is a 100 mm x 100 mm x 3.125 mm (4 in. x 4 in. x 0.125 in.) aluminum plate which has a circular hole located at its center. The diameter of the hole is 24.94 mm (0.9976 in.).

A through cut on one plate and a rear surface partial cut on another plate (Figure 8a) originating at the hole were used as the defects. Both cuts were approximately one inch in length.

5.2 Loading mechanism and test fixture

A loading mechanism was designed to give maximum out of plane displacement of the test specimen (Figure 8b) at the location of the cut defect to give a distinctive holographic signature.

In Figure 8c we show a photograph of the entire test mechanism including the fixture and the test plate loading arm. The loading arm is on the back side of the test plate. The mathematical modeling of the experiment was conducted at Arthur D. Little, Inc.* The model and its experimental verification which are in excellent agreement are described in Part II of this paper, "Comparison of Observation with Prediction".[7]

5.3 Effect of increasing linear fringe frequency in two-exposure FLI

Interpretation of FLI basic equation for increasing linear fringe frequency

The Vector Addition of Phases restricts the loading term $\Delta(x',y')$ in Equation 10, to phases not greater than one-quarter wavelength per linear fringe cycle so that the resulting vector addition of the $(\omega x')$ linear fringe term does not become dominated by the $\Delta(x',y')$ phase term. As previously indicated, this limit can be achieved by carefully controlling the loading forces so that the differential out-of-plane deformations are small or by increasing the linear fringe frequency until it dominates the $\Delta(x',y')$ phase term in the vector addition of phases. This latter method was selected because it satisfies the quarter wave loading constraint, is easy to implement experimentally, and desensitizes the system. In fact, it should be possible to increase the linear fringe frequency to the point where it dominates the $\Delta(x',y')$ phase term for a large loading torque and still show a fringe shift at the location of the crack defect; therefore, two-exposure FLI should be feasible for many practical loading conditions.

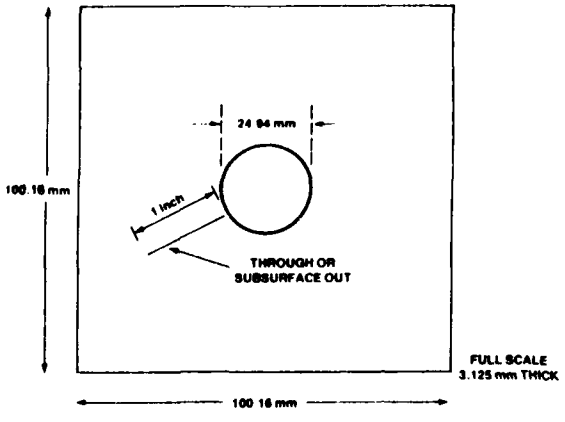

Figure 8a. Aluminum test specimen geometry

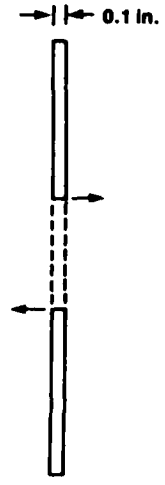

Figure 8b. Force loading used to model hanging weight loading mechanism

*This work was conducted by P.P. Hilton, R.A. Mayville, and D.C. Peirce

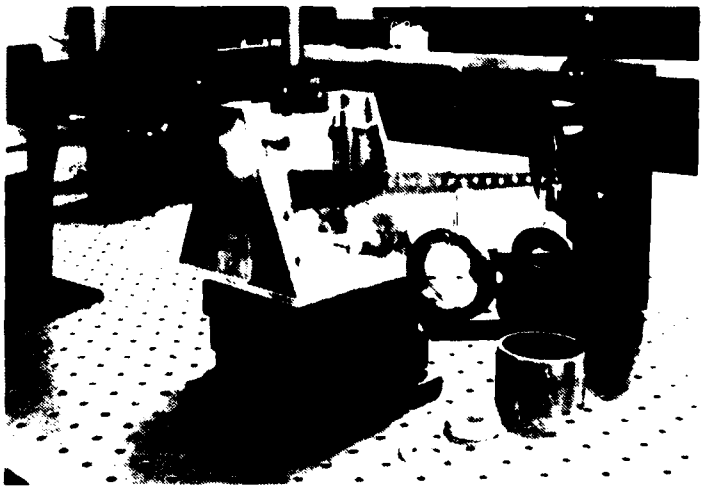

Figure 8c. Photograph of testing set-up showing test specimen and loading mechanism

The ultimate limitation for the frequency of the linear fringes will be determined by the speckle noise in the optical system viewing the hologram. If this limitation yields a non-linear fringe then further desensitization can be achieved by utilizing the more complex two-color, four-exposure moire technique,[6] which requires a photograph of the holographic image and a spatial filtering step applied to the hologram to create the linear fringes showing the defect location.

5.4 Experimental demonstration of FLI for through cuts

A two-exposure FLI experiment was designed and performed on the test plate of Figure 8a with a through cut to demonstrate the FLI technique. A two-exposure hologram was made and reconstructed. The first exposure was for the relaxed state of the test plate and the second exposure was for the stressed state of the test plate, and with a linear fringe. The first hologram (Figure 9a) shows the deformation from the stress. Figures 9b-e show the reconstructed image from the double exposure hologram, where, in addition to the stress in state two, linear fringes of varying frequency have been added.

Figure 9b shows the result when the linear fringe frequency is low, $\omega = 0.5$ cycle/mm. The constraint of one-quarter wave of deformation per fringe cycle has not been met, although the discontinuity at the cut is very visible. Figure 9c is the result for a fringe frequency of 2ω, and 9d is for 4ω. Figure 9e illustrates the case for a frequency of 8ω. In the 8ω case, speckle effects lowered the fringe contrast so the fringes could not be seen. The effect of 8ω was achieved by reducing the load by one half and adding fringes at a frequency of 4ω. The fringe shift at the defect is visible at the higher frequencies.

Obviously, with a linear fringe of frequency $\omega \sim 4$ c/mm (Figure 9e) the differential surface deformation meets the quarter wave/period limitation except in the vicinity of the cut where a violent phase deviation is evident. This was the first demonstration of the FLI principle.

5.5 FLI Experiments with specimens having rear-surface cuts

Since the cut in Figure 9a and 9b is easily visible, a more dramatic demonstration of the FLI principle was made using rear-surface cuts penetrating part way through the plate. A similar test plate to the one used for the through cut was made. A 1/16 inch wide saw cut, 3/32 inch deep was made on the back side of the test plate. The cut is 1 inch long, starts at the center hole and is at an angle -45° to the vertical axis. A double exposure hologram of the plate was made by adding a differential load between the exposures. The process was repeated and linear fringes were added by rotating the illuminating beam between the exposures. The results are shown in Figure 10a and 10b. Figure 10a is the usual interferogram obtained from double exposure holographic interferometry. By carefully examining the photograph the slight bend of the contour fringes can be detected, but the effect is subtle. Figure 10b shows the interferogram obtained for the same plate stress, but with the linear fringes added. The defect area is quite apparent. Since the cut itself is not visible on the surface of the plate, this experiment demonstrates the feasibility of the two-exposure holographic FLI technique for detecting subsurface flaws and defects.

These experiments have been modeled using finite element analysis and agreement between the model and the experiment is excellent as described in Part II of this paper.[7]

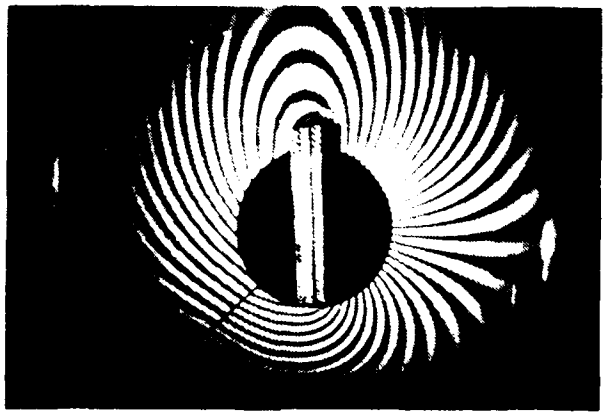

Figure 9a. Reconstructed image from double exposure hologram for the case of a stressed plate having a through cut without the addition of linear fringes

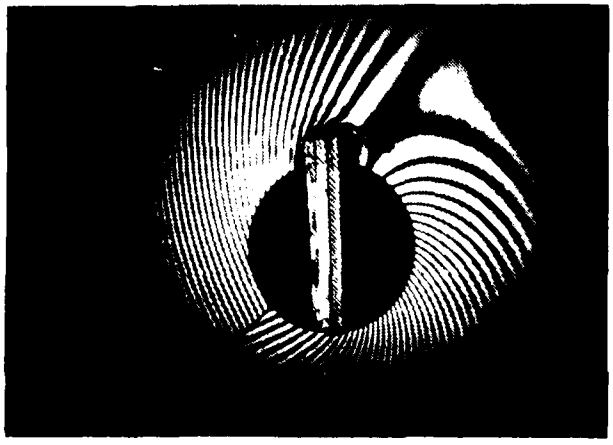

Figure 9b. ω = 0.5 cycles/mm

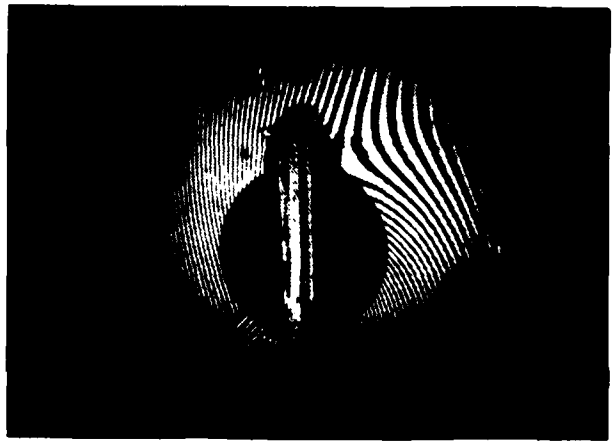

Figure 9c. ω = 1 cycle/mm

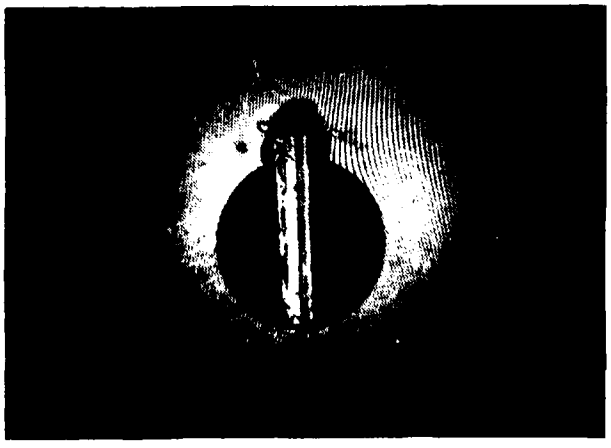

Figure 9d. ω = 2 cycles/mm

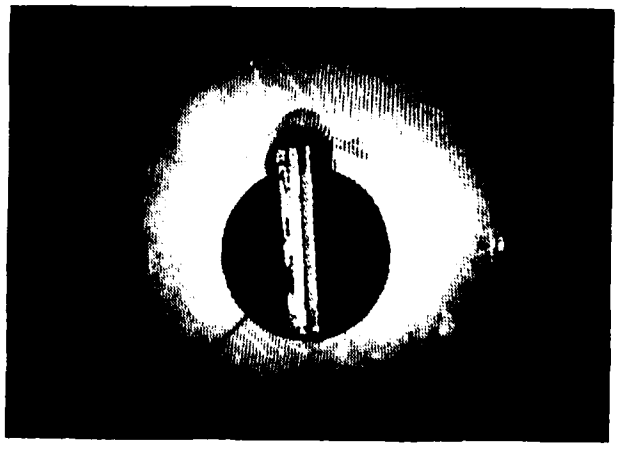

Figure 9e. ω = 4 cycles/mm

Figure 9b-9e. Experimental results showing feasibility for two-exposure FLI for a through cut. Reconstructed images from FLI process in Figure 9a with linear fringes of various frequencies added to control the noise pattern shown in Figure 9a.

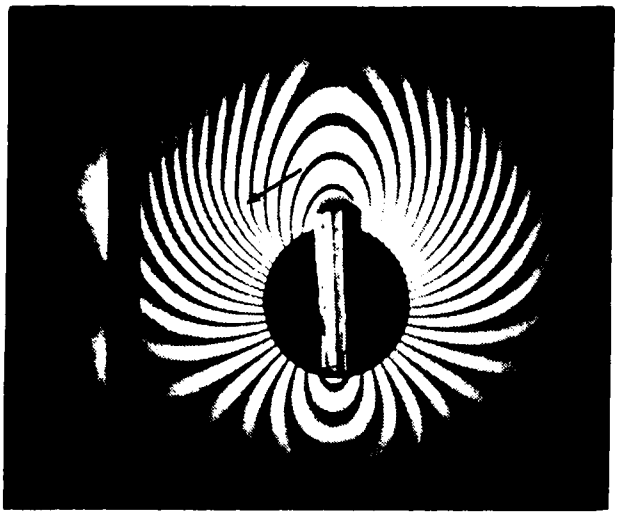

Figure 10a. Reconstructed image from FLI without the addition of linear fringes for a subsurface cut.

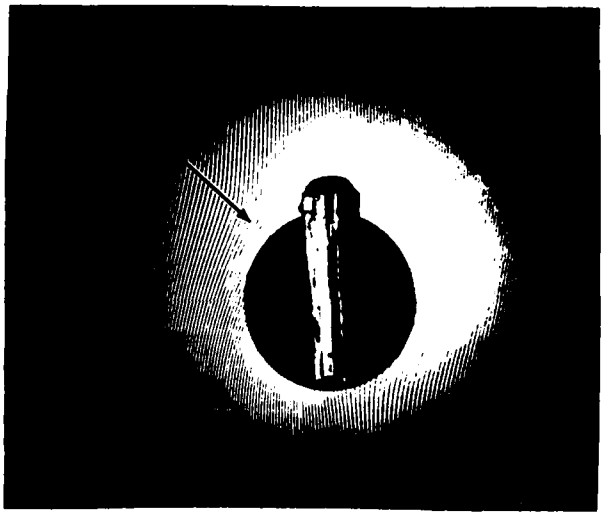

Figure 10b. Reconstructed image from FLI with linear fringes added to predominate the noise and show the location of the subsurface cut.

Figure 10. Demonstration of FLI for subsurface cuts

6. Potential for automatic readout

The linear fringe in the two-exposure Holographic FLI process readily lends itself to using an automatic readout. Although this has yet to be implemented, we present conclusive evidence that effects are present at the defect site in the linear fringe holographic reconstruction which can be detected and used for the automatic readout. To show these effects, we use a diffractometer, a two-dimensional spatial Fourier transforming system as shown in Figure 11. In Figure 12 we show the diffraction pattern from parts of the reconstructed image of a two-exposure FLI hologram at a defect free region and at the site of the through-cut shown in Figure 9e. Figure 12a shows the Fourier signature of the linear fringe (diffractometer was at region to left of defect). We recognize the d.c. term and the two first orders of the linear fringe transform. In Figure 12b, we see the signature at the defect sight (the through cut). The fringe shift at the cut location results in a different d.c. term and two sets of first-orders for the two linear fringes at the cut. The diffractometer outputs clearly show there exists a signature at the defect site distinguishable from the defect free region. Similar results were obtained for the rear surface cut as shown in Figure 13.

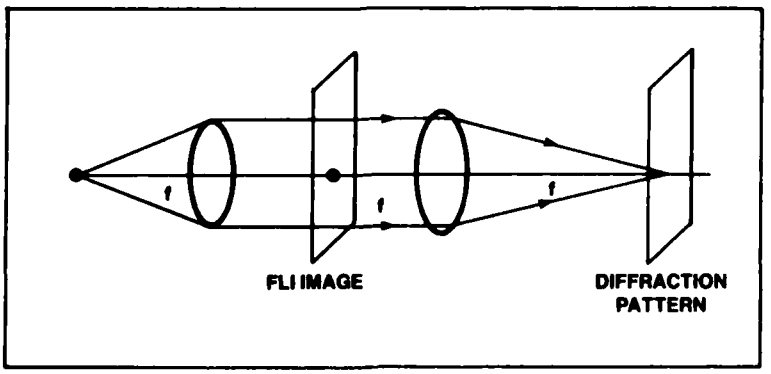

Figure 11. Schematic of optical diffractometer

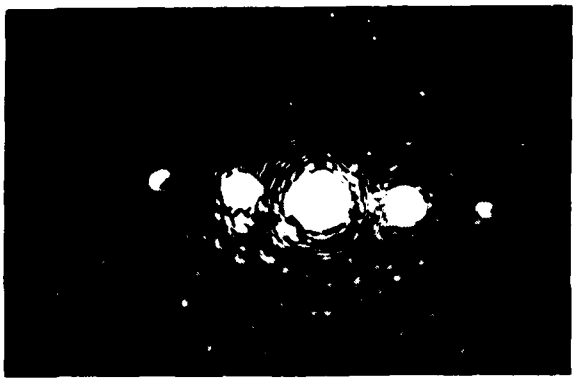

Figure 12a

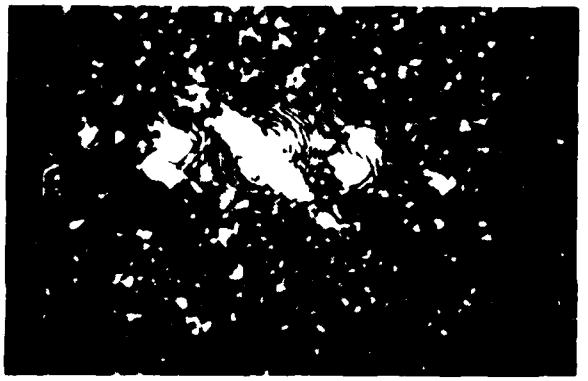

Figure 12b

Figure 12. Fourier signature of through cut

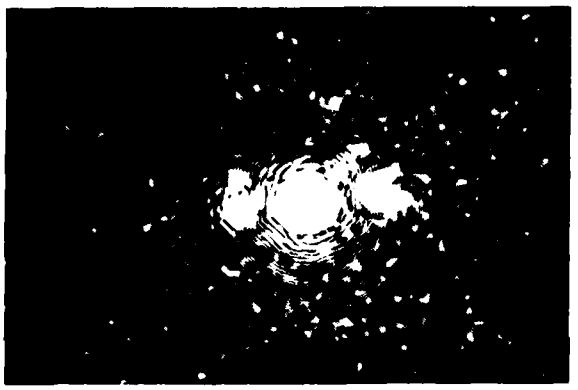

Figure 13a

Figure 13b

Figure 13. Fourier signature of rear surface cut

These results demonstrate that measurable and detectable results characterize defects measured by the FLI Technique. These effects can be exploited in the development of an automatic readout system.

7. Summary and conclusions

The results obtained with static loading techniques were significant and include:

- The experimental feasibility of the FLI concept has been demonstrated.
- FLI removes fringe clutter and simplifies defect location.
- Experimental results showed linearization of fringes and location of both a through cut and a rear-surface cut.
- Experiments with a Fourier diffractometer showed that both the through cut and the rear-surface cut had Fourier signatures significantly different from those of the carrier fringe.

  Automatic readout techniques are possible with such characteristic signatures using image processing software and digital Fourier Transform methods.

- Modeling efforts also showed simplified crack detection with fringe linearization and are in excellent agreement with the experimental results (see Part II of this paper).[7]

Acknowledgements

This work was sponsored by AFOSR on Contract F49620-82-C-0001. Special thanks are also given to P.D. Hilton, R.A. Mayville and D.C. Peirce of Arthur D. Little for consultation on the loading mechanisms used in the experiments.

References

1. Vest, C.M., *Holographic Interferometry*, John Wiley & Son, Inc., New York, NY, 1979.

2. Erf, R.K. editor, *Holographic Non-Destructive Testing* Academic Press, N.Y. and London (1974).

3. N. Abramson, *The Making and Evaluation of Holograms*, Academic Press, N.Y. (1981).

4. TRW Systems Group, "Feasibility Demonstration of Applying Advanced Holographic Systems Technology to Identify Structural Integrity of Naval Aircraft," Interim Report on Contract No. N62269-72-C-0400, 23 March 1973.

5. Smith, H.M., *Principles of Holography*, Wiley-Interscience, N.Y. 1969, pp. 194-5.

6. G.O. Reynolds, D.A. Servaes and J.B. Develis "Holographic Fringe Linearization Interferometry (FLI) for Defect Detection; Part III Load Desensitization with Moire Techniques," in *Applications of Holography* L. Huff, editor Proc SPIE Vol. 523 Paper #28 1985.

7. P.D. Hilton, et al, "Holographic Fringe Linearization Interferometry (FLI) for Defect Detection; Part II Comparison of Observation with Prediction" in *Applications of Holography*, L. Huff, Editor Proc SPIE Vol. 523 Paper #27 1985.

8. Develis, J.B., and Reynolds, G.O., *Theory and Applications of Holography*, Addison Wesley, Reading, MA (1967).

Appendix

Mathematical development of linear fringes in a sideband Fresnel Hologram

The purpose of this appendix is to show that linear fringes can be created in a double exposure sideband Fresnel hologram by shifting the object beam between the exposures. The mathematical development will follow that given in Chapter 3 of Reference 8.

The diffracted field emanating from an object illuminated with a tilted reference wave in the second exposure is obtained by modifying Equation 3-36 of Reference 8 to give

$$R(x) = [-e^{ik_1 z_1} C e^{ik_1 x^2/2z_1}] \int D(\xi) \exp(ik_1[\xi^2/2z_1 - \xi x/z_1]) \times e^{ik_1 \beta_0 \xi} d\xi \tag{A-1}$$

where β_0 is the tilt angle of the beam striking the object and $\sin \beta_0 \cong \beta_0$.

The intensity distribution in the sideband Fresnel hologram produced by this wavefront is

$$I(x) = [Ke^{ik_1 \theta x} + R(x)]^2 \tag{A-2}$$

where θ is the angle between reference and object beams.

If we consider only the term in Equation A-2 corresponding to the real image, we obtain a modified version of Equation 3-81 in Reference 8. Thus,

$$I_R(x) = K'^* K C^* e^{-ik_1 z_1} e^{-ik_1 x^2/2z_1} e^{ik_1 \alpha_0 x} D^*(x), \tag{A-3}$$

where

$$D^*(x) = \int_{z_1 = 0} D^*(\xi) e^{-ik_1(\xi^2/2z_1 - \xi x/z_1 + \beta_0 \xi)} d\xi \cdot \tag{A-4}$$

When the distribution described by Equation A-3 is reconstructed with a beam of wavelength λ_2, the amplitude in the reconstructed image is given by:

$$\psi_{imR}(\alpha) = A \int_{z_2 = 0} e^{-ik_1 x^2/2z_1} D^*(x) e^{ik_1 x\theta} e^{ik_2(x-\alpha)^2/2z_2} dx, \tag{A-5}$$

where A includes all the obliquity factors. Substituting Equation A-4 into A-5, we obtain

$$\psi_{imR}(\alpha) = Ae^{ik_2\alpha^2/2z_2} \int_{z_2=0} \left[\int_{z_1=0} D^*(\xi) e^{-ik_1\xi^2/2z_1} \times e^{ik_1 x\xi/z_1} e^{-ik_1\beta_0\xi} \right] \exp\left\{ \frac{ix^2}{2} \left[\frac{k_2}{z_2} - \frac{k_1}{z_1} \right] \right\} \times e^{ik_1 x\theta} e^{ik_2 x\alpha/z_2} dx, \tag{A-6}$$

which is a modified version of Equation 3-84 in Reference 8.

Applying the focussing condition $k_1 z_2 = k_2 z_1$ to Equation A-6 yields

$$\psi_{imR}(\alpha) = Ae^{ik_2\alpha^2/2z_2} \int\int D^*(\xi) e^{-ik_1\xi^2/2z_1} \times e^{ik_1\xi(x/z_1 - \beta_0)} d\xi \; e^{ix(k_1\theta - k_2\alpha/z_2)} dx \cdot \tag{A-7}$$

In Equation A-7, the ξ integral is the Fourier transform of a Fresnel wavefront. This gives

$$\psi_{imR}(\alpha) = Ae^{ik_2\alpha^2/2z_2} \int_{z_1=0} D^*\left(-\frac{x}{\lambda_1 z_1} + \frac{\beta_0}{\lambda_1}\right) e^{ik_1/2z_1\left(\beta_0 - \frac{x}{z_1}\right)^2} \times e^{2\pi i x\left(\frac{\theta}{\lambda_1} - \frac{\alpha}{\lambda_2 z_2}\right)} dx, \tag{A-8}$$

where tilda denotes a Fourier transform operation.

Making the change of variable

$$x' = \frac{x}{\lambda_1 z_1} + \beta_0/\lambda_1 \tag{A-9}$$

and carrying out the Fourier transform operation indicated in Equation A-8, we get,

$$\psi_{imR}(\alpha) = Ae^{ik_2\alpha^2/2z_2}\ e^{2\pi i\left(\frac{\beta_0\theta z_1}{\lambda_1} - \frac{\alpha\beta_0 z_1}{\lambda_2 z_2}\right)} \times (-\lambda_1 z_1)\, D^*(\alpha - z_1\theta)\, e^{-(2\pi i/2z_1)(\alpha - z_1\theta)^2}. \tag{A-10}$$

A comparison of Equation A-10 with Equation 3-89 in Reference 8 shows that the only difference between the reconstructed image of a sideband Fresnel hologram and one created with a tilted object wave is the linear phase factor (LPF) in α, i.e.,

$$LPF = e^{2\pi i\left(\beta_0\left(\frac{\theta}{\lambda_1}\right)z_1 - \frac{\alpha\beta_0 z_1}{\lambda_2 z_2}\right)}. \tag{A-11}$$

Equation A-11 shows that the phase factor resulting from the tip is linear in α and has a frequency proportional to the tip angle β_0, the hologram construction distance, z_1, the reconstruction distance, z_2, and the reconstruction wavelength, λ_2.

Thus, if a double exposure hologram were made in which the only difference was a tilt of the object beam in one of the exposures, then the reconstructed image would be laced with linear cosine fringes of the form,

$$1 + \cos 2\pi\left(\frac{\beta_0 z_1}{\lambda_1} - \frac{\alpha\beta_0 z_1}{\lambda_2 z_2}\right). \tag{A-12}$$

This shows that tilting the object beam in the hologram results in linear fringes across the image. The analysis of the virtual image yields a similar result.

APPENDIX B

Holographic Fringe Linearization Interferometry (FLI) for Defect Detection: Part II - Comparison of Observation with Prediction

by

D.C. Pierce, P.D. Hilton, R.A. Mayville
Arthur D. Little, Inc.
15 Acorn Park
Cambridge, Massachusetts 02140

G.O. Reynolds, D.A. Servaes, L. Ramos-Izquierdo
Honeywell Electro-Optics Division
110 Fordham Road, Wilmington, Massachusetts 01887

and

J.B. DeVelis
Merrimack College, North Andover, Massachusetts 01860
Currently on sabbatical at Tufts University, Medford, Massachusetts 02153

Reprinted from: SPIE Vol. 523, p. 176, Applications of Holography (1985)

Reprinted from SPIE Vol 523 Applications of Holography

Holographic fringe linearization interferometry (FLI) for defect detection: part II - comparison of observation with prediction

by

D.C. Peirce, P.D. Hilton, R.A. Mayville
Arthur D. Little, Inc.
15 Acorn Park
Cambridge, MA 02140

G.O. Reynolds, D.A. Servaes, L. Ramos-Izquierdo
Honeywell, Inc.
110 Fordham Road
Wilmington, MA 01887

and

J.B. DeVelis
Merrimack College
Turnpike Street
North Andover, MA 01845

Abstract

We present results from our program on fringe linearization for double exposure holographic interferometry for the detection of defects in large areas of metal structures. A model is developed to simulate the expected holographic results, and its predictions are compared to the observations as an aid in refining this nondestructive evaluation procedure. The test specimens are aluminum plates containing circular holes and supported on three sides. Between holographic images a bending moment is applied across the hole. The specimens contain either a through cut or a part-through cut designed to approximate through and part-through cracks respectively. The interference holograms are created by double exposure. Between the first and second exposures the bending moment is applied, and the incident beam is rotated creating fringes which result from specimen deformation and beam rotation. The degree of beam rotation controls the extent to which the fringes are linearized. The supporting finite element modeling and analysis is performed using the ANSYS computer code and plate elements. Fringe linearization is accomplished by adding a rigid body deformation to the deformation field. We will discuss the excellent agreement between experimental FLI results and the finite element predictions for the case of a specimen with a part-through crack in the back surface and not optically visible.

Introduction

Fringe linearization is a valuable technique that enhances the ability of double exposure holographic interferometry to detect defects. As described in Part I[1], the frequency of the linear fringes can be increased to a point where the interferogram becomes insensitive to all disturbances in the exposed body. In order for defects to be detected from the fringe pattern, the linear fringe frequency must be great enough to smooth out almost all deformation of the specimen, yet it must not be so great that it also smooths out any signature left by the defects.

In this part of the set of three papers, experiments used to study flaw detection by fringe linearization are compared to a numerical model of the test configuration. The experimental procedure, which corresponds closely to the testing program desribed in Part I, is described briefly. Greater emphasis here is placed on the numerical model, which employs the commercial finite element code ANSYS[2] to model the deformation of the test plate. We will discuss the agreement between the test and the model results, which suggests that models of this type may play an important supporting role in guiding fringe linearization interferometry experiments.

The experimental configuration

The test specimens for this study were four inch square aluminum plates, 0.125 inches thick, containing one inch diameter holes in the center. Each plate was clamped on three sides, as shown in the fixture in Figure 1. A bending load was imposed via the long metal piece extending out from the hole in Figure 1. This moment arm hooked into the hole, contacting the plate near the top of the hole on the back side of the plate and near the bottom of the hole on the side of the plate visible in the figure. To obtain a differential

loading between holographic exposures, the moment arm was loaded with weights. Either part-through or through cracks could be cut in the plate at arbitrary locations. For the present discussion, only the crack configurations shown in Figure 2 are considered.

To create the interference holograms, two exposures were made for each case. Between these exposures, the moment arm was loaded with weights to produce an excess bending moment of 3.5 to 4.0 inch-pounds at the hole. In addition, the incident beam was rotated between exposures to linearize the fringes. The beam rotation for most of the experiments here was 600 microradians; this number was most accurately determined by counting the fringe frequency on the specimen in a location where the linear fringes were dominant. For a given laser wavelength, the amount of beam rotation is directly proportional to this fringe frequency.

The numerical model

To model the test configuration, finite element meshes were constructed using the commercial computer code ANSYS[2]. One such mesh is shown in Figure 3, in which the flaw extends upward and to the left from the hole. The boundary conditions imposed on the model correspond to those in the experiment: both side boundaries and the bottom boundary were all clamped; the top boundary was left free. The moment applied to the test plate was simulated in the model by equal and opposite out-of-plane forces applied at the top and bottom of the hole. The magnitude of these forces was such that the total applied torque was 3.6 inch-pounds.

Structurally, therefore, the model can be made to correspond to the experiment in all respects. A mechanical analogue for the beam rotation is also easy to provide, and this allows fringe linearization to be part of the model as well. The mechanical analogue is in fact a rigid-body rotation of the plate. Just as the field of linear fringes dominates other fringe patterns as the beam rotation is increased, so does the displacement field of the rigid-body rotation dominate other displacement fields as the mechanical rotation is increased. Indeed, the experimental fringe linearization could also be accomplished by rotation of the specimen, but in practice, the beam rotation can be performed much more easily.

The model boundary conditions associated with the rigid-body rotation can be somewhat tricky. First, an axis of rotation for the model must be chosen to agree with the intended beam rotation. This axis will always lie in the plane of the specimen, and in the usual case, it will pass vertically through the center of the hole. Other rotation axes may be desirable, however, for detecting flaws of a particular orientation. Once the rotation axis is selected, the nodes on the clamped boundaries must be assigned rotations with respect to the coordinate axes so that the plate rotation has the appropriate value (here, 600 microradians) with respect to the chosen rotation axis. In addition, these nodes must be assigned out-of-plane displacements according to their distance from the rotation axis. When imposed correctly, these additional boundary conditions model the experimentally observed fringe linearization extremely well.

Through cracks in the plate were modeled simply by releasing connections along an appropriate line of nodes. Because the model plate consisted of two-dimensional finite elements, modeling a part-through crack required a special procedure. The surfaces of the through crack were separated slightly, and the gap was filled with small additional elements. These additional elements were assigned a thickness of 0.005 inches, four percent of the nominal plate thickness. These elements thus modeled the effect of a thin ligament. The ligament thickness in the model is less than that in the actual plate (0.03 inches); the model ligament thickness was selected by comparing model and experimental fringe patterns. A direct model of the effect of ligament thickness would require a three-dimensional analysis, and such analysis is planned in future work. Corresponding to the presence of a part-through flaw, the current ligament model serves to enforce displacement continuity across the closed side of the defect; this continuity naturally does not occur for the through crack.

Results and discussion

Two sets of results will be presented in detail; both of these demonstrate the accuracy and utility of the finite element structural analysis in modeling the holographic technique proposed in Part I.

The first results are for the crack geometry shown in Figure 2(a). Only the part-through flaw will be discussed. The double exposure holograms obtained in the laboratory were obtained from the back surface of the plate, i.e., the surface on which the crack was not visible. Figure 4 shows the interferogram for the plate without any linear fringes. The fringes which appear in the figure have smoothly varying slopes, and a cursory inspection indicates nothing that might signify the presence of a flaw. If one knows that a part-

through crack emanates from the upper left corner of the hole, however, one notices a modestly sharp bend of the fringes in this region, especially compared to the similar fringes to the upper right of the hole. These bends are not obvious, however, and they would be particularly difficult to detect using an automated scanning procedure. The computer model of the same loading is shown in Figure 5. Here again, the effect of the crack can be observed if one knows its location. Without such knowledge, however, the bend in fringes to the upper left of the hole has no apparent distinction from other bends in the plot, which arise due to the discrete nature of the finite elements used to model the plate. (In Figure 5, and subsequent computer plots, the dashed line corresponds to zero displacements.) The fringe patterns from the experiment and the analysis agree quite well, but one implication of this agreement is that flaw detection may prove difficult using conventional double exposure interferograms. In Part I, this difficulty was emphasized as a primary motivation for development of a fringe linearization technique.

Linear fringes were next superposed on Figure 4, with the result shown in Figure 6. As noted previously, the beam rotation used was 600 microradians, and the moment loading was 3.5 inch-pounds. The linear fringes smooth out the fringe pattern of Figure 4, but the barely noticeable flaw signature in Figure 4 is the dominant feature of Figure 6. The linear fringes have essentially wiped out all the smoothly varying slopes of Figure 4, so that the discontinuous slopes associated with the part-through cut immediately catch one's attention. In addition, the homogeneity of the linear fringes away from the flaw, together with the sharp bends at the flaw, provide the features needed for an automatic detection procedure, as discussed in Part I.

Figure 7 shows the finite element analysis performed to correspond to Figure 6. While the inadequate resolution of the output device makes the fringes jagged in places, the agreement with the experiment is excellent. The linear fringes dominate over the entire plate, except at the flaw, where the sharp bend in fringes occurs, as in the experiment.

Because the agreement between experiment and analytical model is so close, we can use the structural analysis to provide guidance as to how one might facilitate and optimize holographic detection of flaws. For example, if a particular type of flaw is being sought after, both an axis and magnitude of beam rotation could be determined ahead of time to maximize the likelihood that if the particular type of flaw exists, it will have a significant effect on the linear fringes. In addition, appropriate loading configuration and magnitude may be worked out numerically without the expense of an extended experimental program. Additional analyses performed for the part-through cut discussed above indicated that locating the axis of beam rotation 45° from the crack orientation provided the best holographic signature of the flaw; other rotation axes led to linear fringes which made the flaw more obscure. A rule of thumb for detection of a crack emanating from a hole can thus be stated as follows: fringe linearization should be employed, and the rotation axis (or axes) should be oriented 45° from the suspected crack (or cracks). When the flaws are randomly located, a range of beam rotation axes is probably necessary.

We also considered the crack configuration in Figure 2(b). With the same bending load configuration as was applied to Figure 2(a), the interferogram in Figure 8 was produced. As in Figure 4, the crack gives rise to a sharp bend, barely noticeable, in the fringes which cross the crack location. In the corresponding finite element calculation, this bend was not even distinguishable from other sharp bends arising from the discrete nature of the finite elements; see Figure 9. Linear fringes were applied to the finite element model of the plate in the hope that these would render the crack location detectable. The results are furnished in Figure 10. Unfortunately, this figure seems to be identical to what one would expect to see if there were no defects present in the plate. The positive side of the analysis was borne out by the actual experiment on the plate with the part-through flaw, with linear fringes. Exactly as in the model, an undisturbed field of linear fringes was observed, just like those in the defect free areas of Figure 6. Figure 11 shows an attempt, using our model, to reveal the flaw by simulating rotation of the object beam about an axis oriented 45° to the crack. Again, however, the flaw cannot be detected.

Conclusions and future work

The state of affairs just described shows simultaneously the benefits of the computer model and the limitations of reliance on a single load configuration to reveal defects with the holographic technique. For both crack configurations shown in Figure 2, the computer model has shown excellent agreement with the interferograms produced experimentally. Given that a simple structural analysis can model so well the loading and displacements seen here, we would expect the structural model to be an invaluable tool in pursuing viability of the fringe linearization technique for practical applications. Research studies could be performed to determine by computer which beam rotations and loading modes are best suited for interferometric detection of a particular crack. Here, we have observed the utility of a bending load in revealing a crack emanating from a hole; in addition, we can probably conclude that the same loading is not as effective for a crack which does not intersect the

hole.

Other types of loading are under consideration, and current plans are to study these further. An additional loading mechanism appropriate for the hole in the plate is insertion of a tapered or shrink-fit plug into the hole as described in Vest's book.[3] Indeed, this loading rendered the crack of Figure 2(b) visible, both without linear fringes (Figure 12) and with them (Figure 13). At this point, we have not yet modeled these interferograms by computer. The conclusion remains, however, that different flaw geometries are made most susceptible to detection by different loadings. For many situations, and certainly for practical defect detection in, say, aircraft structures, particular static loadings do not provide a range of mechanical disturbances wide enough to reveal all possible flaws. Continuation of this research is therefore expected to focus in large measure on dynamic excitation of mechanical vibrations, in the hope that a broader spectrum of response is activated. Interferograms are naturally more difficult to obtain when the time between exposures becomes very important, as a double-pulsed laser is necessary; extension of the computer models described above should provide guidance as to the time intervals required. Dynamic and modal structural analysis are available to predict times and amplitudes of vibration so that validation studies can be carried out with a minimum of guesswork.

Acknowledgements

The support of this work by the Air Force Office of Scientific Research is gratefully acknowledged.

References

1. Reynolds, G.O., Servaes, D.A., and Ramos-Izquierdo, L., "Holographic Fringe Linearization Interferometry (FLI) for Defect Detection: Part I - The Basic Concept," in Application of Holography, L. Huff Chairman/Editor, Proceedings, SPIE, Volume 523, Number 26, 1985.

2. DeSalvo, G.J. and Swanson, J.A., ANSYS Engineering Analysis System User's Manual, Revision 4.0, Swanson Analysis Systems 1982.

3. Vest, C.M., Holographic Interferometry, John Wiley and Sons 1979.

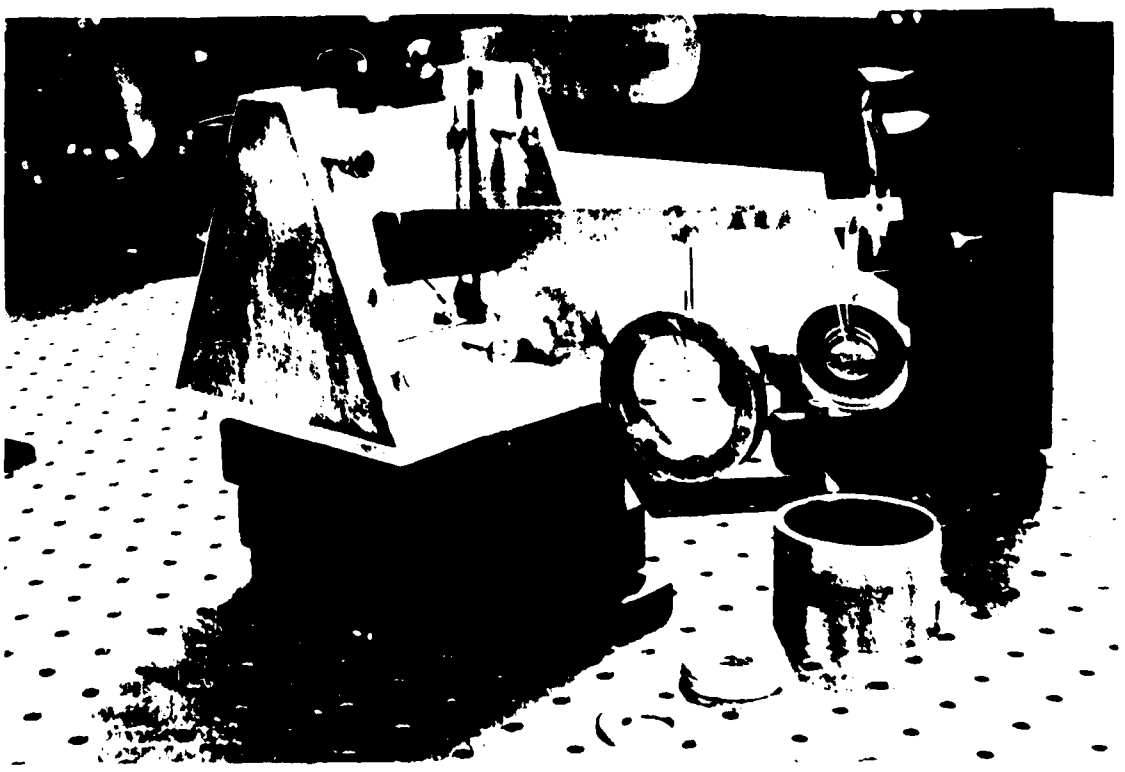

Figure 1. Loading fixture used to produce deformation for the experimental interferograms.

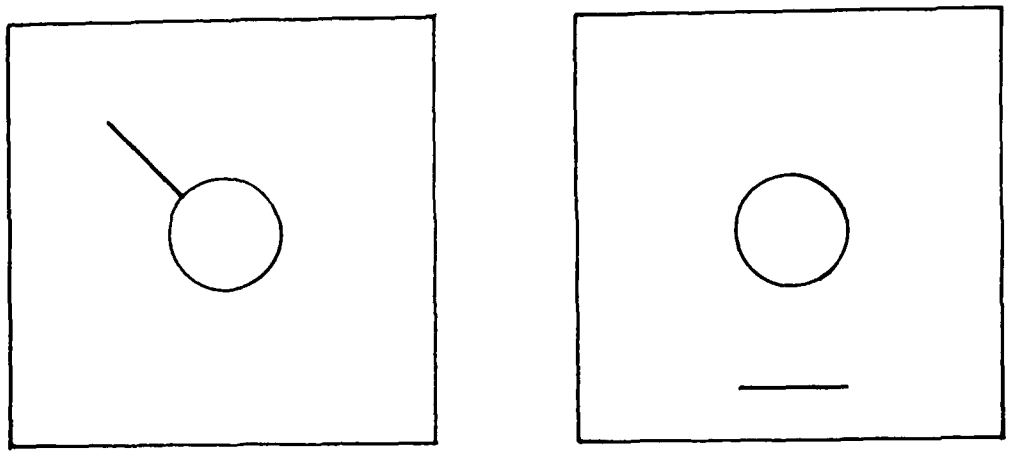

Figure 2. Crack configurations studied in this paper. (a) One inch crack emanating from hole. (b) One inch crack one inch below the hole.

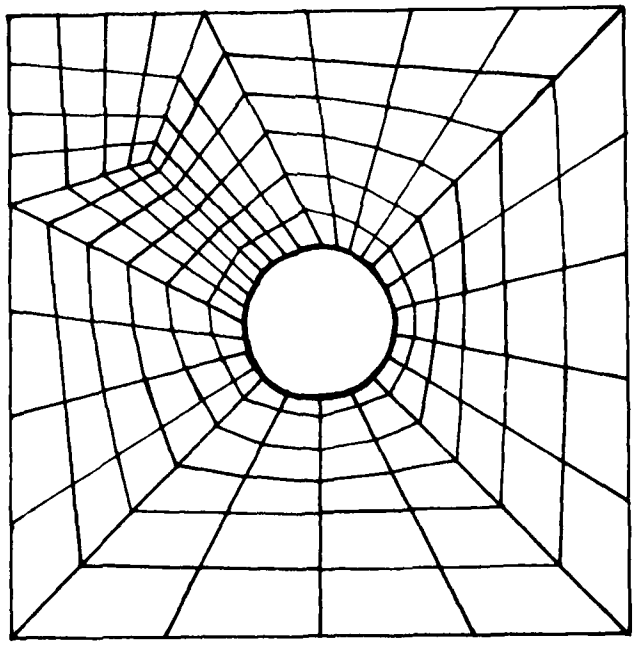

Figure 3. Typical finite element mesh for crack in Figure 2 (a).

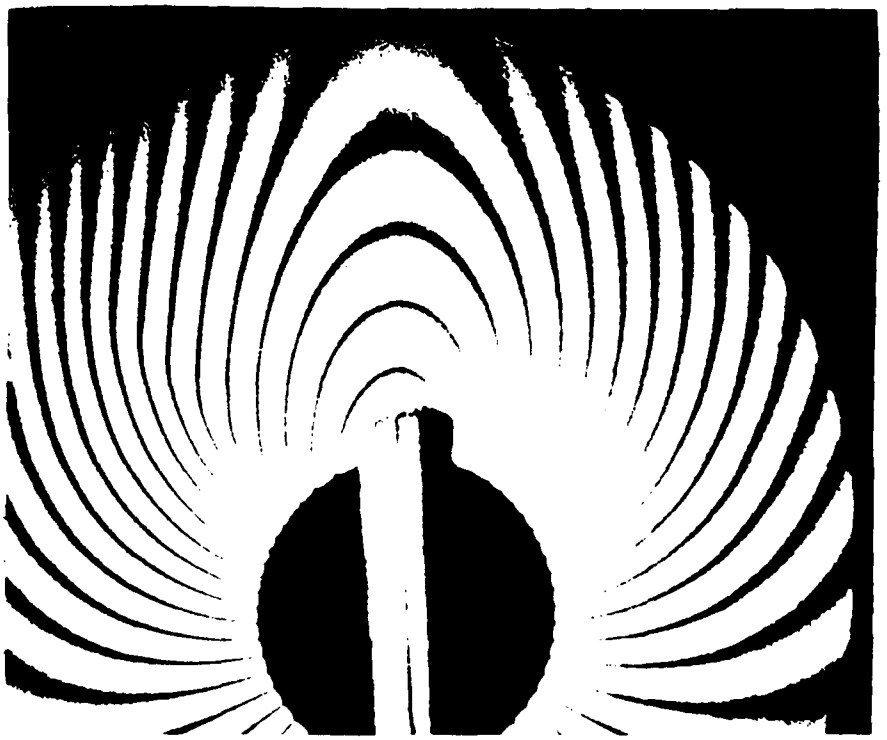

Figure 4. Interferogram for crack in Figure 2(a). No linear fringes are added.

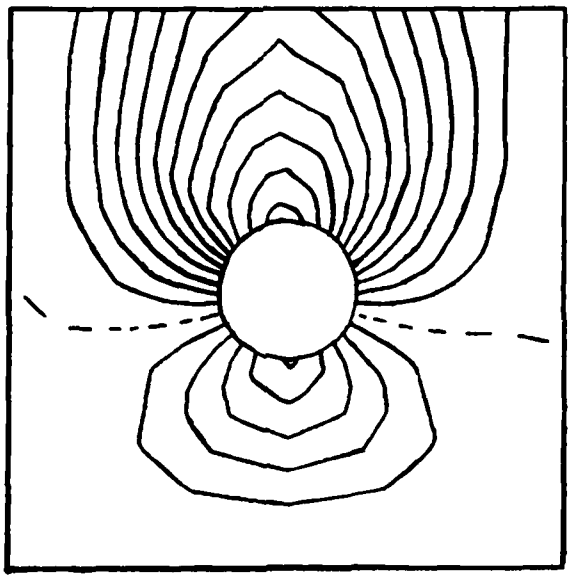

Figure 5. Computer model corresponding to Figure 4.

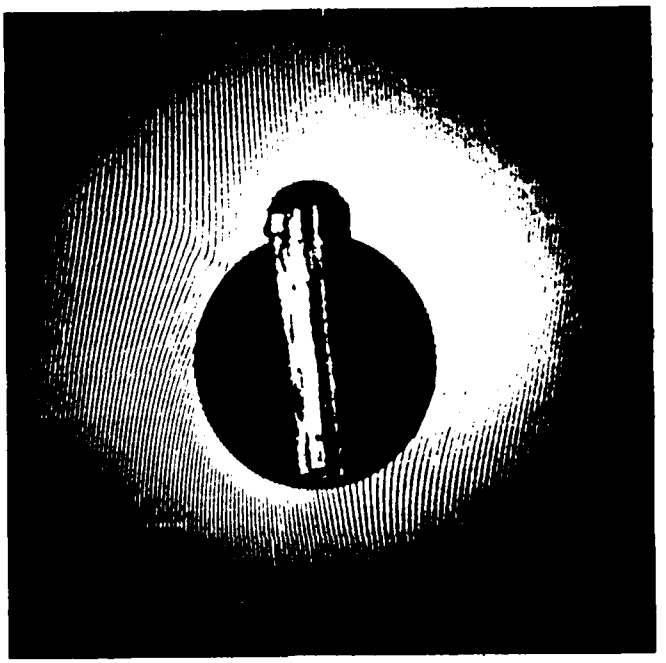

Figure 6. Interferogram for crack in Figure 2(a), with linear fringes added.

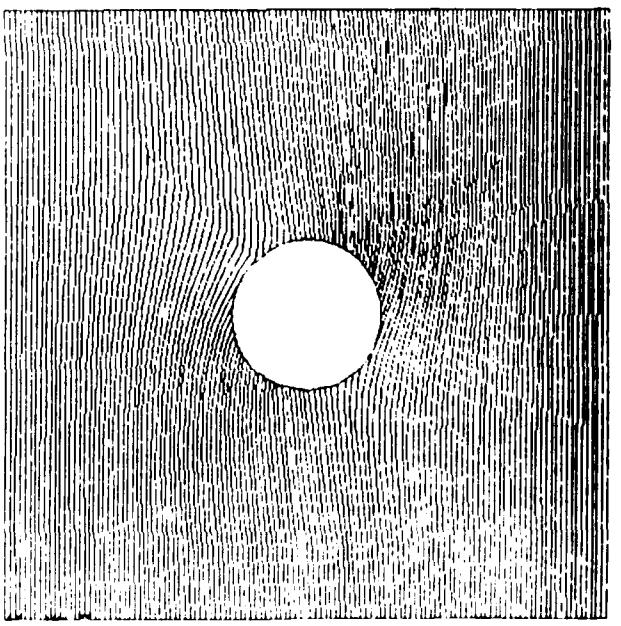

Figure 7. Computer output corresponding to Figure 6.

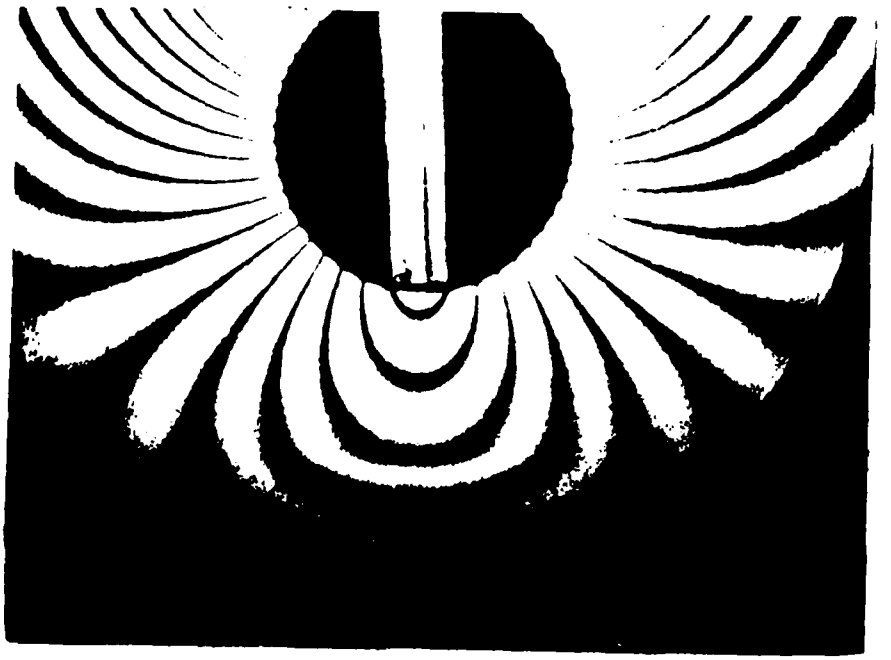

Figure 8. Interferogram for crack in Figure 2(b), without linear fringes.

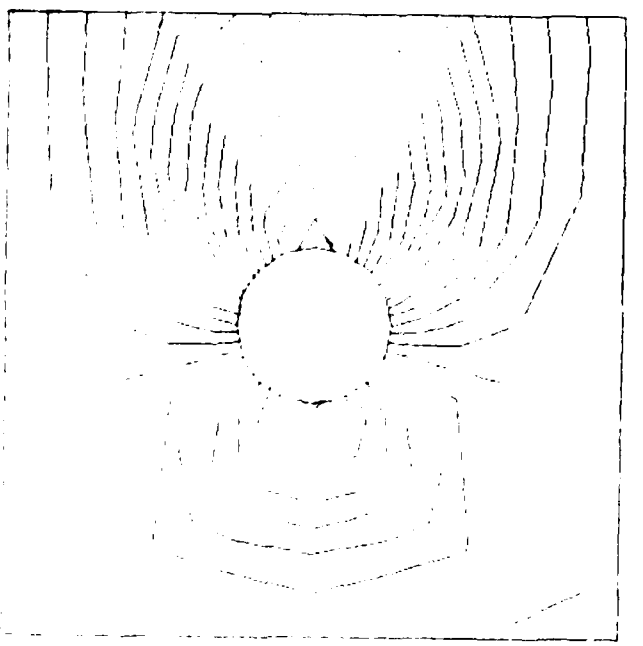

Figure 9. Finite element model of Figure 8.

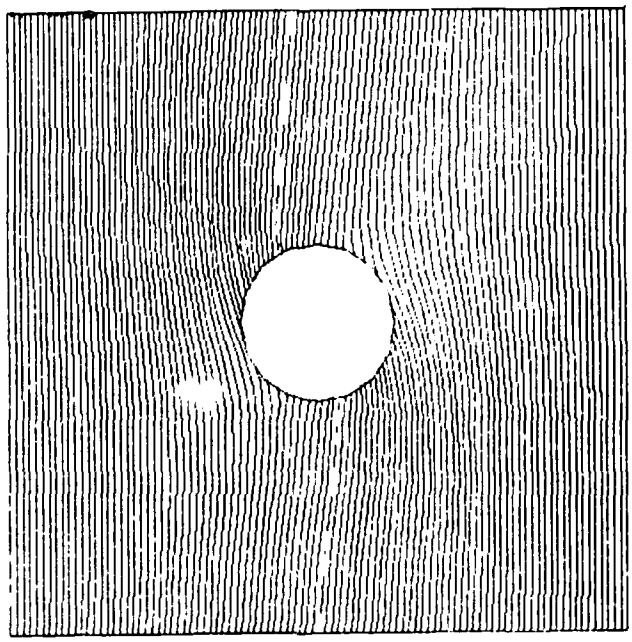

Figure 10. Addition of linear fringes to Figure 9.

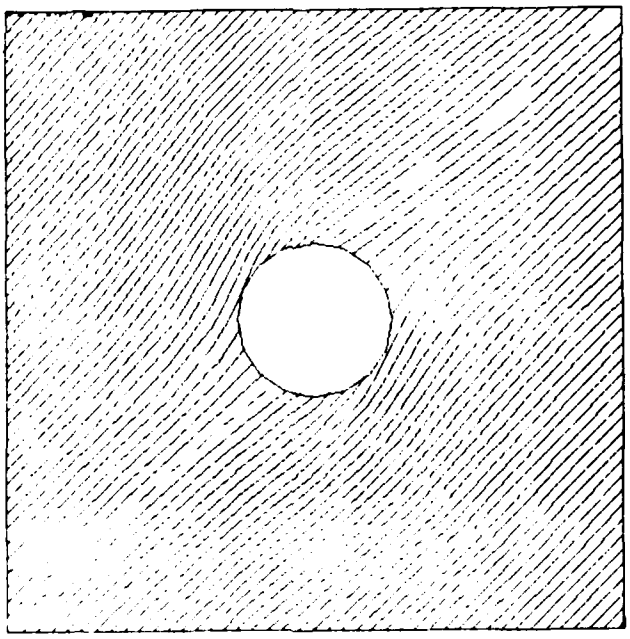

Figure 11. Linear fringes added to Figure 9 by rotation about an axis 45° to the vertical.

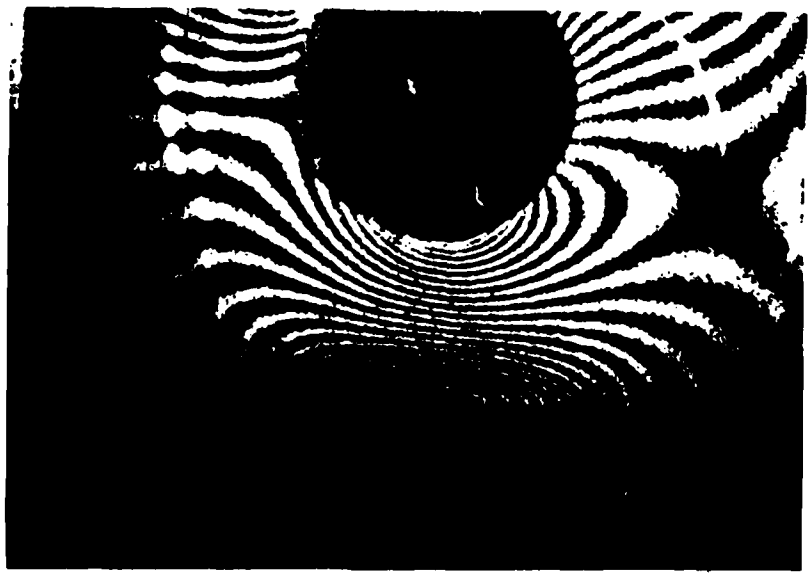

Figure 12. Interferogram of crack in Figure 2(b) with plug loading.

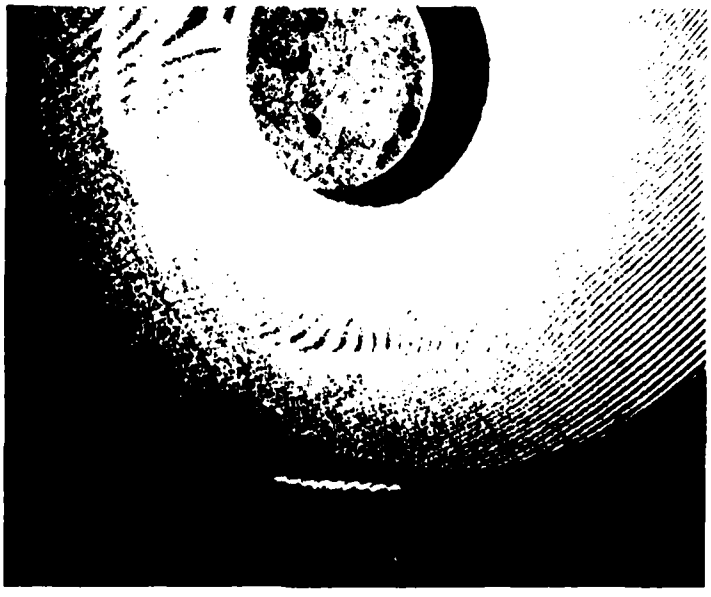

Figure 13. Addition of linear fringes to Figure 12.

APPENDIX C

Holographic Fringe Linearization Interferometry (FLI) for Defect Detection: Part III - Load Desensitization with Moire Techniques*

by

G.O. Reynolds, D.A. Servaes, L. Ramos-Izquierdo
Honeywell Electro-Optics Division
110 Fordham Road, Wilmington, Massachusetts 01887

and

J.B. DeVelis
Merrimack College, North Andover, Massachusetts 01860
Currently on sabbatical at Tufts University, Medford, Massachusetts 02153

Reprinted from: SPIE Vol. 523, p. 186, Applications of Holography (1985)

Reprinted from SPIE Vol. 523 Applications of Holography

Holographic fringe linearization interferometry (FLI) for defect detection Part III Load desensitization with moire techniques*

G.O. Reynolds, D.A. Servaes, and L. Ramos-Izquierdo

Honeywell Electro-Optics Division
110 Fordham Road, Wilmington, Massachusetts 01887

J.B. DeVelis

Merrimack College, North Andover, Massachusetts 01860
Currently on sabbatical at Tufts University, Medford, Massachusetts 02153

Abstract

Holographic FLI technique provides a means of reducing fringe clutter noise. Holographic interferometry measures position changes of the order of the wavelength of the light used. Moire techniques provide a means of desensitizing holographic interferometry. Moire techniques may be employed with FLI with the objective of automating the defect detection process. It may be necessary to employ a spatial frequency filtering step to remove fringe clutter noise.

Experimental results show the feasibility of the FLI concept with moire desensitization.

Introduction

In Part I of this series of papers, "Holographic Fringe Linearization Interferometry (FLI) for Defect Detection: The Basic Concept," it was shown that the basic FLI process is described by the FLI equation

$$\cos\,[\omega_o x + \Delta(x,y)] \tag{1}$$

where the phase term, $\omega_o x$, describes the linear fringes created from tilting the object beam between exposures and the $\Delta(x,y)$ phase term are results from the differential loading of the test specimen between exposures. To make the $\omega_o x$ phase term the dominant term so that the resulting FLI image will display the clean linear fringes, we must either restrict the out-of-plane displacements due to the loading so that the $\Delta(x,y)$ phase term is one-quarter wave per linear/fringe cycle or increase the linear fringe phase term until it dominates the vector addition.

It is easy to increase the linear fringe frequency — increase the tilt angle of the object beam — but there are practical considerations. The fringes should have high visibility for defect detection. This puts an upper limit on the linear fringe frequency.

In this paper we show that fringe desensitization can be achieved by using moire methods and describe a two-color method used by Varner[1] to yield desensitization.

Applications of moire methods to holographic interferometer

Non-periodic functions

Two-color holographic contouring

In holographic interferometry, moire-type effects have been introduced to contour three dimensional objects using non-periodic carriers[2,3]. In this work multiple source, multiple index and multiple wavelength, effects have been utilized to create the moire effect. The desensitized capability of the two wavelength method is given by the factor $\Delta k = 2\pi\,(1/\lambda_1 - 1/\lambda_2)$ which results in a change in the contour interval of

$$\Delta l = \lambda_1 \lambda_2 / 2\,\Delta\lambda \tag{2}$$

*Work sponsored by AFOSR on Contract F49620-82-C-0001

For a single wavelength the contour interval is $\lambda/2$. The two colors create a contour interval which is $\lambda/\Delta\lambda$ times larger than the single wavelength contour interval.

It is this moire desensitization method which can be utilized to overcome the loading limitations of the holographic FLI process. In particular, we will extend the method described by Abramson[6] to achieve a desensitization with the FLI concept by utilizing moire methods.

The Abramson experiment

In this experiment a doubly-exposed hologram of a centrifugal pump was made. Between holographic exposures the internal pressure of the pump was changed, and a large rigid body motion, rotation, was also introduced to the pump. This rotation produced a great number of almost vertical straight fringes. The desired information concerning the pressure deformation is hidden by the unwanted vertical fringes on the reconstructed image as shown in Figure 1. The resulting moire fringe (difference fringe) represents the difference between the rigid body motion (rotation) and the rotation plus the expansion due to pressure change as shown in Figure 2. Thus, the moire method shows the deformation of the pump due to the pressure change between exposures. Therefore, the moire technique, a desensitizing process, has been used to recover a small phase change in a hologram (deformation due to pressure) which was dominated by a large linear phase disturbance (rigid body rotation). Note: If a transparency is made on a copier, the reader can recover the pattern of Figure 2 by overlaying the ruling of Figure 2 on Figure 1.

Inverting the Abramson method

The Abramson technique can be modified for use in the FLI process for those situations where the deformation of the object causes a large phase disturbance that dominates the linear fringe, i.e. the deformation due to the load violates the quarter wave per linear fringe cycle criterion established earlier. In this situation we will consider the random fringe that results from the body deformation as the carrier, and use the Abramson method to recover the linear fringe.

This recovery of the linear fringe is accomplished by making two similar double exposure holograms differing only in that in one, a linear fringe has been added by tipping the object beam between the two exposures. Two such exposures are shown in Figure 3 and Figure 4 where the load was introduced by two thumb screws mounted on the backside of the plate.

When the negatives used to make Figures 3 and 4 are sandwiched together, the linear fringe is revealed as shown in Figure 5. Note: The linear fringe yielded black lines on the sandwich, consequently the nearly clear line on the positive print. This experiment demonstrates that linear fringes can be recovered by the method of holographic moire so that two-color holographic moire could be used as a desensitization technique in the FLI process.

Four exposure, one color, two hologram moire — subtraction

In the holographic moire technique described by Abramson[6] (See Figures 1 and 2) the moire fringe can be mathematically described by subtracting the phases of the two interferograms. i.e.

$$[\omega_o x + \Delta(x,y)] - \omega_o x = \Delta(x,y). \tag{3}$$

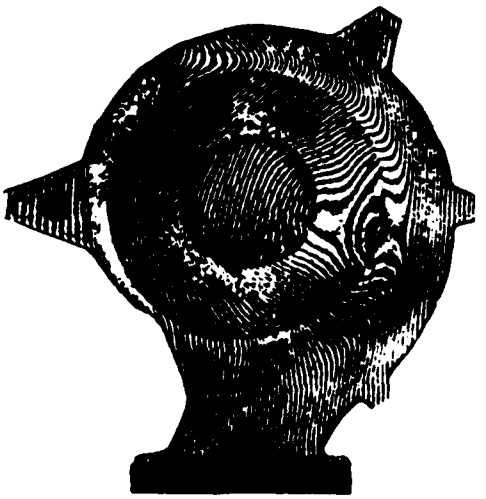

Figure 1. Reconstructed image from a doubly exposed hologram made of a centrifugal pump with a height of about 1 meter. Between the two exposures the internal pressure of the pump was changed and the pump was subjected to a large rigid body motion (i.e., rotation) [after Abramson[6]]

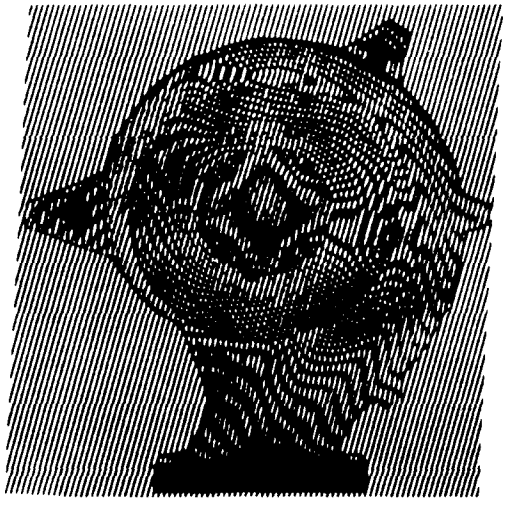

Figure 2. **Moire fringe of a periodic grating with Figure 1 showing the desensitized reconstructed image of Figure 1. Notice the low frequency (moire) fringes not present in Figure 1 which are associated with the out of plane deformation due to the pressure change given to the pump between exposures. [after Abramson[8]]**

Figure 3. **Reconstructed image (holographic interferogram) from double exposure hologram #1**

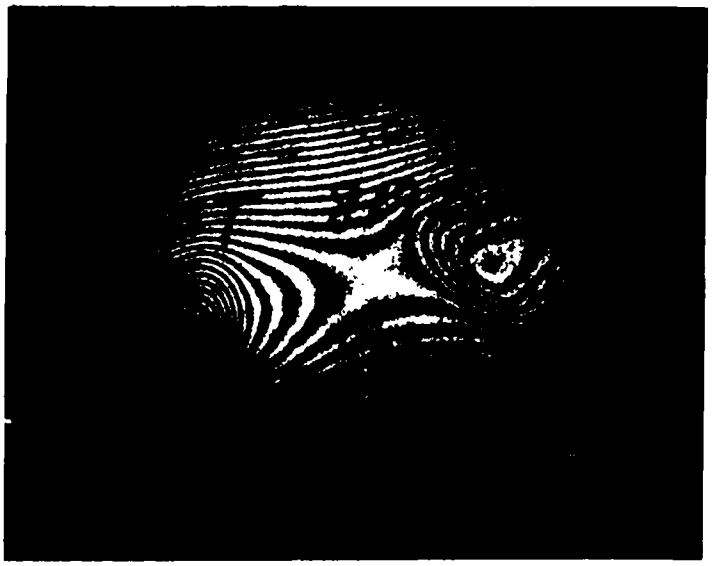

Figure 4. Reconstructed image (holographic interferogram) from double exposure hologram #2. The linear fringe is not observable.

Figure 5. Moire of the two random noise interferograms indicating the presence of the linear fringe

Since four-exposure, two-hologram FLI is the opposite of the Abramson case, (i.e. noise carrier) the resulting phase is

$$[\omega_o x + \Delta(x,y)] - \Delta(x,y) = \omega_o x. \tag{4}$$

In four-exposure FLI with a Phase, $\Delta(x,y)$, due to differential loading the two double exposure holograms can be represented as

$$H_1 = |e^{i\phi_1(x,y)} + R|^2 + |e^{i\phi_2(x,y)} + R|, \tag{5}$$

where H_1 is the sum of exposure 1 and exposure 2.

$$H_2 = |e^{i\omega_o x} e^{i\phi_2(x,y)} + R|^2 + |e^{i\phi_1(x,y)} + R|^2, \tag{6}$$

where $\phi_4(x,y)$ $\phi_2(x,y) + \Delta$, and H_2 is the sum of exposure 3 and exposure 4. In equation (5) and equation (6), $\phi_1(x,y)$ and $\phi_2(x,y)$ represent the out-of-plane displacements due to the two different forces, R is the holographic reference wave and Δ is the phase resulting from the differential loading.

When these two holograms are reconstructed and moired, the moire fringe (difference frequency) is

$$\cos(\omega_x x + \Delta). \tag{7}$$

The phase shifts from the differential loading phase modulate the linear fringe. Since these phase shifts should be larger at the defect locations, the four-exposure FLI holograms should be amenable to automatic readout.

The experiments for this phase of the research were completed using a Laser Technology, Inc. instant hologram recording system. The system, using a monobath chemistry process, developed the hologram in place, and the interference between the hologram virtual image and the test object can be seen immediately. The test object can be stressed and the object beam direction changed so that their effects can be observed in real time. This system allowed us to perform controlled, FLI experiments to demonstrate the moire desensitization. The following procedure was used.

1. A hologram of state 1 is made and processed in the real time recording system.

2. A lever arm was attached to the center of the plate as shown in Figure 6. (Static loading was chosen because we made a computer model for it; also, static loading is easily controlled and repeatable.) The real time holographic system enables us to vary the fringe pattern on the interferogram until high frequency noise fringes were obtained. The resulting interferogram from the real time holographic system (an interferogram between state 1 of the surface recorded on the hologram and state 2 due to the hanging weights) was photographed, Figure 7.

3. The linear fringe was then added by swinging the object beam and the new interferogram was photographed, Figure 8. Note: The loading is so large that the deformation contours dominate and the linear fringes are not visible.

4. The resulting pattern obtained from the moire of Figure 7 and 8 shows the linear fringe, Figure 9.

Figure 9 demonstrates the feasibility of the FLI moire process. However, the linear fringes are superimposed upon the clutter so that a spatial filtering step is required to remove the clutter.

Four exposure, one laser, one hologram

The four exposure moire process can also be achieved on a single hologram[8]. A four exposure hologram will certainly yield confusion. The images produced during reconstruction seem to be an unwieldly number. If the four states are different we should see the four states and an interferogram from the four states, two at a time, for an additional six images. If the states are properly selected, useful information can be obtained.

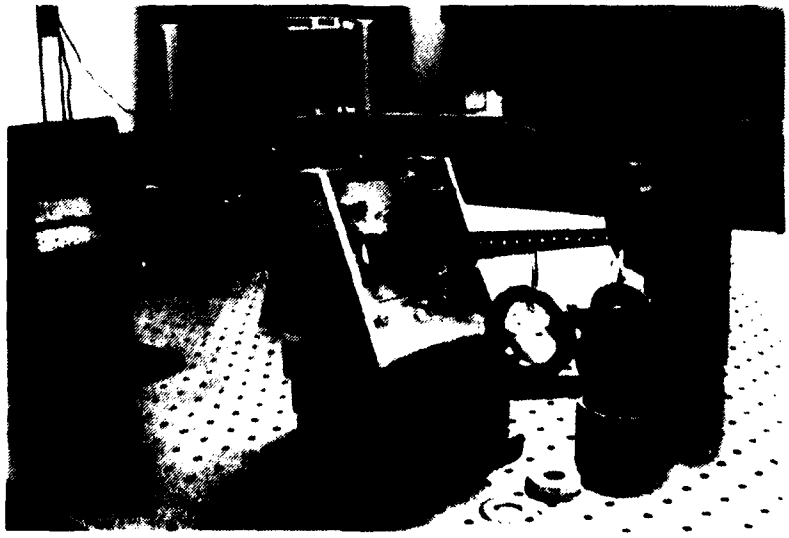

Figure 6. Photograph of fixture for stressing test plate

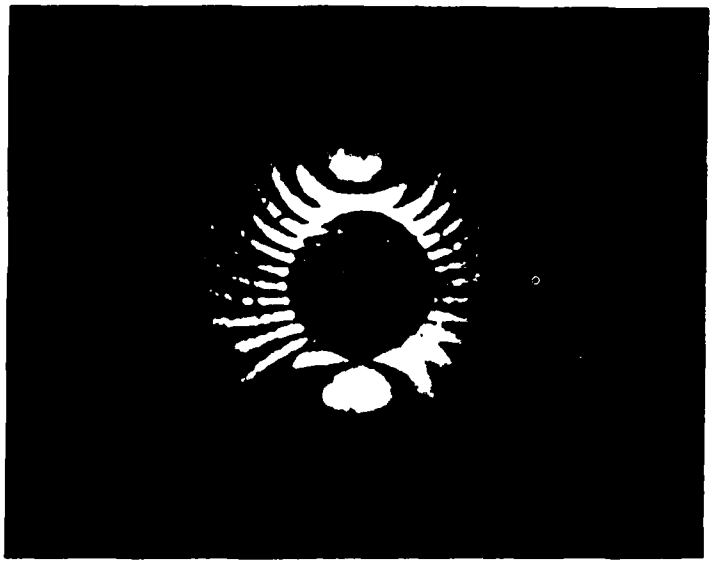

Figure 7. ***Interferogram*** **between state #1 of test plate (relaxed), and state #2 (hanging weights) made in real time holographic system**

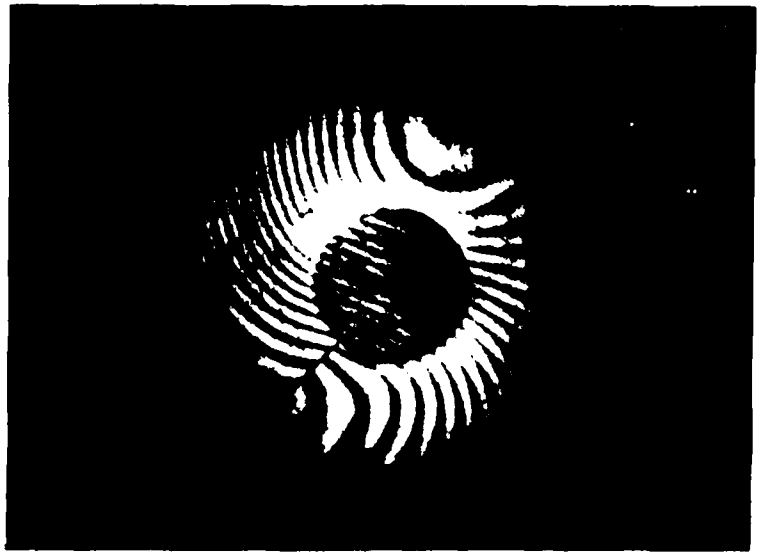

Figure 8. Interferogram between state #1 of the test plate (relaxed) and state #2 (hanging weights) with shifted object beam made in real time holographic system. The fringes rotate on the central plug because it is stiff and experiences a tilt from the hanging weights. Also note that the noise fringes are shifted at the position of the crack i.e., the vector addition gave a better angle of the fringes to the crack illustrating the ultimate importance of fringe direction to crack orientation

The following experiment demonstrates the desensitization that can be achieved and shows the process can be utilized with the linear fringe.

The states of the holographic apparatus for the four exposure hologram are:

State 1. Object relaxed. Exposure 1.

State 2. Object loaded to produce an interferogram. Exposure 2.

State 3. Object load increased such that the interference frequency between State 3 and State 1 and State 2 is too high to be visible. Exposure 3.

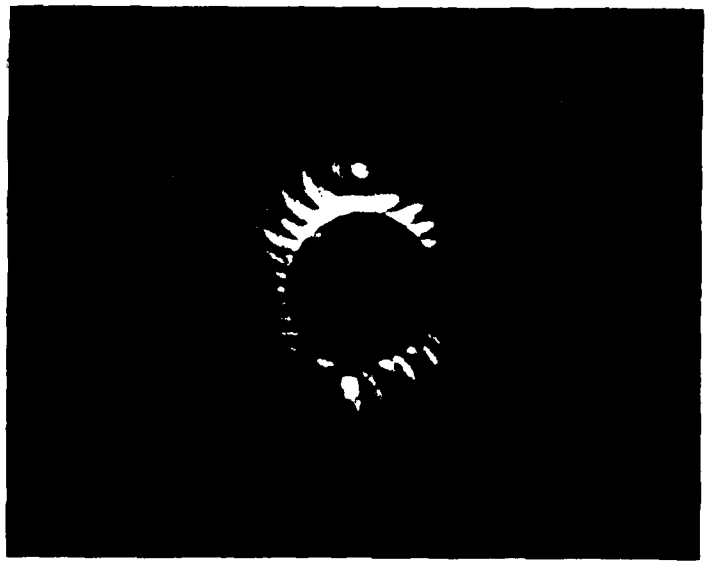

Figure 9. Moire of the interferograms in Figures 4 and 5 indicating the presence of the linear fringes (negative 10 degrees off the vertical)

State 4. Additional object load to state 3, similar to the difference between state 1 and state 2, plus an additional small load and an object beam tip to produce linear fringes. Exposure 4.

The images on reconstruction will be an image of the four states (and they should all appear the same) and the interference contours between state 1 and state 2 and the contours between state 3 and state 4. We can expect these interferograms to moire.

The result of the four exposure, one laser hologram is shown in Figure 10. The moire is the equivalent of a plate that had been loaded with a small load, as shown in Figure 11. The loading for state two produces an interferogram shown in Figure 12.

A linear fringe can be added by swinging the object beam between state 3 and state 4. Figure 13 shows how the beam swing modifies the interferogram move pattern. Figure 14 is the same as Figure 13 with a larger beam swing. The higher frequency linear fringe dominates the high frequency information in the interferogram and simplifies the interpretation. This technique may be used to implement automatic interferogram interpretation.

Figure 10. Four exposure moire. The moire is between two interferograms viewed from the hologram. The moire compares to the low load interferogram shown in Figure 11.

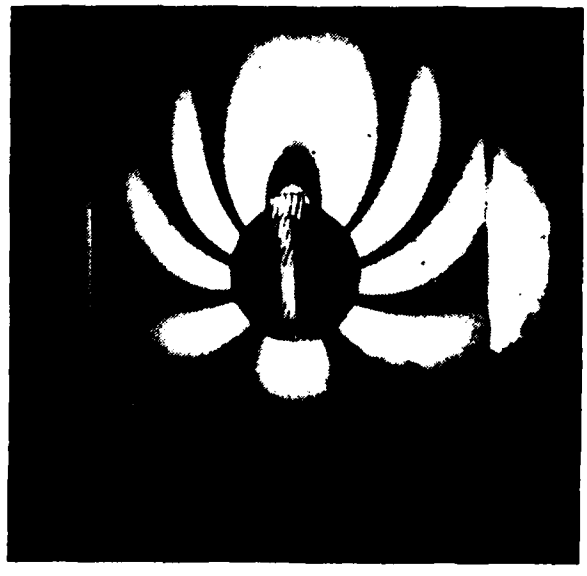

Figure 11. Double exposure holographic interferogram. Plate is deformed by a small load.

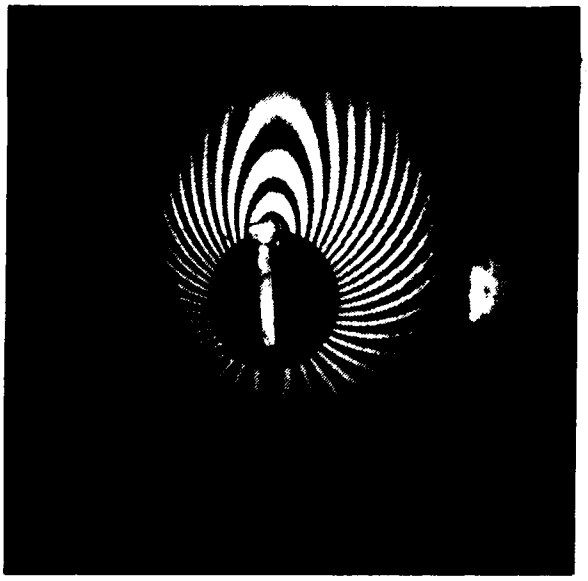

Figure 12. Interferogram obtained with double exposure hologram with load used in state two. This interferogram is nearly identical with the interferogram obtained with the loading used between state 3 and state 4.

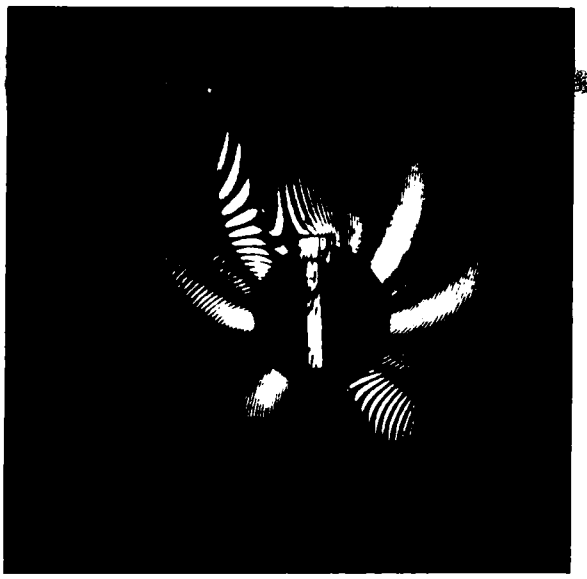

Figure 13. Four exposure moire with beam swing between exposure 3 and exposure 4. This should be compared to Figure 10.

Figure 14. Same as Figure 13, a four exposure moire with beam swing between state 3 and state 4. The beam swing is larger and consequently dominates more of the high frequency information in the interferogram.

Four-exposure, two-laser, two-hologram FLI

Instead of moireing with a grating as done by Abramson[6] we considered using a four-exposure, two-laser, two hologram FLI process to recover the linear FLI fringes from the holographic moire of the random noise pattern produced by the dynamic loading. Experimentally, one can use two pulsed lasers, (different colors) as sources to illuminate the object. One of the lasers will have a beam swinging mirror in the object beam so that linear fringes are introduced into one of the holograms by tilting the object beam between exposures

The initial pulses from the two lasers will occur simultaneously, and dynamic loading techniques will be used. This will ensure that both lasers (hence both holograms), see the same initial state of the surface. The second two pulses will be simultaneous so that both double exposure holograms have essentially the same noise pattern. Photographing the reconstructed images from the two holograms and moireing them will show the linear fringes (small phase) and the higher frequency defects such as subsurface cracks. Filtering of the moire fringes should result in high contrast FLI fringes showing the location of the defects as fringe shifts. The four-exposure, two-laser, two-hologram FLI process can be simplified by recording the holograms on the same film and obtaining the moire beats directly as suggested by Varner[8].

If the two lasers have different wavelengths, then the change in linear fringe frequency is given by $(K_1 - K_2)\,\alpha_o$ where

$$K_n = \frac{2\pi}{\lambda_n} \quad ; \; n = 1, 2 \tag{9}$$

and α_o is the angle of the mirror which is tipped to introduce the linear fringes.

For example, if the two lasers are frequency doubled YAG ($\lambda_1 = 0.53\ \mu m$) and Pulsed Ruby ($\lambda_2 = 0.69\ \mu m$) then $\Delta\lambda/\lambda_1\lambda_2 = 0.3/\lambda_2$ so that the frequency of the linear fringe is 30% lower than it would be for double pulsed holography with a ruby laser. Thus, the moire fringes resulting from using two different lasers have a period characteristic of a laser with a much longer wavelength.

Conclusion

FLI provides a mechanism for automating the locating of defects that can be identified with holographic interferometry. Our studies show methods that enable the apparent displacement of test objects between double exposures to be reduced. These techniques coupled with the understanding acquired from verifiable modeling provide an exciting atmosphere for future experiments.

Acknowledgement

We want to acknowledge the capable help of Adrian Ho for laboratory experiments aiding in the preparation of this paper.

References

1. R.S. Longhurst, *Geometrical & Physical Optics*, John Wiley & Sons, N.Y. (1967) p. 278.
2. D.M. Meadows et al, "Generation of Surface Contours by Moire Patterns," Appl Opt 9(4)942 April (1970).
3. J.R. Varner, "Desensitized Hologram Interferometry," Appl Opt 9(9)2098 Sept. (1970)
4. Optical Engineering 21(4) July-Aug (1982). Many incoherent moire measurement methods are described in this issue.
5. J.R. Varner, "Holographic Contouring: Alternatives and Applications," SPIE Seminar Proceedings, Vol. 25 (1971) p. 239.
6. N. Abramson, *The Making and Evaluation of Holograms*, Academic Press, N.Y. (1981) p. 222.
7. G.O. Reynolds, D.A. Servaes, L. Ramos-Izquierdo, "Holographic Fringe Linearization Interferometry (FLI) for Defect Detection – Part I – The Basic Concept." SPIE meeting, Los Angeles, CA, Jan. 1985.
8. J.R.Varner, "The Use of Contour Maps for Measuring Surface Displacement," in *Holographic Non-Destructive Testing*, ed. by R.K. Erf, Academic Press, N.Y., (1974) p. 270.

APPENDIX D

Holographic Fringe Linearization Interferometry (FLI) for Defect Detection

by

G.O. Reynolds
Honeywell Electro-Optics Division
110 Fordham Road, Wilmington, Massachusetts 01887

Reprinted from: ACTA Polytechnical Scandinavica, Applied Physics, Series No. 150, Image Science '85, Vol. 2 Ph150, p. 53, 1985

HOLOGRAPHIC FRINGE LINEARIZATION INTERFEROMETRY (FLI) FOR DEFECT DETECTION

George O. Reynolds, Honeywell Electro-Optics Division, Wilmington, MA

ABSTRACT

The Holographic FLI process consists of swinging the object beam between exposures of a double exposure hologram to add a linear fringe to the reconstructed image. The amount of beam swing controls the extent to which the fringes are linearized. Finite element analysis using the ANSYS code yields results in excellent agreement with experiment.

1. INTRODUCTION

In this paper, we show that the complicated interference pattern resulting from double-exposure holography can be reduced to a simple linear fringe pattern using Fringe Linearization Interferometry.[1,2,3,4] Furthermore, fringe shifts on the resulting linear fringe pattern clearly indicate the location of through cuts and sub-surface cuts in test plates under static loading conditions.

The fringe shifts at the site of the defects (cracks and sub-surface cracks) in the Holographic FLI method have characteristic Fourier signatures that are amenable to automatic readout techniques for defect location. This is experimentally demonstrated in a Fourier diffractometer where the interference effects at the site of defects using Holographic FLI have demonstrably different diffraction patterns (Fourier signatures) from those in the linear fringe region where no defects are present.

2. THE BASIC FLI PROCESS

In the FLI process the first hologram is made when the object is in state #1. Between exposures the object beam is moved through an angle, $\delta\phi$, and the load on the object is changed to create state #2 of the object. A second exposure on the same film is made of the object in state #2. The reference beam is identical for both holograms. Upon reconstruction, the holographic images from the two exposures combine coherently and the phase difference describing the two different states of the object forms an interference pattern (laced with linear fringes) superimposed upon the image of the object. By controlling the frequency of the linear fringes, it is possible to remove the fringe shifts associated with small displacements (clutter) and keep the information concerning the larger displacements (defects) as a phase shift on the linear fringes.

Analysis shows that the intensity distribution in the reconstructed image of a double exposure FLI Holographic Interferogram is

$$I(X) = |f(x,t)|^2 \, [2 + 2\cos(kx_o x'/f + K\,[\Delta\phi x'') + \Delta\psi(x')])], \qquad (1)$$

where kx_o/f is the linear fringe frequency,

$\Delta\phi(x'')$ is the differential surface displacement due to the defect at the position of the defect, x'', $\Delta\psi(x')$ is the differential surface displacement of the remainder of the test object, and $|f(x,t)|^2$ is the normal holographic image of the object at the time t.

Equation (1) shows that, in general, a complex fringe pattern is super-imposed upon the object. If we assume that

$$x_o x'/f \quad > \Delta\psi(x'), \tag{2}$$

and

$$x_o x'/f \quad < \Delta\phi(x'') > > \Delta\psi(x'), \tag{3}$$

then, Equation (1) becomes

$$I(x') = |f(x',t)|^2 \{2 + 2\cos\{kx_o x'/f + K\,\Delta\phi x''\}\}\,. \tag{4}$$

Equation (4) shows that under the assumptions given in Equations (2) and (3), the reconstructed interferometric image is laced with linear fringes having fringe shifts at the locations of the defects.

It is apparent from these results that if Holographic FLI is to be feasible and viable, we must control the linear fringe phase terms, $x_o x/f$, so that it dominates the phase term, $\Delta\psi(x',y')$ resulting from the differential loading. Experimentally, this task was accomplished by increasing the fringe frequency until the $x_o x/f$ phase term dominates the $\Delta\psi(x', y')$ phase term resulting from the differential loading. Obviously, if the defect is to be found as a shift of the linear fringes at the defect site then its out of plane displacement must be greater than $\lambda/4$ per linear fringe period as described in Equation (2).

3. DEMONSTRATION OF THE HOLOGRAPHIC FLI CONCEPT

A. Specimen, Loading, Mechanism and Test Fixture

The test specimen (Figure 1) designed for the FLI experiments is a 100 mm x 100 mm x 3.125 mm (4 in. x 4 in. x 0.125 in.) aluminum plate which has a circular hole located at its center. The diameter of the hole is 24.94 mm (0.9976 in.).

A through cut on one plate and a rear surface partial cut on another plate originating at the hole were used as the defects. Both cuts were approximately one inch in length. The test plates were placed in a stable fixture and attached on three sides.

A loading mechanism consisting of a lever arm attached to the edges of the hole was designed to give maximum out of plane displacement of the test specimen (Figure 2) at the location of the cut defect to give a distinctive holographic signature. Weights were hung from the lever arm between exposure to create the differential loads statically.

B. The Numerical Model

The experiments have been modeled using finite element analysis and agreement between the model and the experiment was found to be excellent. To model the test configuration, finite element meshes were constructed using the commercial computer code ANSYS[5] for the crack configurations shown in Figure 10. One such mesh is shown in Figure 3, in which the flaw extends upward and to the left from the hole. The boundary conditions imposed on the model correspond to those in the experiment: both side boundaries and the bottom boundary were all clamped: the top

boundary was left free. The moment applied to the test plate was simulated in the model by equal and opposite out-of-plane forces applied at the top and bottom of the hole as illustrated in Figure 2. The magnitude of these forces was such that the total applied torque was 3.6 inch-pounds.

Structurally, therefore, the model can be made to correspond to the experiment in all respects. A mechanical analogue for the beam rotation is also easy to provide, and this allows fringe linearization to be part of the model as well. The mechanical analogue is in fact a rigid-body rotation of the plate. Just as the field of linear fringes dominates other fringe patterns as the beam rotation is increased, so does the displacement of field of the rigid-body rotation dominate other displacement fields as the mechanical rotation is increased. Indeed, the experimental fringe linearization could also be accomplished by rotation of the specimen, but in practice, the beam rotation can be performed much more easily.

Once the rotation axis is selected, the nodes on the clamped boundaries must be assigned rotations with respect to the coordinate axes so that the plate rotation has the appropriate value (here, 600 microradians) with respect to the chosen rotation axis. In addition, these nodes must be assigned out-of-plane displacements according to their distance from the rotation axis. When imposed correctly, these additional boundary conditions model the experimentally observed fringe linearization extremely well.

C. Results and Discussion

The results of the analysis for the geometry in Figure 1 demonstrate the accuracy and utility of the finite element structural analysis in modeling the holographic FLI technique. Only the results obtained with the part through flaw will be discussed here. Other examples are given in the literature.[6,7] The computer model with differential loading between exposures gives the results shown in Figure 4. The effect of the crack can be observed as a modestly sharp bend of the fringes in the region of the crack. These bends are not obvious and would be particularly difficult to detect using an automated scanning procedure. Without a prior knowledge of the crack location, however, the bend in fringes to the upper left of the hole has no apparent distinction from other bends in the plot, which arise due to the discrete nature of the finite elements used to model the plate. (In Figure 4 and subsequent computer plots, the dashed line corresponds to zero displacements.)

The fringe patterns from the experiment and the analysis agree very well,[6,7] but one implication of this agreement is that flaw detection may prove difficult using conventional double exposure interferograms. This difficulty was a primary motivation for development of a linear fringe technique.

Linear fringes were next superimposed on Figure 4 with the result shown in Figure 5. The beam rotation used was 600 microradians, and again the moment loading was 3.5 inch-pounds. The linear fringes smooth out the fringe pattern of Figure 4, but the barely noticeable flaw signature in Figure 4 is the dominant feature of Figure 5. The linear fringes have essentially wiped out all the smoothly varying slopes of Figure 4, so that the discontinuous slopes associated with the part-through cut immediately catch one's attention. In addition, the homogeneity of the linear fringes away from the flaw, together with the sharp bends at the flaw, provide the features needed for an automatic detection procedure.

The inadequate resolution of the output device used in plotting the results of the finite element analysis makes the fringes jagged in places. However, the agreement with the experi-

ment results is excellent.[6,7] The linear fringes dominate over the entire plate, except at the flaw, where the sharp bend in the fringes occur. In the experiment the FLI results are even more dramatic because the FLI fringes are continuous.

4. POTENTIAL FOR AUTOMATIC READOUT

The linear fringe in the two-exposure Holographic FLI process readily lends itself to using an automatic readout. Although this has yet to be implemented, conclusive experimental evidence was obtained showing that effects are present at the defect site in the linear fringe holographic reconstruction which can be detected and used for the automatic readout. These effects were obtained by using a two-dimensional spatial Fourier transforming system to display the signatures.

5. SUMMARY AND CONCLUSIONS

Other types of loading are under consideration, and current plans are to study these further. For many situations, and certainly for practical defect detection in, say, aircraft structures, particular static loadings do not provide a range of mechanical disturbances wide enough to reveal all possible flaws. Continuation of this research is therefore expected to focus in large measure on dynamic excitation of mechanical vibrations, in the hope that a broader spectrum of response is activated. Interferograms are naturally more difficult to obtain when the time between exposures becomes very important, as a double-pulsed laser is necessary; extension of the computer models described above should provide guidance as to the time intervals required. Dynamic and model structural analysis are available to predict times and amplitudes of vibration so that validation studies can be carried out with a minimum of guess work.

This study demonstrates that measurable and detectable results characterize defects measured by the FLI Technique. These effects can be exploited in the development of an automatic readout system.

ACKNOWLEDGEMENTS

This work was sponsored by AFOSR on Contract F49629-82-C-0001.

The author wishes to thank his colleagues, J. DeVelis, L. Ramos, and Don Servaes of Honeywell EOD, and P. Hilton, R. Mayville and D. Peirce of A.D. Little for their contributions to this work which is described more fully in References 6 and 7.

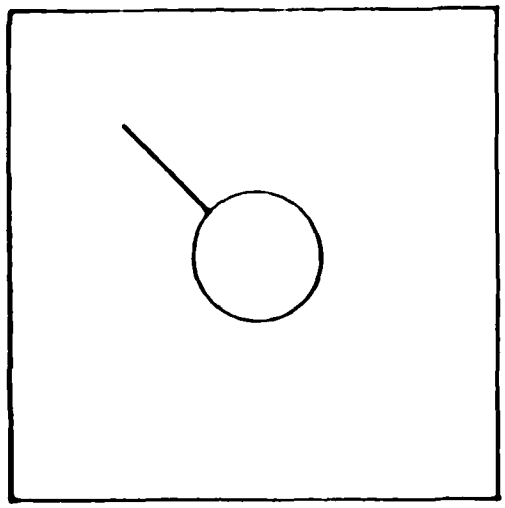

Figure 1. Crack Configurations Studied in This Paper. One Inch Crack Emanating from One Inch Hole in a 4 Inch Plate

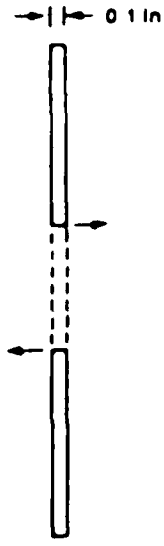

Figure 2. Force Loading Used to Model Hanging Weight Loading Mechanism

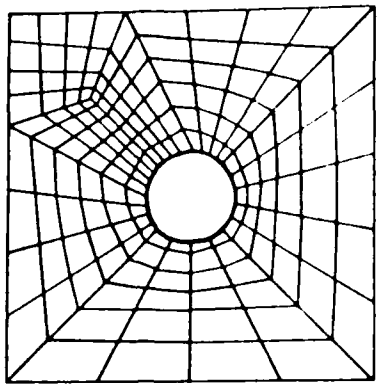

Figure 3. Typical Finite Element Mesh for Crack in Figure 1

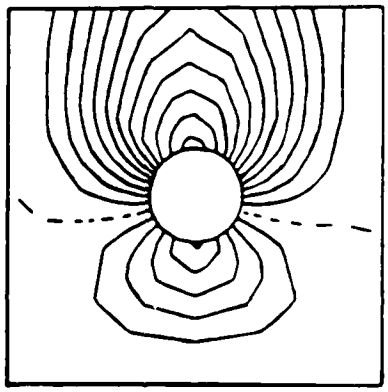

Figure 4. Computer Model Results Corresponding to Figure 1 with Differential Loading Between Exposures

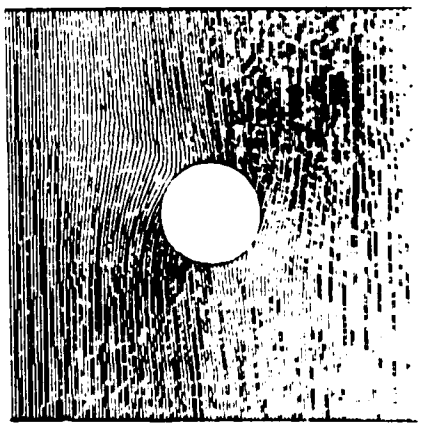

Figure 5. Reconstructed Image from FLI Model with Linear Fringe Added to Predominate the Clutter Fringes and Show the Location of the Subsurface Cut

REFERENCES

1. Vest, C.M., Holographic Interferometry, John Wiley & Son, Inc., New York, NY 1979.

2. Erf, R.K. Editor, Holographic Non-Destructive Testing, Academic Press, NY and London (1974).

3. N. Abramson, The Making and Evaluation of Holograms, Academic Press, NY (1981).

4. TRW Systems Group, "Feasibility Demonstration of Applying Advanced Holographic Systems Technology to Identify Structural Integrity of Naval Aircraft", Interim Report on Contract No. N62269-72-C-0400, 23 March 1973.

5. DeSalvo, G.J. and Swanson, J.A., ANSYS Engineering Analysis System User's Manual, Revision 4.0; Swanson Analysis Systems, P.O. Box 65, Houston, PA 15342 (1982).

6. G.O. Reynolds et al "Holographic Fringe Linearization Interferometry (FLI) for Defect Detection; Part I The Basic Concept" in Applications of Holography", L. Huff Editor, Proceedings SPIE Vol. 523, Paper No. 26, 1985.

7. G.O. Reynolds et al "Holographic Fringe Linearization Interferometry (FLI) for Defect Detection", to be published, Optical Engineering, September-October, 1985.

APPENDIX E

Holographic Fringe Linearization Interferometry (FLI) for Defect Detection

by

G.O. Reynolds, D.A. Servaes, L. Ramos-Izquierdo
Honeywell Electro-Optics Division
110 Fordham Road, Wilmington, Massachusetts 01887

and

J.B. DeVelis
Merrimack College, North Andover, Massachusetts 01860
Currently on sabbatical at Tufts University, Medford, Massachusetts 02153

and

D.C. Pierce, P.D. Hilton, R.A. Mayville
Arthur D. Little, Inc.
15 Acorn Park
Cambridge, Massachusetts 02140

Reprinted from: Optical Engineering Vol. 24 (5), pg. 757, (1985)

A reprint from

Optical Engineering

24(5), 757-768 (September/October 1985).

ISSN 0091-3286

HOLOGRAPHIC FRINGE LINEARIZATION INTERFEROMETRY FOR DEFECT DETECTION

G. O. Reynolds
D. A. Servaes
L. Ramos-Izquierdo

Honeywell Electro-Optics Division
110 Fordham Road
Wilmington, Massachusetts 01887

J. B. DeVelis

Merrimack College
Physics Department
North Andover, Massachusetts 01845

D. C. Peirce
P. D. Hilton
R. A. Mayville

Arthur D. Little, Inc.
15 Acorn Park
Cambridge, Massachusetts 02140

Holographic fringe linearization interferometry for defect detection

G. O. Reynolds
D. A. Servaes
L. Ramos-Izquierdo
Honeywell Electro-Optics Division
110 Fordham Road
Wilmington, Massachusetts 01887

J. B. DeVelis*
Merrimack College
Physics Department
North Andover, Massachusetts 01845

D. C. Peirce
P. D. Hilton
R. A. Mayville
Arthur D. Little, Inc.
15 Acorn Park
Cambridge, Massachusetts 02140

Abstract. In normal double-exposure holography with impulse loading, it is very difficult to locate defects because fringe clutter, which is due to random motion between exposures, often dominates the fringe shifts caused by the presence of subsurface defects (cracks, disbonds, etc.). We attempted to simplify the defect location problem by developing a concept more amenable to automatic readout techniques. Our approach to incorporate this change is quite simple. We swing the object beam between the two exposures, which adds a linear fringe to the reconstructed image. Proper selection of the fringe frequency (angle of object beam swing) and the loading force creates a reconstructed image laced with linear fringes that have fringe shifts at the defect locations that are highly visible. We describe the theory of the process. Experiments performed with static load illustrate that the defect is seen as fringe shifts on a linear carrier. Both through cuts and rear-surface cuts in a metal test plate were used to simulate defects. We further show that the defects have characteristic Fourier signatures different from those of the carrier.

Subject terms: holography; holographic interferometry; holographic nondestructive evaluation; diffractometers; finite element analysis; ANSYS code.

Optical Engineering 24(5), 757-768 (September/October 1985).

CONTENTS

1. Introduction
2. Objective of holographic fringe linearization interferometry (FLI)
3. Basic theory of holographic FLI
   3.1. Object beam shifting to create linear fringes
   3.2. Fourier transform holographic FLI analysis
   3.3. Fringe localization with holographic FLI
4. Understanding FLI/vector addition of phases
   4.1. Experiment demonstrating the vector addition of phases
   4.2. Basic holographic FLI process
   4.3. Interpretation of vector fringe addition leading to the loading limitation
5. Experimental demonstration of holographic FLI
   5.1. Test specimen
   5.2. Loading mechanism and test fixture
   5.3. Effect of increasing linear fringe frequency in two-exposure FLI
   5.4. Experimental demonstration of FLI for through cuts
   5.5. FLI experiments with specimens having rear-surface cuts
6. Numerical model
   6.1. Results and discussion
   6.2. Alternate loading methods
7. Potential for automatic readout
8. Summary and conclusions
9. Acknowledgments
10. Appendix: Mathematical development of linear fringes in a sideband Fresnel hologram
11. References

1. INTRODUCTION

Double-exposure holographic interferometry has been successfully demonstrated in a number of applications including nondestructive testing and metrology.[1-4] This technique holds promise for many nondestructive evaluation (NDE) applications. However, it has been limited in reaching its full potential due to its inability to interpret the complicated interference patterns that result from the test specimen being in different mechanical and/or thermal states at the time of the two exposures.

In this paper, we show that the complicated interference pattern resulting from double-exposure holography can be reduced to a simple linear fringe pattern using fringe linearization interferometry (FLI), a modification of conventional double-exposure holographic interferometry. Furthermore, fringe shifts on the resulting linear fringe pattern clearly indicate the location of through cuts and subsurface cuts in test plates under static loading conditions.

The fringe shifts at the site of the defects (cracks and subsurface cracks) in the holographic FLI method have characteristic Fourier signatures that are amenable to automatic readout techniques for defect location. This is experimentally demonstrated in a Fourier diffractometer, where the interference effects at the site of defects using holographic FLI have demonstably different diffraction patterns (Fourier signatures) from those in the linear fringe region where no defects are present.

2. OBJECTIVE OF HOLOGRAPHIC FLI

The objective of holographic FLI is to replace the complicated interference pattern resulting from conventional double-exposure holographic interferometry by a simple linear fringe pattern. Holographic FLI is potentially capable of detecting and locating defects in inspection applications involving large areas.

In the FLI technique, linear fringes are introduced in the formation step of double-exposure holographic interferometry by utilizing a beam deflector in the object beam between the two holographic exposures. The addition of the linear fringes to the interferogram makes the pattern much easier to interpret. A distinctive signature

*Currently on sabbatical at Tufts University, Medford, Mass

Invited Paper HO-108 received Feb 28, 1985, accepted for publication April 8, 1985, received by Managing Editor May 28, 1985. This paper is a revision of Papers 523-26 and 523-27 which were presented at the SPIE conference on Applications of Holography, Jan 21-23, 1985, Los Angeles, Calif. The papers presented there appear (unrefereed) in SPIE Proceedings Vol 523.

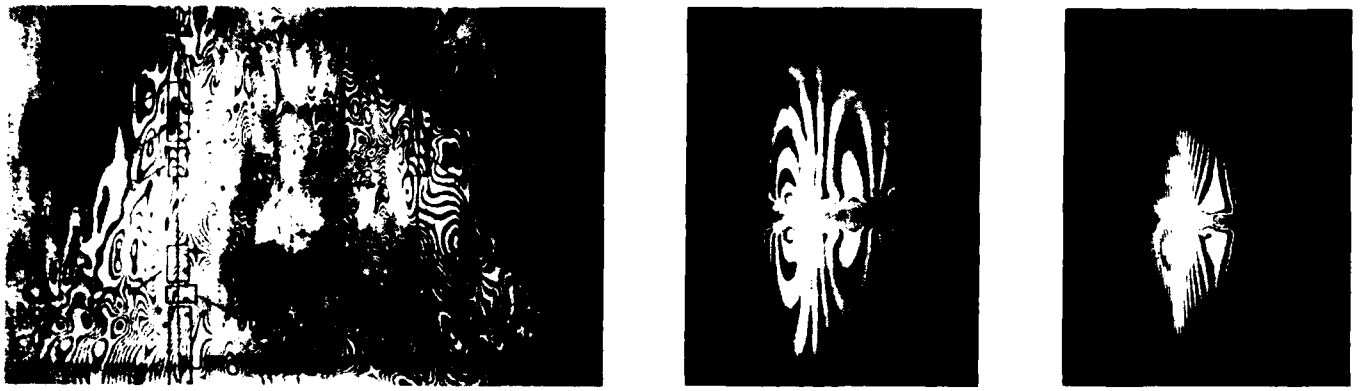

(a) (b) (c)

Fig. 1. Double-exposure holographic interferograms. (a) Complicated fringe pattern on a 48 in. by 25 in. panel using the double-pulsed holographic NDT technique. An impulse loading technique was utilized. The areas of stress corrosion cracking are indicated by fringe shifts in the boxed-in areas (from Ref. 4). (b) Holographic interferogram of Coke can stressed with elastic band. (c) FLI version of Fig. 1(b).

(fringe shift) at the site of a defect is maintained, while the clutter pattern is reduced to a field of linear fringes.

In Fig. 1(a) we have a typical cluttered fringe pattern resulting from double-exposure holographic interferometric testing of a panel. The stress corrosion cracking is indicated and highlighted by the fringe shifts in the boxed-in areas. It is apparent that locating the desired fringe shift information within the complicated fringe pattern is quite difficult.

In Fig 1(b) we show another, less complicated, fringe pattern. This pattern resulted from a double-exposure hologram of an aluminum can stressed with an elastic band. Between exposures the elastic band was cut, causing a large local deformation at the position of the elastic.

In Fig. 1(c), we see the effect of adding the linear fringe pattern by tilting the object beam between exposures of the two holograms. We see that the complicated fringe pattern in Fig. 1(b) has been simplified to the linear fringe pattern of Fig. 1(c) with a phase shift at the region of the elastic band where the differential force was appiied. The fringes are not quite linear but rather more quadratic in nature because of the curvature of the object. A higher frequency linear fringe is needed to linearize these quadratic fringes. It is the simplification of this interference pattern that forms the basis for the holographic FLI concept.

3. BASIC THEORY OF HOLOGRAPHIC FLI

3.1. Object beam shifting to create linear fringes

The principle of shifting the object wave between exposures in double-exposure holographic interferometry to create linear cosine fringes in the reconstructed interferogram has been illustrated in the literature.[5] The fringes have a period $\lambda/\delta\theta$ in object space, where $\delta\theta$ is the amount of angular shift between the object beams and λ is the wavelength of the laser light. An analysis utilizing Fourier transform holography and a finite-sized object is given here to illustrate the principle of FLI.

3.2. Fourier transform holographic FLI analysis

The Fourier transform configuration (Fig. 2) will be analyzed for simplicity. An analysis for sideband Fresnel holographic FLI appears in the Appendix. Fourier transform holograms reconstruct by performing Fourier transforms, rather than the more complicated procedure of focusing Fresnel transforms, which is necessary for sideband Fresnel holograms.

In the FLI process the first hologram is made when the object beam is in state No. 1. Between exposures the object beam is moved through an angle $\delta\theta$, and the load on the object is changed to create state No. 2 of the object. A second exposure on the same film is made

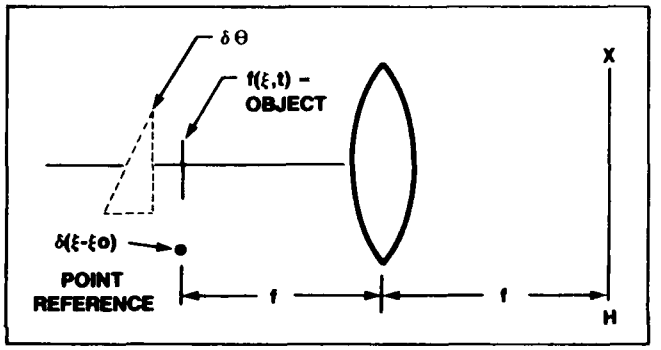

Fig. 2. Schematic of Fourier transform hologram system for double-exposure interferometry using a lens of focal length f.

of the object in state No. 2. The reference beam is identical for both holograms. Upon reconstruction, the holographic images from the two exposures combine coherently, and the phase difference describing the two different states of the object forms an interference pattern (laced with linear fringes) superimposed upon the image of the object. By controlling the frequency of the linear fringes, it is possible to remove the fringe shifts associated with small displacements (clutter) and keep the information concerning the larger displacements (defects) as a phase shift on the linear fringes. [Fig. 1(c)]. We will now describe this process mathematically using the Fourier transform hologram recording process illustrated schematically in Fig. 2.

The irradiance in the hologram plane of Fig. 2 for the first exposure is

$$H(x) = |e^{ikx\sin(\xi_o/f)} + \tilde{f}(x,t)|^2 , \tag{1}$$

where $\sim$ denotes a Fourier transform and $f(x,t)$ represents the surface deformations on the complex test object at time t.

If a prism of angle $\delta\theta$ is used to shift the direction of the object wave and another hologram is recorded on the same recording medium (note: in double-exposure holographic interferometry, a different state of the dynamic object, $f(x,t_1)$, is usually captured on the hologram), the irradiance of the second hologram is

$$H(x) = |e^{ikx\sin(\xi_o/f)} + \tilde{f}(x-x_o,t_1)|^2 , \tag{2}$$

where from the shift theorem of Fourier analysis

$$x_o = f\tan(\delta\theta) . \tag{3}$$

Reconstruction of the two holograms described in Eqs. (1) and (2) with a lens of focal length f results in a reconstructed image centered at the position $x' = \xi_o\theta$ of the reconstructed image plane given by

$$I(x) = \text{image} = \left|f(x',t) + f(x',t_1)e^{ikx_ox'/f}\right|^2 . \quad (4)$$

We will now investigate the implications of Eq. (4) for various conditions of interest.

Case 1: linear fringes

If $f(x',t) = f(x',t_1)$, then

$$I(x') = [f(x',t)]^2\left|1 + e^{ikx_ox'/f}\right|^2$$

$$= [f(x',t)]^2\left[2 + 2\cos\left(\frac{kx_ox'}{f}\right)\right]; \quad (5)$$

i.e., the image of the object is laced with "linear" cosine fringes of frequency $\nu = \tan(\delta\theta)/\lambda$.

Case 2: response of the defect

To extend this analysis to include the response of a defect, assume that the defect of interest causes a differential surface displacement $\Delta\phi(x'')$ at the position of the defect when loaded between the two exposures. This displacement behaves as an optical phase function in the hologram. A simplified analysis would assume $f(x',t) = 1$, and $f(x',t_1) = e^{ik\Delta\phi(x'')}$ in Eq. (4). The revised image of Eq. (5) would be

$$I(x') = \text{ideal image} = 2 + 2\cos\left[\frac{kx_ox'}{f} + k\Delta\phi(x'')\right] , \quad (6)$$

where x'' denotes the position of the defect in the x' coordinate system.

The surface displacement differential appears as a phase modulation of the linear fringes and has a shape, size, and location, $\Delta\phi(x'')$, characteristic of the defect. We call this the ideal image because of the simplifying assumptions used in deriving Eq. (6).

Case 3: response of the defect and random surface displacements (clutter noise)

In any situation where the object surface undergoes a differential loading between the two exposures, $f(x',t_1)$ in Eq. (4) would be

$$f(x',t_1) = f(x',t)e^{ik[\Delta\phi(x'') + \Delta\psi(x')]} , \quad (7)$$

where $\Delta\phi(x'')$ is the differential surface displacement due to the defect at the position of the defect x'', and $\Delta\psi(x')$ is the differential surface displacement of the remainder of the test object.

Use of Eq. (7) in Eq. (5) yields

$$I(x) = |f(x,t)|^2\left(2 + 2\cos\left\{\frac{kx_ox'}{f} + k[\Delta\phi(x'') + \Delta\psi(x')]\right\}\right) , \quad (8)$$

where $|f(x,t)|^2$ is the normal holographic image of the object at time t.

Equation (8) shows that in general a complex fringe pattern is superimposed upon the object. If we assume that

$$\frac{x_ox'}{f} > \Delta\psi(x') \quad (9)$$

and

$$\frac{x_ox'}{f} < \Delta\phi(x'') \gg \Delta\psi(x') , \quad (10)$$

then Eq. (8) becomes

$$I(x') = |f(x',t)|^2\left\{2 + 2\cos\left[\frac{kx_ox'}{f} + k\Delta\phi(x'')\right]\right\} . \quad (11)$$

Equation (11) shows that under the assumptions given in Eqs. (9) and (10) the interferometric image is laced with linear fringes with fringe shifts at the locations of the defects.

The result in Eq. (8) illustrates that the normal fringe pattern of holographic interferometry is phase-modulated onto the cosine carrier, which is created by shifting the object wave between the exposures. Therefore, we see that the basis of holographic FLI is to create linear fringes in two-exposure holographic interferometry by shifting the object beam between exposures of the two holograms and to control either the loading and/or the fringe frequency to ensure that the assumptions given in Eqs. (9) and (10) are experimentally realizable. This approximation is nearly realized in Fig. 1(c), where the loading was extremely localized and very large.

3.3. Fringe localization with holographic FLI

The issue of fringe localization in holographic interferometry has been thoroughly investigated.[1] The linear fringes resulting from tilting the object beam between exposures in holographic FLI appear to be localized in the space on and about the object. These fringes can be made to appear in front of or behind the reconstructed object or actually on the object surface. In the research presented in this paper the latter situation is most desirable. A thorough mathematic analysis[1] shows that the fringe localization depends upon the geometry of the holographic recording and viewing systems.

In holographic interferometry, the fringe localization depends upon the curvature of the object illumination wavefront at the object surface. The curvature of the reference beam is unimportant as long as it is equivalent to the curvature of the reconstruction wave. To guarantee that the linear fringes in holographic FLI will be localized on the surface of the reconstructed object, we utilize collimated illumination for the object beam in forming the holograms. The actual experimental holographic recording arrangement used in the experiments is shown in Fig. 3.

4. UNDERSTANDING FLI/VECTOR ADDITION OF PHASES

4.1. Experiment demonstrating the vector addition of phases

The fundamental concept for understanding why the holographic FLI process works is that of the vector addition of phases in the holographic process, as shown in Eq. (8). The phase of the linear fringes resulting from tilting the object beam between exposures of a double-exposure hologram adds vectorially to the phase due to the surface deformation contours caused by differentially loading the object. The system, shown schematically in Fig. 3, was used to demonstrate the vector addition principle for two-exposure holography.

In Fig. 4 we show the results for the case of an object tilt about one axis and a beam rotation about the other axis. Figure 4(a) shows the linear fringes present in the reconstructed image of a double-exposure hologram arising from tipping the test plate about the x-axis between exposures. Figure 4(b) shows linear fringes resulting from rotating the object beam about the y-axis between exposures. Figure 4(c) shows the linear fringes arising from the vector addition of the phases resulting from tilting the test plate as in Fig. 4(a) and rotating the object beam as in Fig. 4(b) between exposures. The resulting fringes in Fig. 4(c) are rotated through an angle. The horizontal and vertical phases have been added vectorially to produce the rotated linear fringe pattern. Figure 4(c) also shows that the higher frequency x-axis phase due to tilting the test plate is larger

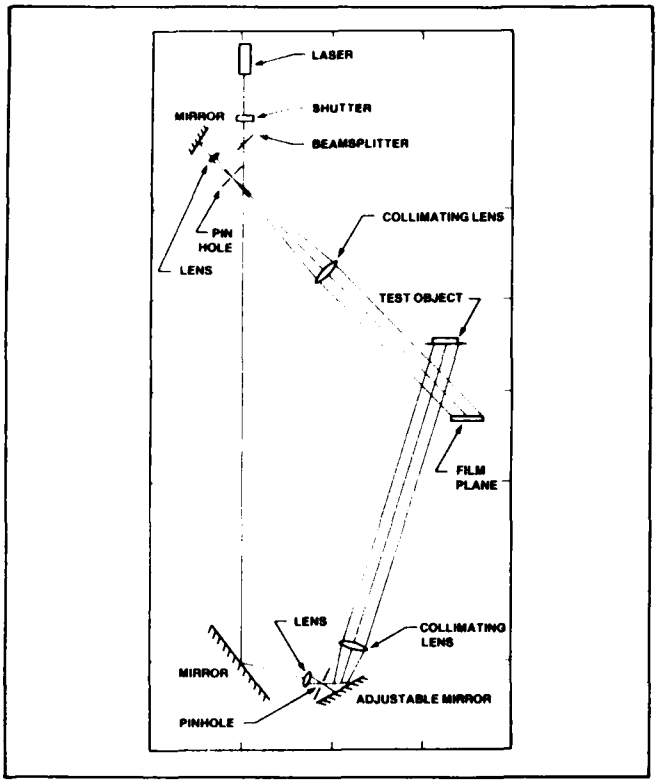

Fig. 3. Experimental arrangement for holographic FLI experiments showing collimated object illumination for obtaining fringe localization on the surface of the reconstructed image.

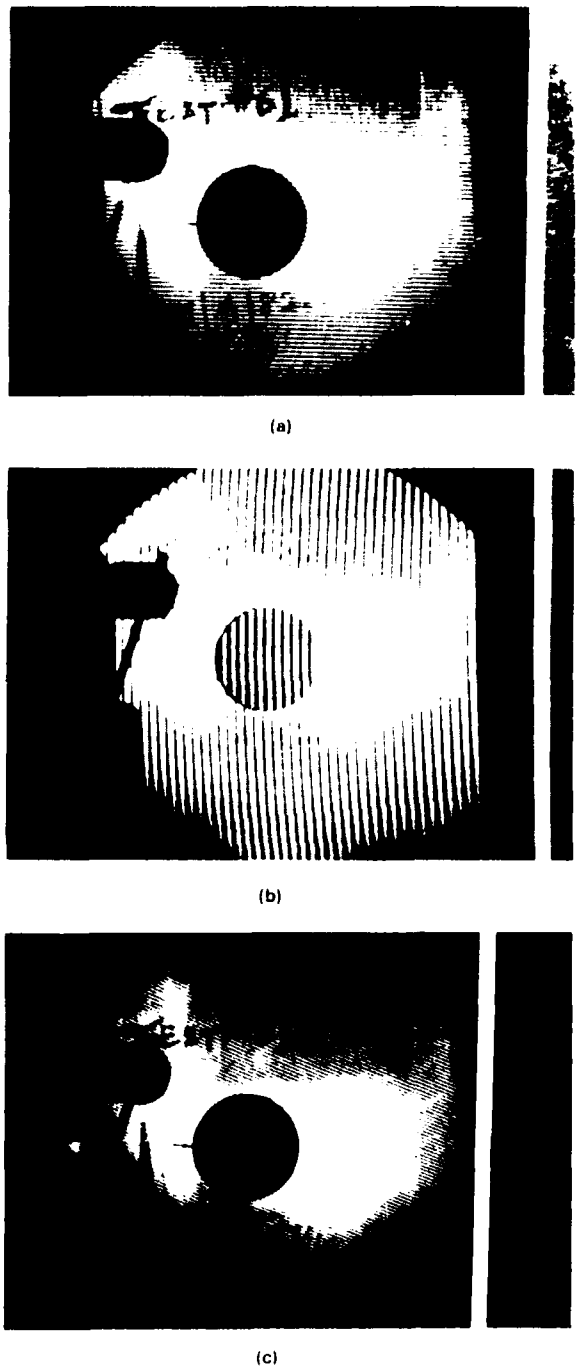

Fig. 4. Experimental demonstration of the vector addition of linear fringes in double-exposure holography. Reconstructed image of double-exposure hologram resulting from (a) tipping the test plate about the x-axis between exposures, (b) rotating the object beam about the y-axis between exposures, and (c) rotating the object beam about the y-axis and tipping the test plate about the x-axis between exposures.

than the y-axis phase resulting from a small rotation of the object beam. Thus when the two are vectorially added in the two-exposure hologram, the x-axis phase greatly controls the amount of rotation.

To demonstrate that it is the vector addition of phases that has occurred in the experiments shown in Fig. 4, we examine the Fourier spectrum of each of the reconstructed images of Fig. 4. In Fig. 5 we show the spectra. Figure 5(a) is the Fourier transform of Fig. 4(a); Fig. 5(b) is the Fourier transform of Fig. 4(b); Fig. 5(c) is the Fourier transform of Fig. 4(c). The higher diffraction orders are due to film nonlinearities.

If we now record and superimpose the position of the first harmonic along the y-axis of Fig. 5(a) [see arrow in Fig. 5(a)] with the first harmonic along the x-axis of Fig. 5(b) [see arrow in Fig. 5(b)] with the first harmonic in the x-y plane of Fig. 5(c) [see arrow in Fig. 5(c)], we obtain the result shown in Fig. 6. Clearly, the first harmonic of Fig. 5(a) has added vectorially to the first harmonic of Fig. 5(b) to give the resultant first harmonic of Fig. 5(c). This series of experiments clearly demonstrates that the holographic FLI process does indeed produce a vector addition of the phases that leads to the desired linear fringe pattern in the reconstructed image.

4.2. Basic holographic FLI process

The experimental procedure for the holographic FLI process is described as follows: (1) Form a conventional hologram with the test specimen in a given stress state. (2) Add an additional loading to the test fixture to change the stress state of the specimen. (3) Tilt the object beam and keep the reference beam fixed. (4) Form the second hologram on the same recording medium with a second exposure. (5) Process and reconstruct the double-exposure hologram.

As shown in Eq. (8), the resulting reconstructed holographic interferogram has cosine fringes of the form

$$\text{Fringes} \sim \cos[\omega x' + \Delta(x',y')] \,, \tag{12}$$

where $(\omega x') = kx_0x'$ represents the phase of the linear fringe obtained from tilting the object beam between exposures of the two holograms and $\Delta(x',y') = k\Delta\phi(x'',y'') + \Delta\psi(x',y')$ represents the phase term describing the difference in the out-of-phase surface deformations resulting from the loading force added prior to form-

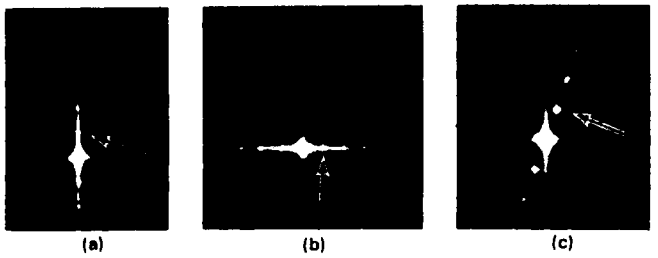

Fig. 5. (a) Fourier spectrum of the reconstructed image of Fig. 4(a) showing the delta functions along the y-axis. (b) Fourier spectrum of the reconstructed image of Fig. 4(b) showing the delta functions along the x-axis. (c) Fourier spectrum of the reconstructed image of Fig. 4(c) showing the delta functions in the (x-y) plane.

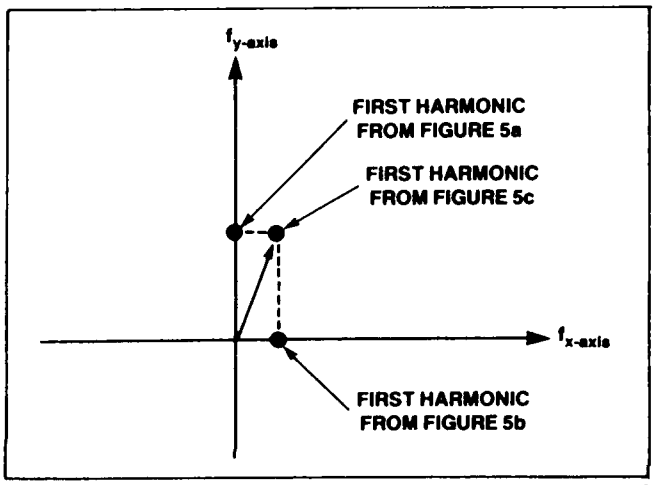

Fig. 6. Fourier plane indicating the superposition of the first harmonics of Figs. 5(a), 5(b), and 5(c) demonstrating the vector addition of phases.

ing the second hologram. Equation (12) is referred to as the FLI equation.

4.3. Interpretation of vector fringe addition leading to the loading limitation

Interpreting the experimental results demonstrated in Fig. 5 in terms of the basic interference equation of two-exposure FLI holography, Eq. (12), led to the following conclusion: If the out-of-plane deformation of the test plate due to differential loading between exposures, which yields the $\Delta(x',y')$ phase term in Eq. (12), is greater than one-quarter wavelength per linear fringe period, given by the $\omega x'$ term in Eq. (12), then the vector addition of fringes will lead to the $\Delta(x',y')$ term dominating the linear fringe term in Eq. (12). This will result in the linear fringe term being dominated by the clutter fringes due to any differential loading, rendering the FLI concept ineffective.

This constraint can be overcome in two ways: (1) fixing the fringe frequency and desensitizing the effect of the deformation by using holographic moire techniques as described elsewhere,[6] or (2) increasing the fringe frequency ω so that the spatial period is smaller than the distance over which the deformation changes by $\lambda/4$.

Thus, the two phase terms in Eq. (12) can be controlled such that either term can predominate over the other. In fact, in Figs. 1(b) and 1(c) we have shown a case in which the linear fringe term was controlled so that it was larger than the phase term due to the deformation $\Delta(x',y')$ but not the phase of the defect $\Delta(x'',y'')$. This effect was achieved by increasing the linear fringe frequency until it dominated the vector addition.

This same effect of linear fringe demonstration could have been accomplished by controlling the differential loading force [giving rise to the $\Delta(x',y')$ phase term in Eq. (12)] to ensure that the resulting deformations are less than one-quarter wavelength per linear fringe period. This is a very severe experimental restriction on the differential loading configuration and is very difficult to implement. We demonstrate that the differential loading phase term $\Delta(x',y')$ can be made to dominate the linear fringe phase term $\omega x'$ by examining the experimental results shown in Fig. 7. In Fig. 7 linear fringes were introduced by shifting the object beam. They have been completely dominated by the random fringe pattern resulting from the differential loading. In this case the load was applied by two thumb screws mounted on the back side of the test plate. The linear fringes can be recovered by using moire holography, as described elsewhere.[6]

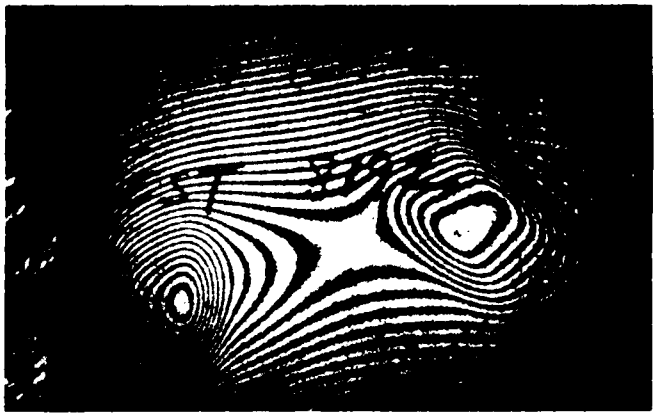

Fig. 7. The addition of a large differential load $\Delta(x,y)$ leads to random fringes that dominate the linear fringes.

It is apparent from these results that if holographic FLI is to be feasible and viable, we must control the linear fringe phase term $\omega x'$ so that it dominates the phase term $\Delta(x',y')$ resulting from the differential loading. Experimentally, this task was accomplished by increasing the fringe frequency until the $\omega x'$ phase term dominated the $\Delta(x',y')$ phase term resulting from the differential loading. Obviously, if the defect is to be found as a shift of the linear fringes at the defect site, then its out-of-plane displacement must be greater than $\lambda/4$ per linear fringe period as described in Eq. (10).

5. EXPERIMENTAL DEMONSTRATION OF HOLOGRAPHIC FLI

5.1. Test specimen

The test specimen [Fig. 8(a)] designed for the FLI experiments is a 100 mm × 100 mm × 3.125 mm (4 in. × 4 in. × 0.125 in.) aluminum plate that has a circular hole located at its center. The diameter of the hole is 24.94 mm (0.9976 in.).

A through cut on one plate and a rear-surface partial cut on another plate [Fig. 8(a)] originating at the hole were used as the defects. Both cuts were approximately one inch in length.

5.2. Loading mechanism and test fixture

A loading mechanism was designed to give maximum out-of-plane displacement of the test specimen [Fig. 8(b)] at the location of the cut defect to give a distinctive holographic signature.

In Fig. 8(c) we show a photograph of the entire test mechanism including the fixture and the test plate loading arm. The loading arm is on the back side of the test plate. The mathematical modeling of the experiment was formulated by modifying the ANSYS computer code. The model and its experimental verification, which are in excellent agreement, are described later in this paper.

5.3. Effect of increasing linear fringe frequency in two-exposure FLI

The vector addition of phases restricts the loading term $\Delta(x',y')$ in Eq. (12) to phases not greater than one-quarter wavelength per linear

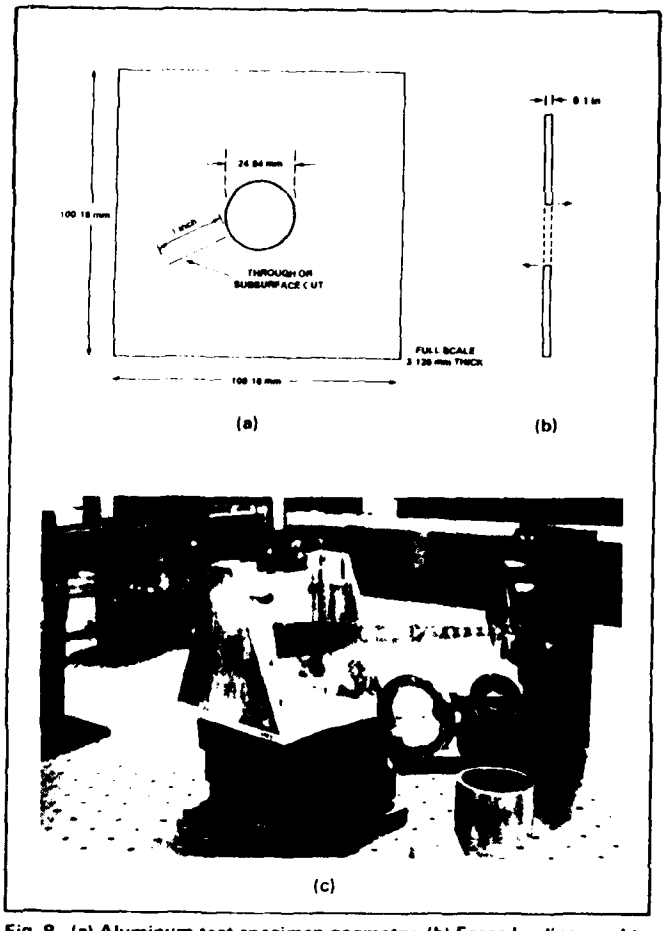

Fig. 8. (a) Aluminum test specimen geometry. (b) Force loading used t(model hanging weight loading mechanism. (c) Photograph of testing setup showing test specimen and loading mechanism.

fringe cycle so that the resulting vector addition of the $\omega x'$ linear fringe term does not become dominated by the $\Delta(x',y')$ phase term. As previously indicated, this limit can be achieved by carefully controlling the loading forces so that the differential out-of-plane deformations are small or by increasing the linear fringe frequency until it dominates the $\Delta(x',y')$ phase term in the vector addition of phases. This latter method was selected because it satisfies the quarter-wave loading constraint, is easy to implement experimentally, and desensitizes the system. In fact, it should be possible to increase the linear fringe frequency to the point where it dominates the $\Delta(x',y')$ phase term for a large loading torque and still show a fringe shift at the location of the crack defect; therefore, two-exposure FLI should be feasible for many practical loading conditions.

The ultimate limitation for the frequency of the linear fringes will be determined by the speckle noise in the optical system viewing the hologram. If this limitation yields a nonlinear fringe, then further desensitization can be achieved by utilizing the more complex two-color, four-exposure moire technique,[6] which requires a photograph of the holographic image and a spatial filtering step applied to the hologram image to create the linear fringes showing the defect location.

5.4. Experimental demonstration of FLI for through cuts

A two-exposure FLI experiment was designed and performed on the test plate of Fig. 8(a) with a through cut to demonstrate the FLI technique. A two-exposure hologram was made and reconstructed. The first exposure was for the relaxed state of the test plate, and the second exposure was for the stressed state of the test plate. The first hologram [Fig. 9(a)] shows the deformation from the stress. Figures 9(b) through (e) show the reconstructed image from the double-exposure hologram, where, in addition to the stress, linear fringes of varying frequency have been added between exposures.

Figure 9(b) shows the result when the linear fringe frequency is low, $\omega = 0.5$ cycle/mm. The constraint of one-quarter wave of deformation per fringe cycle has not been met, although the discontinuity at the cut is very visible. Figure 9(c) is the result for a fringe frequency 2ω, and Fig. 9(d) is for 4ω. Figure 9(f) illustrates the case for a frequency of 8ω. In the 8ω case, speckle effects lowered the fringe contrast so the fringes could not be seen. The effect of 8ω was

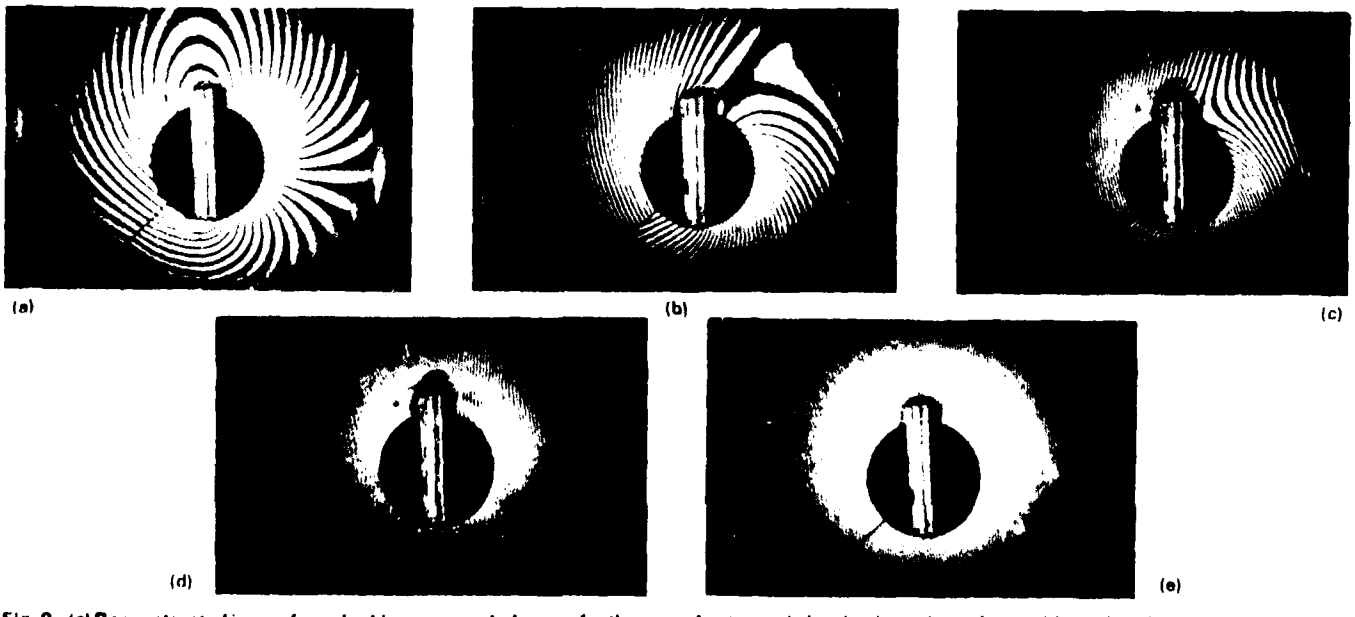

Fig. 9. (a) Reconstructed image from double-exposure hologram for the case of a stressed plate having a through cut without the addition of linear fringes. (b)–(e) Experimental results showing feasibility for two-exposure FLI for a through cut. Reconstructed images from FLI process in Fig. 9(a) with linear fringes of various frequencies added to control the noise pattern shown in Fig. 9(a). In (b) $\omega = 0.5$ cycles/mm, in (c) $\omega = 1$ cycle/mm, in (d) $\omega = 2$ cycles/mm, in (e) $\omega = 4$ cycles/mm.

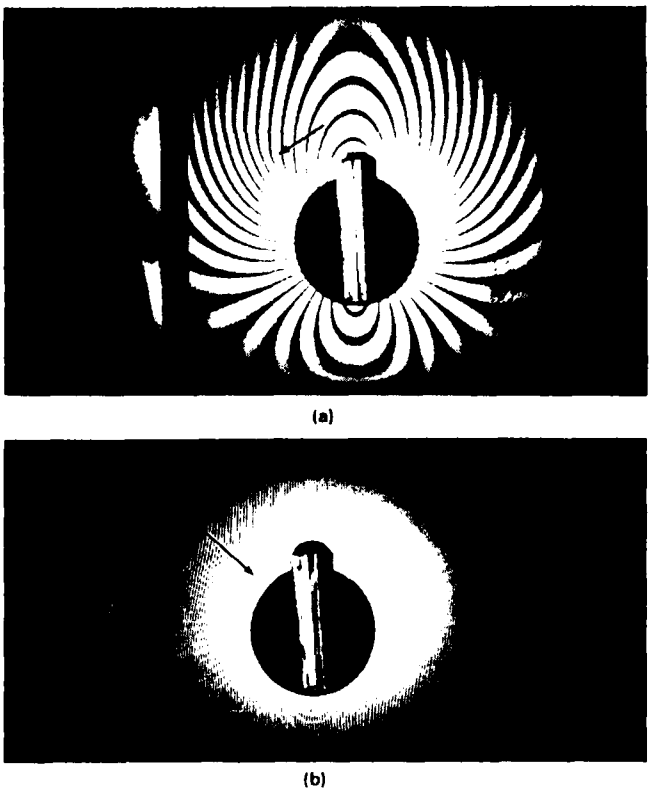

Fig. 10. Demonstration of FLI for subsurface cuts. (a) Reconstructed image from FLI without the addition of linear fringes for a subsurface cut. (b) Reconstructed image from FLI with linear fringes added to predominate the noise and show the location of the subsurface cut.

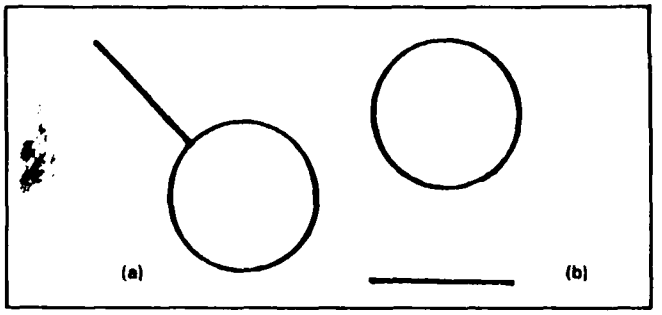

Fig. 11. Crack configurations studied in this paper. (a) One inch crack emanating from hole. (b) One inch crack one inch below hole.

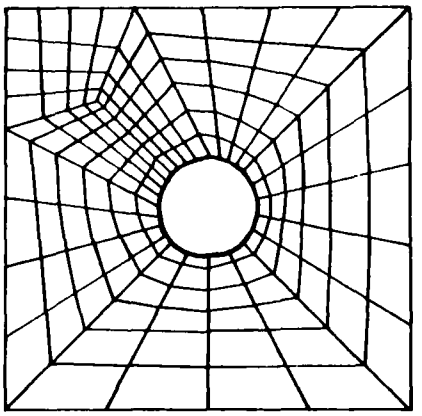

Fig. 12. Typical finite element mesh for crack in Fig. 11(a).

achieved by reducing the load by one-half and adding fringes at a frequency of 4ω. The fringe shift at the defect is visible at the higher frequencies.

Obviously, with a linear fringe of frequency $\omega \sim 4c/\text{mm}$ [Fig. 9(e)] the differential surface deformation meets the quarter-wave/period limitation except in the vicinity of the cut, where a violent phase deviation is evident. This was the first demonstration of the FLI principle.

5.5. FLI experiments with specimens having rear-surface cuts

Since the cut in Figs. 9(a) and 9(b) is easily visible, a more dramatic demonstration of the FLI principle was made using rear-surface cuts penetrating part way through the plate. A similar test plate to the one used for the through cut was made. A 1/16 in. wide saw cut, 3/32 in. deep was made on the back side of the test plate. The cut is 1 in. long, starts at the center hole, and is at an angle ($-45°$) to the vertical axis. A double-exposure hologram of the plate was made by adding a differential load between the exposures. The process was repeated, and linear fringes were added by rotating the illuminating beam between the exposures. The results are shown in Figs. 10(a) and 10(b). Figure 10(a) is the usual interferogram obtained from double-exposure holographic interferometry. By carefully examining the photograph the slight bend of the contour fringes can be detected, but the effect is subtle. Figure 10(b) shows the interferogram obtained for the same plate stress, but with the linear fringes added. The defect area is quite apparent. Since the cut itself is not visible on the surface of the plate, this experiment demonstrates the feasibility of the two-exposure holographic FLI technique for detecting subsurface flaws and defects.

These experiments have been modeled using finite element analysis, and agreement between the model and the experiment is excellent, as described below.

6. NUMERICAL MODEL

To model the test configuration, finite element meshes were constructed using the commerical computer code ANSYS[7] for the crack configurations shown in Fig. 11. One such mesh is shown in Fig. 12, in which the flaw extends upward and to the left from the hole. The boundary conditions imposed on the model correspond to those in the experiment: both side boundaries and the bottom boundary were all clamped; the top boundary was left free. The moment applied to the test plate was simulated in the model by equal and opposite out-of-plane forces applied at the top and bottom of the hole, as illustrated in Fig. 8(b). The magnitude of these forces was such that the total applied torque was 3.6 in.-lb.

Structurally, therefore, the model can be made to correspond to the experiment in all respects. A mechanical analogue for the beam rotation is also easy to provide, and this allows fringe linearization to be part of the model as well. The mechanical analogue is in fact a rigid-body rotation of the plate. Just as the field of linear fringes dominates other fringe patterns as the beam rotation is increased, so does the displacement field of the rigid-body rotation dominate other displacement fields as the mechanical rotation is increased. Indeed, the experimental fringe linearization could also be accomplished by rotation of the specimen, but in practice the beam rotation can be performed much more easily.

The model boundary conditions associated with the rigid-body rotation can be somewhat tricky. First, an axis of rotation for the model must be chosen to agree with the intended beam rotation. This

axis will always lie in the plane of the specimen, and in the usual case it will pass vertically through the center of the hole. Other rotation axes may be desirable, however, for detecting flaws of a particular orientation. Once the rotation axis is selected, the nodes on the clamped boundaries must be assigned rotations with respect to the coordinate axes so that the plate rotation has the appropriate value (here, 600 μrad) with respect to the chosen rotation axis. In addition, these nodes must be assigned out-of-plane displacements according to their distance from the rotation axis. When imposed correctly, these additional boundary conditions model the experimentally observed fringe linearization extremely well.

Through cracks in the plate were modeled simply by releasing connections along an appropriate line of nodes. Because the model plate consisted of two-dimensional finite elements, modeling a part-through crack required a special procedure. The surfaces of the through crack were separated slightly, and the gap was filled with small addditional elements. These additional elements were assigned a thickness of 0.005 in., 4% of the nominal plate thickness. These elements thus modeled the effect of a thin ligament. The ligament thickness in the model was less than that in the actual plate (0.03 in.); the model ligament thickness was selected by comparing model and experimental fringe patterns. A direct model of the effect of ligament thickness would require a three-dimensional analysis, and such analysis is planned in future work. Corresponding to the presence of a part-through flaw, the current ligament model serves to enforce displacement continuity across the closed side of the defect; this continuity naturally does not occur for the through crack.

6.1. Results and discussion

Two sets of results will be presented in detail; both of these demonstrate the accuracy and utility of the finite element structural analysis in modeling the holographic FLI technique.

The first results are for the crack geometry shown in Fig. 11(a). Only the part-through flaw will be discussed. The double-exposure holograms obtained in the laboratory were obtained from the front surface of the plate, i.e., the surface on which the crack was not visible. Figure 10(a) shows the interferogram for the plate without any linear fringes. The fringes that appear in the figure have smoothly varying slopes, and a cursory inspection indicates nothing that might signify the presence of a flaw. If one knows that a part-through crack emanates from the upper left corner of the hole, however, one notices a modestly sharp bend of the fringes in this region, especially compared to the similar fringes to the upper right of the hole. These bends are not obvious, however, and they would be particularly difficult to detect using an automated scanning procedure. The computer model of the same loading is shown in Fig. 13. Here again, the effect of the crack can be observed if one knows its location. Without such knowledge, however, the bend in fringes to the upper left of the hole has no apparent distinction from other bends in the plot, which arise due to the discrete nature of the finite elements used to model the plate. (In Fig. 13 and subsequent computer plots, the dashed line corresponds to zero displacements.) The fringe patterns from the experiment and the analysis agree quite well, but one implication of this agreement is that flaw detection may prove difficult using conventional double-exposure interferograms. This difficulty was previously emphasized as a primary motivation for development of a fringe linearization technique.

Linear fringes were next superposed on Fig. 10(a), with the result shown in Fig. 10(b). As noted previously, the beam rotation used was 600 μrad, and the moment loading was 3.5 in.-lbs. The linear fringes smooth out the fringe pattern of Fig. 10(a), but the barely noticeable flaw signature in Fig. 10(a) is the dominant feature of Fig. 10(b). The linear fringes have essentially wiped out all the smoothly varying slopes of Fig. 10(a), so that the discontinuous slopes associated with the part-through cut immediately catch one's attention. In addition, the homogeneity of the linear fringes away from the flaw, together with the sharp bends at the flaw, provides the features needed for an automatic detection procedure.

Figure 14 shows the finite element analysis performed to correspond to Fig. 10(b). While the inadequate resolution of the output device makes the fringes jagged in places, the agreement with the experiment is excellent. The linear fringes dominate over the entire plate, except at the flaw, where the sharp bend in the fringes occurs, as in the experiment.

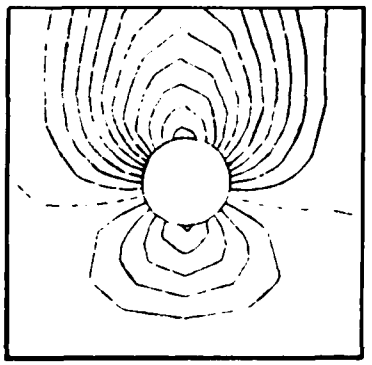

Fig. 13. Computer model corresponding to Fig. 10(a).

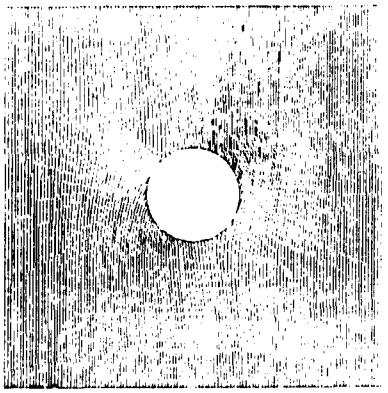

Fig. 14. Computer output corresponding to Fig. 10(b).

Because the agreement between experiment and analytical model is so close, we can use the structural analysis to provide guidance as to how one might facilitate and optimize holographic detection of flaws. For example, if a particular type of flaw is being sought after, both the axis and the magnitude of beam rotation could be determined ahead of time to maximize the likelihood that if the particular type of flaw exists, it will have a significant effect on the linear fringes. In addition, appropriate loading configuration and magnitude may be worked out numerically without the expense of an extended experimental program. Additional analyses performed for the part-through cut discussed above indicated that locating the axis beam rotation 45° from the crack orientation provided the best holographic signature of the flaw; other rotation axes led to linear fringes that made the flaw more obscure. A rule of thumb for detection of a crack emanating from a hole can be stated as follows: fringe linearization should be employed, and the rotation axis (or axes) should be oriented 45° from the suspected crack (or cracks). When the flaws are randomly located, a range of beam rotation axes is probably necessary

We also considered the crack configuration in Fig. 11(b). With the same bending load configuration as was applied to Fig. 11(a), the interferogram in Fig. 15 was produced. As in Fig. 10(a), the crack gives rise to a sharp bend, barely noticeable, in the fringes that cross the crack location. In the corresponding finite element calculation, this bend was not even distinguishable from other sharp bends arising from the discrete nature of the finite elements; see Fig. 16. Linear fringes were applied to the finite element model of the plate in

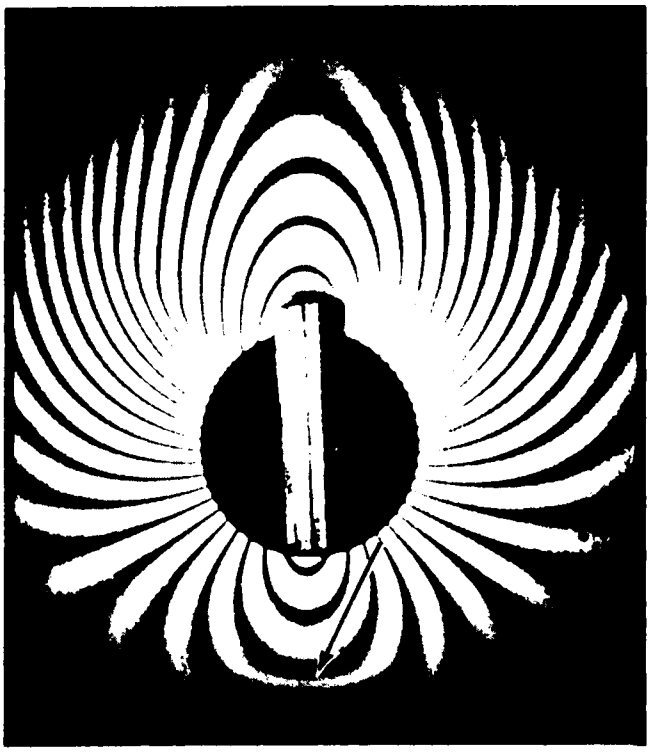

Fig. 15. Interferogram for crack in Fig. 11(b), without linear fringes.

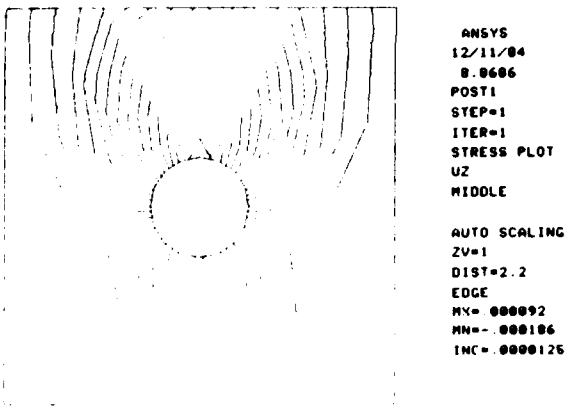

Fig. 16. Finite element model of Fig. 15.

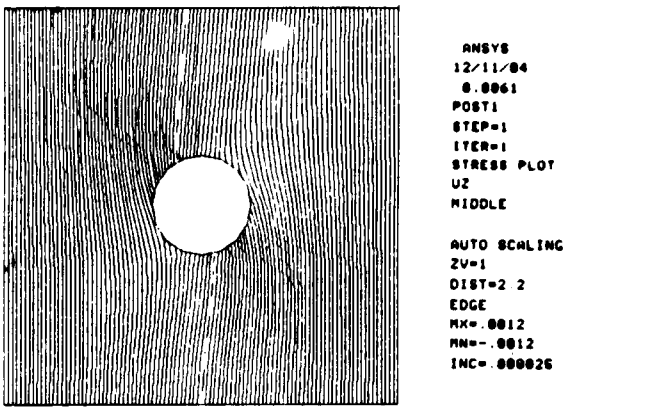

Fig. 17. Addition of linear fringes to Fig. 16.

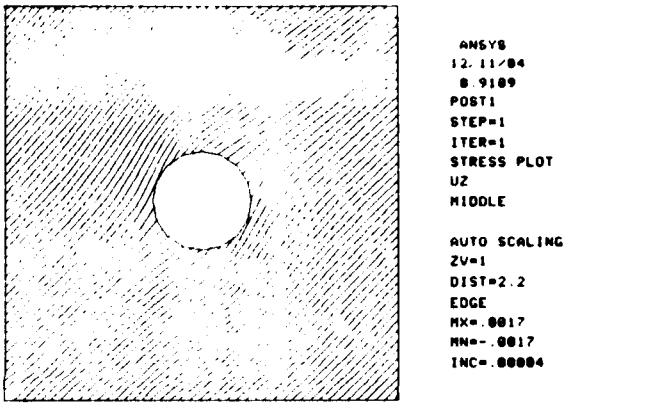

Fig. 18. Linear fringes added to Fig. 16 and rotated about an axis 45° to the vertical.

the hope that these would render the crack location detectable. The results are furnished in Fig. 17. Unfortunately, this figure seems to be identical to what one would expect to see if there were no defects present in the plate. The positive side of the analysis was born out by the actual experiment on the plate with the part-through flaw, with linear fringes. Exactly as in the model, an undisturbed field of linear fringes was observed, just like those in the defect-free areas of Fig. 10(b). Figure 18 shows an attempt, using our model, to reveal the flaw by simulating rotation of the object beam about an axis oriented 45° to the crack. Again, however, the flaw cannot be detected with this loading mechanism.

6.2. Alternate loading methods

The state of affairs just described shows simultaneously the benefits of the computer model and the limitations of reliance on a single load configuration to reveal defects with the holographic technique. For both crack configurations shown in Fig. 11, the computer model has shown excellent agreement with the interferograms produced experimentally. Given that a simple structural analysis can model so well the loading and displacements seen here, we would expect the structural model to be an invaluable tool in pursuing viability of the fringe linearization technique for practical applications. Research studies could be performed to determine by computer which beam rotations and loading modes are best suited for interferometric detection of a particular crack. Here, we have observed the utility of a bending load in revealing a crack emanating from a hole; in addition, we can probably conclude that the same loading is not as effective for a crack that does not intersect the hole.

Other types of loading are under consideration, and current plans are to study these further. An additional loading mechanism appropriate for the hole in the plate is insertion of a tapered or shrink-fit plug into the hole, as described by Vest.[1] Indeed, this loading rendered the crack of Fig. 11(b) visible, both without linear fringes (Fig. 19) and with them (Fig. 20). At this point, we have not yet modeled these interferograms by computer. The conclusion remains, however, that different flaw geometries are made most susceptible to detection by different loadings. For many situations, and certainly for practical defect detection in, say, aircraft structures, particular static loadings do not provide a range of mechanical disturbances wide enough to reveal all possible flaws. Continuation of this research is therefore expected to focus in large measure on dynamic excitation of mechanical vibrations, in the hope that a broader spectrum of responses is activated. Interferograms are naturally

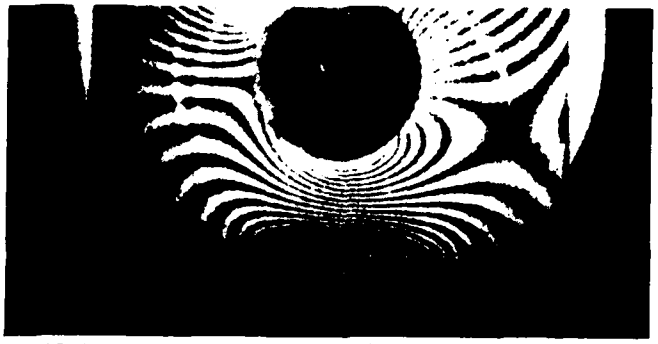

Fig. 19. Interferogram of crack in Fig. 11(b) with tapered plug loading.

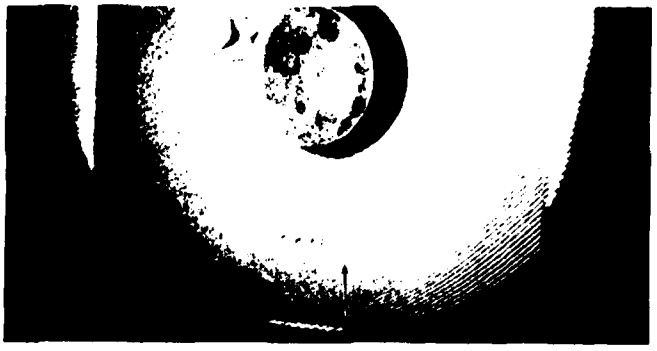

Fig. 20. Addition of linear fringes to Fig. 19.

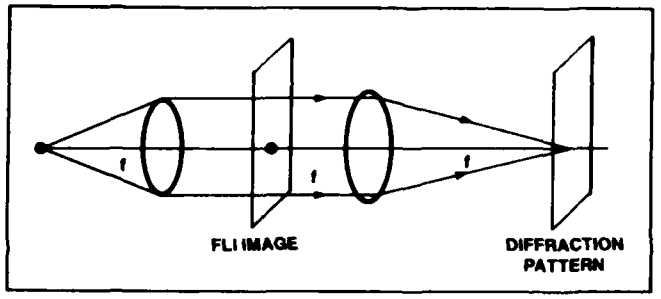

Fig. 21. Schematic of optical diffractometer.

Fig. 22. Fourier signature of through cut; (a) linear fringes, (b) defect.

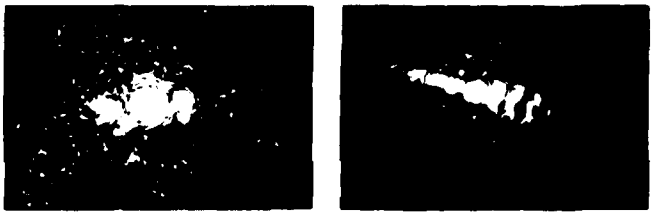

Fig. 23. Fourier signature of rear-surface cut; (a) linear fringes, (b) defects.

more difficult to obtain when the time between exposures becomes very important, since a double-pulsed laser is necessary; extension of the computer models described above should provide guidance as to the time intervals required. Dynamic and model structural analyses are available to predict times and amplitudes of vibration so that validation studies can be carried out with a minimum of guesswork.

7. POTENTIAL FOR AUTOMATIC READOUT

The linear fringe in the two-exposure holographic FLI process readily lends itself to using an automatic readout. Although this has yet to be implemented, we present conclusive evidence that effects are present at the defect site in the linear fringe holographic reconstruction that can be detected and used for the automatic readout. To show these effects we use a diffractometer, a two-dimensional spatial Fourier transforming system shown schematically in Fig. 21. In Fig. 22 we show the diffraction pattern from parts of the reconstructed image of a two-exposure FLI hologram at a defect-free region and at the site of the through cut shown in Fig. 9(e). Figure 22(a) shows the Fourier signature of the linear fringe (diffractometer was directed at a region to left of defect). We recognize the dc term and the two first orders of the linear fringe transform. In Fig. 22(b), we see the signature at the defect site (the through cut). The fringe shift at the cut location results in a different dc term and two sets of first orders for the two linear fringes at the cut. The diffractometer outputs clearly show there exists a signature at the defect site distinguishable from the defect-free region. Similar results were obtained for the rear-surface cut, as shown in Fig. 23.

These results demonstrate that measurable and detectable results characterize defects measured by the FLI technique. These effects can be exploited in the development of an automatic readout system.

8. SUMMARY AND CONCLUSIONS

The results obtained with static loading techniques were significant and include the following: (1) The experimental feasibility of the FLI concept has been demonstrated. (2) FLI removes fringe clutter and simplifies defect location. (3) Experimental results showed linearization of fringes and location of both a through cut and a rear-surface cut. (4) Experiments with a Fourier diffractometer showed that both the through cut and the rear-surface cut had Fourier signatures significantly different from those of the carrier fringe. Automatic readout techniques are possible with such characterisitic signatures using image processing software and digital Fourier transform methods. (5) Modeling efforts also showed simplified crack detection with fringe linearization and are in excellent agreement with the experimental results. (6) Modeling/experimental results indicated the limitations of static loading techniques for finding subsurface defects.

We conclude that holographic FLI has been successfully demonstrated for the detection of defects under conditions of static loading. Further development of the process is necessary before an automatic holographic FLI process can be implemented for field experiments.

9. ACKNOWLEDGMENT

This work was sponsored by Air Force Office of Scientific Research on Contract F49620-82-C-0001.

10. APPENDIX: MATHEMATICAL DEVELOPMENT OF LINEAR FRINGES IN A SIDEBAND FRESNEL HOLOGRAM

The purpose of this appendix is to show that linear fringes can be

created in a double-exposure sideband Fresnel hologram by shifting the object beam between the exposures. The mathematical development will follow that given in Chap. 3 of Ref. 8.

The diffracted field emanating from an object illuminated with a tilted reference wave in the second exposure is obtained by modifying Eq. (3-36) of Ref. 8 to give

$$R(x) = -\exp(ik_1 z_1)C\exp\left(\frac{ik_1 x^2}{2z_1}\right) \times \int D(\xi)\exp\left[ik_1\left(\frac{\xi^2}{2z_1} - \frac{\xi x}{z_1}\right)\right]\exp(ik_1\beta_0\xi)d\xi \ , \quad \text{(A-1)}$$

where β_0 is the tilt angle of the beam striking the object and $\sin\beta_0 \simeq \beta_0$.

The intensity distribution in the sideband Fresnel hologram produced by this wavefront is

$$I(x) = [K\exp(ik_1\theta x) + R(x)]^2 \ , \quad \text{(A-2)}$$

where θ is the angle between reference and object beams.

If we consider only the term in Eq. (A-2) corresponding to the real image, we obtain a modified version of Eq. (3-81) in Ref. 8. Thus,

$$I_R(x) = K'^*KC^*\exp(-ik_1 z_1)\exp\left(\frac{-ik_1 x^2}{2z_1}\right) \times \exp(ik_1\alpha_0 x)\mathcal{D}^*(x) \ , \quad \text{(A-3)}$$

where

$$\mathcal{D}^*(x) = \int_{z_1=0} D^*(\xi)\exp\left[-ik_1\left(\frac{\xi^2}{2z_1} - \frac{\xi x}{z_1} + \beta_0\xi\right)\right]d\xi \ . \quad \text{(A-4)}$$

When the distribution described by Eq. (A-3) is reconstructed with a beam of wavelength λ_2, the amplitude in the reconstructed image is given by

$$\psi_{imR}(\alpha) = A\int_{z_2=0}\exp\left(\frac{-ik_1 x^2}{2z_1}\right)\mathcal{D}^*(x) \times \exp(ik_1 x\theta)\exp\left[\frac{ik_2(x-\alpha)^2}{2z_2}\right]dx \ , \quad \text{(A-5)}$$

where A includes all the obliquity factors. Substituting Eq. (A-4) into Eq. (A-5), we obtain

$$\psi_{imR}(\alpha) = A\exp\left(\frac{ik_2\alpha^2}{2z_2}\right)\int_{z_2=0}\left[\int_{z_1=0} D^*(\xi)\exp\left(\frac{-ik_1\xi^2}{2z_1}\right) \times \exp\left(\frac{ik_1\xi x}{z_1}\right)\exp(-ik_1\beta_0\xi)d\xi\right]\exp\left[\frac{ix^2}{2}\left(\frac{k_2}{z_2} - \frac{k_1}{z_1}\right) \times \exp(ik_1 x\theta)\exp\left(-\frac{ik_2 x\alpha}{z_2}\right)dx\right], \quad \text{(A-6)}$$

which is a modified version of Eq. (3-84) in Ref. 8.

Applying the focusing condition $k_1 z_2 = k_2 z_1$ to Eq. (A-6) yields

$$\psi_{imR}(\alpha) = A\exp\left(\frac{ik_2\alpha^2}{2z_2}\right)\int\int D^*(\xi)\exp\left(\frac{-ik_1\xi^2}{2z_1}\right) \times \exp\left[ik_1\xi\left(\frac{x}{z_1} - \beta_0\right)\right]d\xi\exp\left[ix\left(k_1\theta - \frac{k_2\alpha}{z_2}\right)\right]dx \ . \quad \text{(A-7)}$$

In Eq. (A-7), the ξ integral is the Fourier transform of a Fresnel wavefront. This gives

$$\psi_{imR}(\alpha) = A\exp\left(\frac{ik_2\alpha^2}{2z_2}\right)\int_{z_2=0}\widetilde{D}^*\left(-\frac{x}{\lambda_1 z_1} + \frac{\beta_0}{\lambda_1}\right) \times \exp\left[\left(\frac{ik_1}{2z_1}\right)\left(\beta_0 - \frac{x}{z_1}\right)^2\right] \times \exp\left[2\pi ix\left(\frac{\theta}{\lambda_1} - \frac{\alpha}{\lambda_2 z_2}\right)\right]dx \ , \quad \text{(A-8)}$$

where tilde denotes a Fourier transform operation. Making the change of variable

$$x' = -\frac{x}{\lambda_1 z_1} + \frac{\beta_0}{\lambda_1} \quad \text{(A-9)}$$

and carrying out the Fourier transform operation indicated in Eq. (A-8), we get

$$\psi_{imR}(\alpha) = A\exp\left(\frac{ik_2\alpha^2}{2z_2}\right)\exp\left[2\pi i\left(\frac{\beta_0\theta z_1}{\lambda_1} - \frac{\alpha\beta_0 z_1}{\lambda_2 z_2}\right)\right] \times (-\lambda_1 z_1)\, D^*(\alpha - z_1\theta)\exp\left[-\frac{2\pi i}{2z_1}(\alpha - z_1\theta)^2\right] \ . \quad \text{(A-10)}$$

A comparison of Eq. (A-10) with Eq. (3-89) in Ref. 8 shows that the only difference between the reconstructed image of a sideband Fresnel hologram and one created with a tilted object wave is the linear phase factor (LPF) in α; i.e.,

$$\text{LPF} = \exp\left[2\pi i\left(\frac{\beta_0\theta z_1}{\lambda_1} - \frac{\alpha\beta_0 z_1}{\lambda_2 z_2}\right)\right] . \quad \text{(A-11)}$$

Equation (A-11) shows that the phase factor resulting from the tip is linear in α and has a frequency proportional to the tip angle β_0, the hologram construction distance z_1, the reconstruction distance z_2, and the reconstruction wavelength λ_2.

Thus, if a double-exposure hologram were made in which the only difference was a tilt of the object beam in one of the exposures, then the reconstructed image would be laced with linear cosine fringes of

the form

$$1 + \cos 2\pi\left(\frac{\beta_0 z_1}{\lambda_1} - \frac{\alpha\beta_0 z_1}{\lambda_2 z_2}\right). \quad \text{(A-12)}$$

This shows that tilting the object beam in the hologram results in linear fringes across the image. The analysis of the virtual image yields a similar result.

11. REFERENCES

1. C. M. Vest, *Holographic Interferometry*, John Wiley & Son, Inc., New York (1979).
2. R. K. Erf, ed, *Holographic Non-Destructive Testing*, Academic Press, New York (1974).
3. N. Abramson, *The Making and Evaluation of Holograms*, Academic Press, New York (1981).
4. TRW Systems Group, "Feasibility Demonstration of Applying Advanced Holographic Systems Technology to Identify Structural Integrity of Naval Aircraft," Interim Report on Contract No. N62269-72-C-0400 (23 March 1973).
5. H. M. Smith, *Principles of Holography*, pp. 194-5, Wiley-Interscience, New York (1969).
6. G. O. Reynolds, D. A. Servaes, and J. B. DeVelis, in *Applications of Holography*, L. Huff, ed., Proc. SPIE 523, 186 (1985).
7. G. J. DeSalvo, and J. A. Swanson, *ANSYS Engineering Analysis System Users Manual*, Revision 4.0; Swanson Analysis Systems, P.O. Box 65, Houston, Pa. 15342 (1982).
8. J. B. DeVelis and G. O. Reynolds, *Theory and Applications of Holography*, Addison Wesley, Reading, Mass. (1967).

the form

$$1 + \cos 2\pi\left(\frac{\beta_0 z_1}{\lambda_1} - \frac{\alpha\beta_0 z_1}{\lambda_2 z_2}\right). \quad \text{(A-12)}$$

This shows that tilting the object beam in the hologram results in linear fringes across the image. The analysis of the virtual image yields a similar result.

11. REFERENCES

1. C. M. Vest, *Holographic Interferometry*, John Wiley & Son, Inc., New York (1979).
2. R. K. Erf, ed, *Holographic Non-Destructive Testing*, Academic Press, New York (1974).
3. N. Abramson, *The Making and Evaluation of Holograms*, Academic Press, New York (1981).
4. TRW Systems Group, "Feasibility Demonstration of Applying Advanced Holographic Systems Technology to Identify Structural Integrity of Naval Aircraft," Interim Report on Contract No. N62269-72-C-0400 (23 March 1973).
5. H. M. Smith, *Principles of Holography*, pp. 194-5, Wiley-Interscience, New York (1969).
6. G. O. Reynolds, D. A. Servaes, and J. B. DeVelis, in *Applications of Holography*, L. Huff, ed., Proc. SPIE 523, 186 (1985).
7. G. J. DeSalvo, and J. A. Swanson, *ANSYS Engineering Analysis System Users Manual*, Revision 4.0; Swanson Analysis Systems, P.O. Box 65, Houston, Pa. 15342 (1982).
8. J. B. DeVelis and G. O. Reynolds, *Theory and Applications of Holography*, Addison Wesley, Reading, Mass. (1967).

END

DTIC

5-86